

DISSERTATION

PREDICTING THE PHYSICAL STABILITY OF BIOPOLYMERS  
BY SELF-INTERACTION CHROMATOGRAPHY

Submitted by

Robert W. Payne

Department of Chemistry

In partial fulfillment of the requirements

For the Degree of Doctor Philosophy

Colorado State University

Fort Collins, Colorado

Spring 2008

UMI Number: 3321301

## INFORMATION TO USERS

The quality of this reproduction is dependent upon the quality of the copy submitted. Broken or indistinct print, colored or poor quality illustrations and photographs, print bleed-through, substandard margins, and improper alignment can adversely affect reproduction.

In the unlikely event that the author did not send a complete manuscript and there are missing pages, these will be noted. Also, if unauthorized copyright material had to be removed, a note will indicate the deletion.

**UMI**<sup>®</sup>

---

UMI Microform 3321301

Copyright 2008 by ProQuest LLC.

All rights reserved. This microform edition is protected against unauthorized copying under Title 17, United States Code.

ProQuest LLC  
789 E. Eisenhower Parkway  
PO Box 1346  
Ann Arbor, MI 48106-1346

COLORADO STATE UNIVERSITY

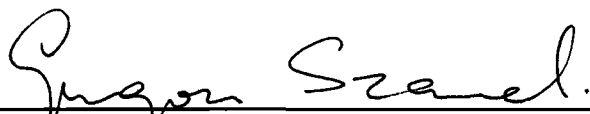
March 24, 2008

WE HEREBY RECOMMEND THAT THE DISSERTATION PREPARED UNDER OUR SUPERVISION BY ROBERT W. PAYNE ENTITLED "PREDICTING THE PHYSICAL STABILITY OF BIOPOLYMERS BY SELF-INTERACTION CHROMATOGRAPHY" BE ACCEPTED AS FULFILLING IN PART REQUIREMENTS FOR THE DEGREE OF DOCTOR OF PHILOSOPHY.

Committee on Graduate Work



George B. Barisas



Grzegorz Szamel



Steven H. Strauss



Olve Peersen



Advisor: Charles S. Henry



Department Head: Anthony K. Rappe

## **Abstract of Dissertation**

### **Predicting the Physical Stability of Biopolymers by Self-Interaction Chromatography**

Biopolymers, including proteins and peptides, are increasingly taking the place of small molecules in manufacturing, health and home applications. The advantage of using biopolymers over small molecules for therapeutic applications include high activity, high specificity and low toxicity. The disadvantages of using biopolymers include large scale production, chemical instability and physical degradation. A biopolymer that shows promise for a specific application will not advance past early development if the protein lacks either chemical or physical stability. Of these two parameters, physical stability is often harder to predict and/or measure. The physical stability of a biopolymer can be improved by site-directed mutagenesis, glycosylation, post-translational modification and adjusting the solvent/co-solvent system. Quantitatively measuring the change in the physical stability of a protein in different solvent/co-solvent systems can increase the number of early developmental stage proteins that advance to commercial scale. Physical stability of proteins can be described by protein-protein interactions and measured by the osmotic second virial coefficient ( $B$ ). However, current methods used to measure  $B$  such as static light scattering are not practical for large screening studies because of large protein consumption, low throughput, method variability and analyte size limitations. An alternative method

to measure B is Self-Interaction Chromatography (SIC), which requires less protein, shorter analysis time, allows for miniaturization and capable of measuring B for small size biopolymer. The ability of SIC to measure B for a therapeutic protein, a peptide and membrane proteins in different solvent/co-solvent systems has been demonstrated in this dissertation.

Robert W Payne  
Chemistry Department  
Colorado State University  
Fort Collins, CO 80523  
Spring 2008

## ACKNOWLEDEMENTS

To my amazing wife and best friend: Lola Payne. Without your love and support this work would have not been possible.

To my family, thank for your love and support. The lessons I learned growing up shaped the person I am now.

To Mark C. Manning. Thank for you all your contributions in the development of this project. Your support and guidance has directed me in my graduate career and beyond.

To Genencor: Dr. Whiten, Douglas Dale and Beth Fryksadale. Thank you for the experience of purifying protein in SF, which opened my eyes to protein processing.

To my committee: Dr. Barisas, Dr. Szamel, Dr. Strauss, Dr. Peersen. Thank for your critical eye, advice and support.

To my advisor: Dr. Henry. Thank you for your guidance, support and standing up for me.

## DEDICATION

This work is dedicated to my wife Lola Payne

## Table of Contents

	Page
Abstract.....	iii
Acknowledgements.....	v
Dedication.....	vi
List of Figures.....	xi
Chapters	
1. Introduction	1
1.1 Chemical and Physical Degradation	2
1.2 Osmotic Second Virial Coefficient (B)	3
1.2.1. Relationship between B and Protein Crystallization	5
1.2.2. Relationship between B and Solubility	6
1.3 Static Light Scattering (SLS)	8
1.4 Self-Interaction Chromatography for Soluble Proteins	8
1.4.1 SIC for Membrane Proteins	12
1.5 Dissertation Summary	12
1.6 Reference	14
2. Therapeutic Agents	18
2.1. Introduction	
2.2. Materials and Methods	21
2.2.1. Chemicals and Reagents	21
2.2.2. Enfuvirtide Sample Preparation	21
2.2.3. Enfuvirtide Column Preparation	22
2.2.4. Anti-Body Fragment Sequences	23
2.2.5. Anti-Body Fragment Sample Preparation	23
2.2.6. Anti-Body Fragment Column Preparation	24
2.2.7. LC System used for Enfuvirtide	25
2.2.8. LC System used for Antibody Fragment	26
2.2.9. Molecular Weight for Enfuvirtide	26
2.2.10. Solubility Measurements for Enfuvirtide	27
2.2.11. Reverse Phase HPLC Method for Enfuvirtide	27
2.3. Results and Discussion	
2.3.1. Enfuvirtide Chromatograms	28
2.3.2. pH Effects on the B of Enfuvirtide.	29
2.3.3. The Effects Salt on Enfuvirtide	33
2.3.4. Peptide Concentration Effects on B Values of Enfuvirtide	36
2.3.5. pH and NaCl Screens For LB-005	38
2.3.6. Sucrose, Glycine and Trehalose for LB-005	40

2.3.7. Comparing the Colloidal Stability of LB-005 to LB-007.	41
2.3.8.Changes in Colloidal Stability of LB-007 with NaCl	43
2.4. Conclusion	45
2.5. References	45
3. Colloidal and Conformational Stability of Proteorhodopsin	
3.1. Introduction	52
3.2. Conformational Stability of pR	53
3.3. Colloidal Stability of a Membrane Protein	54
3.4. Materials and Methods	55
3.4.1. Chemical and Reagents	55
3.4.2. pR Purification of pR Wild Type and Slow Cycle Mutant	56
3.4.3. Photocycling Proteorhodopsin in Solution	58
3.4.4. Photocycling Proteorhodopsin on the Stationary Phase	58
3.4.5. Sodium Dodecyl Sulfate Polyacrylamide Gel Electrophoresis (SDS-Page)	59
3.4.6. Size Exclusion Chromatography (SEC)	59
3.4.7. Bicinchoninic Acid (BCA)	60
3.4.8. Column Preparation	60
3.4.9. LC System	61
3.4.10. Small Scale SIC Instrument	62
3.4.11. Dye Absorption Method	62
3.4.12. Measuring Conformational Changes in pR	63
3.5. Results and Discussion	
3.5.1. SEC Results of the First pR Batch	63
3.5.2. Photocycling of Proteorhodopsin Immobilized on the Stationary Phase	65
3.5.3. Photocycling of Proteorhodopsin in the Mobile Phase	66
3.5.4. Concentration Dependence of Detergent	69
3.5.5. Effects of pH	70
3.5.6. Effects of Salt	73
3.5.7. Denaturing pR with SDS	75
3.5.8. Conformational Stability of pR	78
3.5.9. Measuring B for Mixed Detergent Systems	81
3.5.10. Detecting Detergent Micelles	83
3.6. Conclusion	87
3.7. References	88
4. Small Scale SIC	
4.1. Introduction	95
4.2. Methods and Materials	95

4.2.1. Reagents and Chemicals	96
4.2.2. Column Preparation	96
4.2.3. Column Construction	97
4.2.4. Measuring Protein Concentration by BCA	97
4.2.5. Conventional Scale LC	97
4.2.6. Small Scale LC	98
4.3. Results and Discussion	
4.3.1. Effects of Flowrate on B	99
4.3.2. Column Length	101
4.3.3. Effects of Flowrate on $V_0$	104
4.3.4. Effects of Injection Volume	106
4.3.5. Miniaturized SIC Column	108
4.4. Conclusion	108
4.5. References	110
5. OMPX and Photosynthetic Reaction Center	
5.1. Introduction.	111
5.2. Materials and Methods	
5.2.2. Chemical and Reagents	115
5.2.3. Column Preparation	116
5.2.4. Column Preparation	117
5.2.5. Small Scale SIC	117
5.2.6. Bicinchoninic Acid (BCA)	119
5.3. Results and Discussion.	
5.3.1. Effects of $K_2HPO_4$	119
5.3.2. Effects of PEG	121
5.3.4. Effects of Glycerol	124
5.3.5. Effects of Crystallization Co-solvent	126
5.3.6. Effects of Glycerol vs $E_8C_4$	128
5.4. Conclusion	130
5.5. Reference	130
6. Developing Microchip SIC	
6.1. Introduction.	135
6.2. Designing the Microchip SIC	135
6.3. Alternate Stationary Phase	136
6.4. Measuring Pore Size Distribution	137
6.5. Materials and Methods	
6.5.1. Chemicals and Reagents	138
6.5.2. Microchip Fabrication (Thermoset Polyester)	138
6.5.3. Polymerizing the Monolithic Stationary Phase	139
6.5.4. ISEC	140
6.5.5. BCA	140
6.6. Data and Discussion	140
6.6.1. Prototype of the SIC Microchip	141
6.6.2. Methacrylate Based Stationary Phase	142

6.6.3. ISEC of the Methacrylate Polymer	144
6.6.4. ISEC with Dextran Standards	145
6.6.5. Reproducibility of the Polymer	148
6.6.6. On Column Immobilization of Lysozyme	151
6.6.7. Monolithic SIC	153
6.7. Conclusions	155
6.8. Reference	155
7. Dissertation Summary	
7.1. Summary	158
7.2. Future Work	160
APPENDIX 1: RESEARCH PROPOSAL	163

## List of Figures

Figure		Page
1.1.	Helfritz Type Osmometer <sup>13</sup>	4
1.2.	B values for proteins measured by SLS in solvent/co-solvent conditions that promote protein crystallization. <sup>23</sup>	6
1.3.	A plot of lysozyme solubility vs B for different solvent/co-solvent conditions. <sup>15</sup>	7
1.4.	The amount of surface area of a particle available for protein immobilization.	10
1.5.	The empirical correlation between MW of protein and the corresponding molecular volume of the protein in solution.	12
2.1.	The effects of salt concentration on the SIC retention time, 0 M (Black), 0.5 M (Blue), 1 M (Red). Experimental conditions: pH 9, 20 mM sodium carbonate, injection volume 10 $\mu$ l, flow rate 0.1 mL/min.	29
2.2.	The effect of pH on solubility (RED) and B (BLUE) for enfuvirtide. Experimental conditions for SIC: All buffers contained 20 mM sodium carbonate, pH was adjusted with sodium chloride or hydrochloric acid, injection volume 10 $\mu$ l, flow rate 0.5 mL/min.	31
2.3.	Salt dependence of B and the weight-averaged molecular weight of enfuvirtide. Experimental conditions: Buffers contained 20 mM sodium carbonate, injection volume 10 $\mu$ l, flow rate 0.5 mL/min, pH 9.	34
2.4.	Effects of sodium citrate and ammonium sulfate on B. (Experimental conditions: All buffers contained pH 9, 20 mM sodium carbonate, injection volume 10 $\mu$ l, flow rate 0.5 mL/min)	36
2.5.	Effect of peptide concentration on the B values of enfuvirtide. (Experimental conditions: Buffers contained pH 8, 20 mM sodium carbonate, injection volume 10 $\mu$ l, flow rate 0.5 mL/min).	38

2.6.	The effects of increasing the NaCl concentration from 0 to 0.20 M at pH 3, 5, and 7 on LB-005 virial coefficients. Instrument Settings: Mobile Phase: 10 mM K <sub>2</sub> HPO <sub>4</sub> , Flow Rate = 0.1 mL/min, injection volume 1 μL, wavelength 280nm	40
2.7.	The change in B as an effect of sucrose, glycine and trehalose. Instrumental Settings: 10 mM K <sub>2</sub> HPO <sub>4</sub> , pH 7, flowrate= 0.1 mL/min, injection volume 1 μL, wavelength 280 nm.	42
2.8.	Comparing B for LB-005 to LB-007 at pH 5, 6 and 7. Instrumental settings: Mobile phase: 10mM potassium phosphate, flow rate: 0.1 mL/min, injection volume 10 μL, wavelength 280nm.	43
2.9.	The effects of increasing NaCl concentration from 0 to 1 M at pH7 of LB-007. Instrumental settings: Mobile Phase: 10 mM K <sub>2</sub> HPO <sub>4</sub> , flowrate =0.1 mL/min, injection volume 10 μL, wavelength 280 nm	44
3.1.1.	pR injected on to SEC column to determine sample purity. Experimental Conditions: Mobile phase was composed of 0.1 M Na <sub>2</sub> HPO <sub>4</sub> at pH 7.3, injector volume 10uL, flowrate of 1 mL/min and wavelength set to 280 and 500nm.	64
3.1.2.	SDS Page Gel using a Novex 4-12% Bis –Tris Gel w/MES of dialyzed wild type pR. Wild type pR in lane 1 is 1 μL wild type pR and lane 2 is 1:10 dilution of wild type pR with deionized water. Lane 3 is the mW standard measured in kDa.	65
3.1.3.	Photocycling of proteorhodopsin in solution at pH 12 and pH 7. Buffer conditions 20mM TRIS, 0.03% DMS.	67
3.1.4.	Photocycling immobilization of pR at pH 7 and pH 12. Buffer conditions 20 mM MES in 0.1% DDM.	68
3.1.5.	Measuring the change in magnitude and direction of B with increasing % of DDM. SIC conditions: Mobile phase: 20 mM MES, pH 7, flow rate: 0.1 mL/min, injection volume 1 μL, wavelength 520 nm.	70
3.1.6.	B was measured for mutant pR (A) and wild type pR (B) at various pH and detergent concentration using SIC Instrumental conditions: Mobile phase: 20mM TRIS, flow rate: 0.1 mL/min, injection volume 1 μL, wavelength 520nm.	72

3.1.7.	B measurements for mutant (A) and wild-type pR (B) at various concentrations of NaCl and K <sub>2</sub> HPO <sub>4</sub> using SIC. Instrumental conditions: mobile phase pH 9, 20 mM MES, flow rate 0.1 mL/min, injection volume 1 μL, wavelength 520 nm.	74
3.1.8.	pR in its native conformation absorbs at 280 nm and 531 nm in pH 7, 20 mM MES, 0.05% DDM (A). As the concentration of SDS increases from 0 to 10mM, pR loses its native conformation by the change in color.	76
3.1.9.	The spectrum of PR denaturing (A) and trending the absorbance of 531 and 387 nm (B) in pH 7, 20 mM MES, 0.05% DDM (A).	77
3.1.10.	Conformational Stability of pR measured by changes of the retinal absorbance at 531 nm, (A) DDM vs tween 20, DDM vs Chaps (B) and Chaps vs tween 20 (C) in pH 7 and 20 mM MES.	80
3.1.11.	Colloidal Stability of pR measured by changes in B, (A) DDM vs tween 20, (B) DDM vs Chaps and (C) Chaps vs Tween 20 in pH 7 and 20 mM MES.	82
3.1.12.	Evans Blue shift in wavelength maximum caused by the presence of the micelles at pH 7, 20 mM MES.	84
3.1.13.	Shifts in wavelength caused by formation of Micelles, (A) DDM vs Tween 20, (B) DDM vs Chaps and (C) Chaps vs Tween 20 in pH 7 and 20 mM MES.	86
4.1.1.	Example of chromatogram collected off of the small scale SIC, black line is UV data of acetone and OmpX, red line is 2 <sup>nd</sup> derivate of the signal from injector, negative line indicates sample injection.	99
4.1.2.	Effects of flowrate and NaCl Concentration of B. Experimental Conditions: column length 33cm. Buffer conditions pH 4.5, 0.1M acetic acid, injection volume 10μL and detector 280 nm.	101
4.1.3.	Effects of decreasing column length on B. Experimental conditions: flow rate: 0.1 mL/min. Buffer conditions pH 4.5, NaCl 0, 0.5 and 1 M, 0.1M acetic acid, injection volume 10 μL, detector 280 nm.	103
4.1.4.	Effects of flow rate and column length on V <sub>o</sub> . Experimental	105

conditions: pH 4.5, 0.1 M acetic acid, injection volume 10  $\mu\text{L}$ , wavelength 280 nm.

- 4.1.5. Effects of increasing injection volume on B (A) and chromatograms (B) Experimental conditions: flow rate: 0.1 mL/min. Buffer conditions pH 4.5, 0.1M acetic acid, detector 280 nm. 107
- 4.1.6. Chromatograms of lysozyme with increasing NaCl, Small Scale SIC column. Instrumental settings: Mobile phase 0.1 M acetic acid, pH 7, injection volume 0.5  $\mu\text{L}$ , wavelength 280 nm. 109
- 5.1.1. RHO crystallized by sitting drop setup at room temperature in the following buffer conditions, 3.5% heptano-1,2,3-triol, 0.1% lauryl dimethylamine oxide, 2.0% dioxane, and 0.75 M potassium phosphate (pH 7.4).<sup>5</sup> 112
- 5.1.2. The structure of OmpX from *Escherichia coli*, crystallized in 30% (v/v) 2-propanol, 20% (v/v) glycerol, 0.2 M  $\text{CaCl}_2$  and 0.1 M sodium acetate, pH 4.6 114
- 5.1.3. RHO immobilized on amino particles after washing with coupling buffer. Coupling buffer contained 0.02 M MES, 6% LDAO at pH 6. 118
- 5.1.4. The effects of different  $\text{K}_2\text{HPO}_4$  concentrations (0 to 0.8 M) on the B values (A) and peak symmetry (B) on RHO. Buffer conditions: pH 6, 0.02 M MES and 6% LDAO Instrumental Settings flow rate: 60  $\mu\text{L}/\text{min}$ , injection volume 0.5  $\mu\text{L}$ , wavelength 280nm. 120
- 5.1.5. RHO at different PEG concentrations, 0% (Black) and 12% (Red) measured by small scale by SIC. Instrumental settings: Mobile phase: 10mM TRIS, flow rate: 60  $\mu\text{L}/\text{min}$ , injection volume 0.5  $\mu\text{L}$ , wavelength 280nm. 122
- 5.1.6. The effects of different PEG concentrations (0 to 30% w/v) at pH 8.5. 0.5%  $\text{C}_8\text{E}_4$ , 20 mM TRIS-HCl, 20mM NaCl. Experimental Condition: Flow rate 25  $\mu\text{L}/\text{min}$ , injection volume 0.5  $\mu\text{L}$ , wavelength 280 nm. 123
- 5.1.7. Effects of different glycerol concentrations on OMPX at 0 to 30% at pH 4.5, 0.1M sodium acetate, 0.2 mM  $\text{CaCl}_2$ . Figure A shows chromatograms of OmpX vs glycerol 0% (Black), 10% (Red) and 20% (Blue). Experimental Condition: Flow rate 25  $\mu\text{L}/\text{min}$ , injection volume 0.5  $\mu\text{L}$ , wavelength 280 nm. 125

5.1.8.	The effects of different 2-propanol (B) (0 to 30%) and sodium acetate (A) (0.05 to 0.3 M) at pH 4.6, 20% Glycerol, 200 mM CaCl <sub>2</sub> , 100mM sodium acetate. Experimental Condition: Flow rate 25 μL/min, injection volume 0.5 μL, wavelength 280 nm.	127
5.1.9.	The effects of different concentration glycerol and E <sub>8</sub> C <sub>4</sub> at pH 4.6, 20% Glycerol, 200 mM CaCl <sub>2</sub> , 100mM sodium acetate. Experimental Condition: Flow rate 25 μL/min, Injection Volume 0.5 μL, wavelength 280 nm.	129
6.1.1.	A prototype the TEP Microchip SIC, the fittings attached on the chip by glue.	142
6.1.2.	SEM images take of monolithic column with increasing DOOH concentrations, 35% DOOH (A), 40% DOOH (B)	143
6.1.3.	Figure 6.1.3. Trending the change in polystyrene probes of increasing molecular weight. Instrumental settings: Mobile phase THF, 0.1 mL/min, injection volume 5 μL, detector set at 280 nm.	145
6.1.4.	Figure 6.1.4. Trending the change in Dextran probes of increasing molecular weight. Instrumental settings: Mobile phase 120 mM NaCl, 6mM Na <sub>2</sub> HPO <sub>4</sub> , pH 7 Flowrate: 0.030 mL/min, injection volume 0.5 μL, RI detector.	147
6.1.5.	SEM images take of two monolithic columns formed from the sample polymer mixture.	149
6.1.6.	Figure 6.1.6. Measured the reproducibility of the monolithic column with the same DOOH concentration by ISEC. Instrumental settings: Mobile phase 120 mM NaCl, 6mM Na <sub>2</sub> HPO <sub>4</sub> , pH 7, flowrate 0.030 mL/min, injection volume 0.5 μL, RI detector.	150
6.1.7.	Figure 6.1.7. Trending the change in absorbance of lysozyme in the mobile phase during on column immobilization of a monolithic column. Image A shows a control and live column after protein immobilization. Data showing online coupling of lysozyme (A) and (B)	152

6.1.8. The effects of increasing NaCl concentration from 0 to 1 M at pH 154  
4.5 of lysozyme. Instrumental settings: Mobile Phase: 0.1. M  
Acetic acid, pH 4.5, flowrate =0.01 mL/min, injection volume 0.5  
 $\mu$ L, wavelength 280 nm

## 1. Introduction

**1. Introduction.** Biopolymers such as proteins and peptides are increasingly taking the place of small molecules in manufacturing and therapeutic agents.<sup>1-4</sup> The advantage of using biopolymers over small molecules for therapeutic applications include high activity, high specificity and low toxicity.<sup>5,6</sup> The disadvantages of using biopolymers include challenges associated with large scale production, chemical instability and physical degradation.<sup>5,7</sup> A biopolymer, such as a protein, that shows promise for a specific application will not advance past early stage development if the protein lacks either chemical or physical stability. Of these two parameters, physical stability is often harder to predict and/or measure, because it is not tied to the presence of a single or small group of amino acids.<sup>8</sup> The physical stability of proteins and peptides can be improved by site-directed mutagenesis, glycosylation, post-translational modification and adjusting the solvent/co-solvent systems with the latter being the most common.<sup>2,3,5,9</sup> Quantitatively measuring the change in the colloidal stability of a protein in different solvent/co-solvent system could increase the number of early stage proteins that advance to the commercial scale. The current methods used to measure the colloidal stability of proteins are not practical for large screening studies, due to the high quantity of protein consumed and low sample throughput.

This work is focused on refining Self-Interaction Chromatography (SIC), a

technique that can be used to measure B and therefore the colloidal stability of proteins. SIC is attractive compared to existing methods because it has a low sample consumption, increased sample throughput and decreased method variability. Refining the SIC technique has made it possible to quantitatively trend the colloidal stability of proteins in large screening studies. Sample consumption was decreased by scaling down the SIC method, requiring new developments in instrumentation and new software. B values for a therapeutic peptide were measured and developed a new stationary phase was developed for microchip SIC. Additionally, I have also extended studies to membrane proteins, which are a particularly unstable class of biopolymers.

**1.1. Chemical and Physical Degradation.** The amino acid sequence and the resulting folded structure determines the physical and chemical characteristics of a protein. A protein can be degraded chemically or physically during production and/or downstream processing, altering its activity, specificity and toxicity. Chemical degradation occurs when a covalent bond is either formed or cleaved resulting in a change in the chemical structure.<sup>5,9</sup> Examples of chemical degradation in proteins include hydrolysis, oxidation and deamidation.<sup>5</sup> The physical stability of a protein, both conformational and colloidal is dependent on the chemical stability, as chemical modification can lead to physical instability.<sup>5,9</sup> Physical stability describes the colloidal stability of the protein in solution, which includes aggregation, precipitation and solubility.<sup>5,9</sup> Colloidal stability of a protein in solution can be described by protein-protein interactions, which can be difficult

to measure for proteins.<sup>10,11</sup> For many proteins colloidal stability is a problem resulting in financial loss due to low production yields, toxicity issues with therapeutic agents and low activity for manufacturing.<sup>1-3,6,12</sup>

**1.2. Osmotic Second Virial Coefficient (B).** Protein-protein self-interaction can be described by the osmotic second virial coefficient (B), a dilute solution parameter. B was originally used as a thermodynamic property to describe the direction and magnitude of two body interactions in solution.<sup>13</sup> B was correlated empirically to protein crystal growth by George W. Wilson, and later to solubility.<sup>2,10,14-18</sup> Historically B was determined by membrane osmometry, which measures the difference in osmotic pressure between the sample and a reference at equilibrium, Figure 1.1.<sup>13</sup> An ideal solution occurs when repulsive and attractive interactions are equal in solution. When a sample deviates from the ideal solution, Van't Hoff's equation is expanded using the second virial coefficient (B), Equation 1.<sup>13</sup>

$$\Pi = RTc \left( \frac{1}{M_w} + Bc + \dots \right) \quad 1.$$

In Equation 1,  $\pi$  is osmotic pressure, c is concentration (in mass units) of the solute, R is universal gas constant 8.3145 J/mol\*K, T is absolute temperature and  $M_w$  is molecular weight. On a molecular level, when osmotic second coefficient (B) is positive, repulsive conditions dominate leading to an increase in protein solubility. A negative B indicates attractive interactions are dominating, leading to results ranging from crystallization to precipitation.<sup>9,17,19</sup>

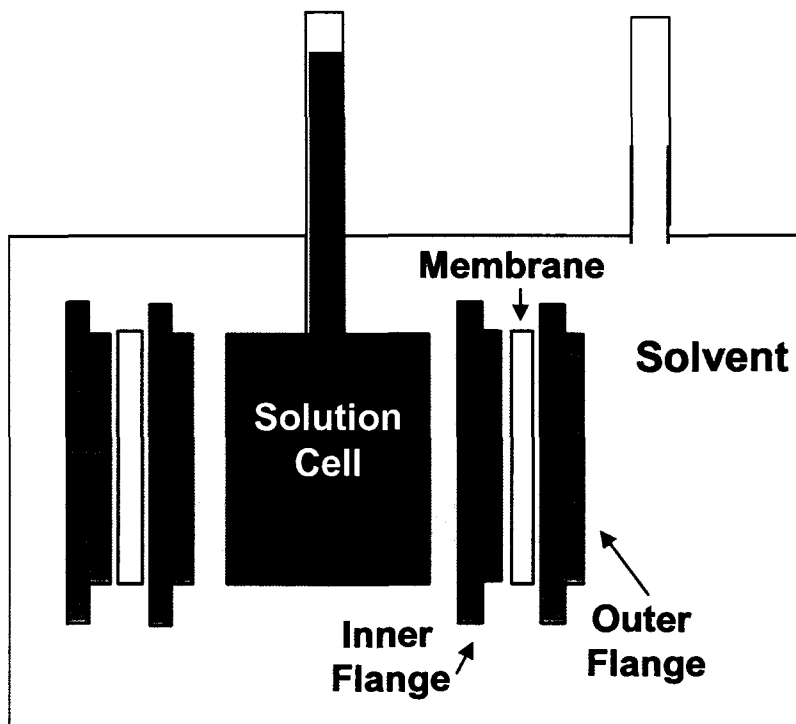


Figure 1.1. Helfritz Type Osmometer.<sup>13</sup>

Using McMillian and Mayers theory, which treats the solvent as a homogenous background,  $B$  can be related to the potential mean force (PMF) of a two-body interaction, Equation 2.<sup>11,13</sup>

$$B = \left( \frac{-2\pi}{M_w} \right) \int_0^{\infty} (e^{-W/kT} - 1) r_{12}^2 dr_{12} \quad 2.$$

In equation 2,  $W$  is the interaction between two proteins in solutions,  $k$  is the Boltzmann constant and  $r_{12}$  is the intermolecular center-to-center distance between the center of two bodies.<sup>11,13</sup> PMF is the sum of all forces between two bodies in a solvent, including excluded volume, charge-charge, charge-dipole, dipole-dipole, dipole-induced-dipole interactions, Van der Waals interactions and

the hydrophobic effect.<sup>11,13</sup> Changes in B caused by different solvent/co-solvent systems can be therefore attributed to changes in PMF. The excluded volume of the protein is defined as a sphere in Equation 2 and has positive contribution to B.<sup>11,13</sup> Flory and others have shown a molecular weight dependence on B, where the magnitude of B is affected by molecular weight.<sup>13,20,21</sup>

**1.2.1. Relationship between B and Protein Crystallization.** B was utilized for determining buffer conditions that favored protein crystallization in an effort to develop a pre-screening method.<sup>14,15, 22</sup> The reason for using B was to develop a quantitative method for choosing buffer conditions that yielded x-ray quality protein crystals.<sup>10</sup> Wilson was the first to make the connection between protein crystallization and B by static light scattering (SLS) for buffer conditions that promoted protein crystallization, Figure 1.2.<sup>10,14,15</sup> The work showed empirically that proteins crystallized between  $-2 \times 10^{-4}$  to  $-8 \times 10^{-4}$  mol mL g<sup>-2</sup>, now referred to as

the crystallization slot ,Figure 1.2.<sup>10,14,15</sup> The magnitude and direction of B for the crystallization slot corresponds to weak attractive two body interactions. These weak protein interactions allow for the correct orientation of a protein in the crystal without aggregation. The crystallization slot also applies to membrane protein crystallization as established by Dr. Loll.<sup>7, 24</sup> Using B as parameter screen for buffer conditions that favor crystallization for soluble proteins is now widely accepted.

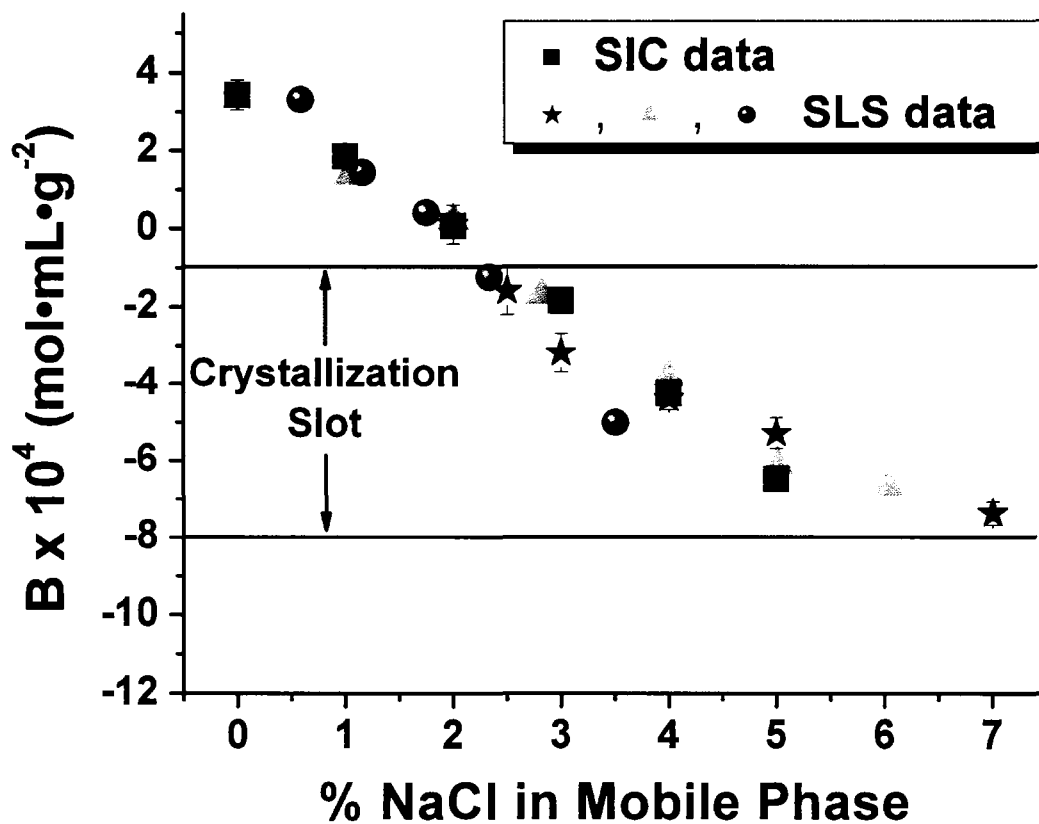


Figure 1.2. B values for proteins measured by SLS in solvent/co-solvent conditions that promote protein crystallization.<sup>23</sup>

**1.2.2. Relationship between B and Solubility.** When B values are above the crystallization slot, protein-solvent interactions are favored. This corresponds to repulsive protein-protein interactions dominating, causing an increase in colloidal stability and protein solubility.<sup>17</sup> The correlation between B and protein solubility has been observed for a number of model proteins.<sup>10,14,15</sup> As shown in Figure 1.3, as the solubility of lysozyme increases, B increases. Additionally, Wilson

derived based on static mechanics between B and solubility, Equation 4.

$$B = \frac{-\Delta\mu_2}{RT} \frac{1}{2M_2S} - \frac{\ln s}{2M_2S} \quad 4.$$

In Equation 4, R is the gas constant 8.3145 J/mol\*K, T is temperature and  $M_2$  is the molecular weight of the protein. The solubility of the protein is defined as s value in g/mL. The value  $\Delta\mu_2$  is the difference in chemical potential of the protein in solution and chemical potential of the protein in crystal lattice.<sup>15</sup> While, equation 4 is important, it is not practical because many proteins and peptides not been crystallized.

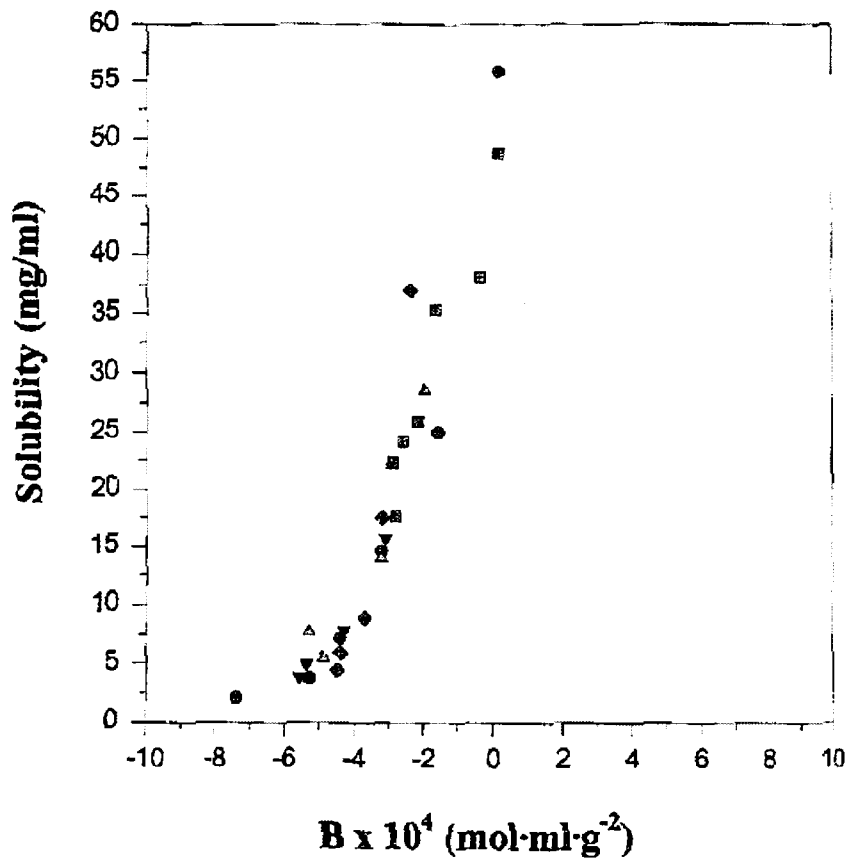


Figure 1.3. A plot of lysozyme solubility vs B for different solvent/cosolvent have conditions.<sup>15</sup>

By using the relationship between  $B$  and solubility, screening studies have measured changes in protein-protein interactions, which correlate to changes in protein solubility for a number of proteins.<sup>2, 3, 17, 18</sup> The use of  $B$  as a parameter to screen for maximizing colloidal stability of proteins has not been accepted. The reason for this is the lack solubility data and  $B$  measurements for additional proteins.

**1.3. Static Light Scattering (SLS).** Currently SLS is the preferred method to measure  $B$  for polymers and proteins.<sup>14, 16</sup> SLS measures  $B$  and other static parameters such as average molecular weight of a polymer by measuring the intensity of scattered light, Figure 1.3.<sup>23</sup> SLS is not practical for high throughput screening for proteins because of the large amount of protein (milligrams) required for a measurement, lengthy analysis times (hours), low throughput, scattering caused by co-solvents resulting in an increase in noise, and a minimum size requirement for the analyte.<sup>23</sup> The scattering caused by the addition of co-solvents such as detergents above the critical micelle concentration (CMC) and polyethylene glycol (PEG) has limited measurement of  $B$  to soluble proteins. Analytical ultracentrifugation and membrane osmometry have also been used to measure  $B$ , but suffer limitations similar to those of SLS.<sup>2</sup> An alternative method is needed to measure changes in  $B$  using less than 1 mg of protein, if  $B$  is to become widely accepted as an important measure of protein stability.

**1.4. Self-Interaction Chromatography for Soluble Proteins.** Self-Interaction

Chromatography (SIC) is a relatively new method for measuring B, which consumes magnitudes less protein than SLS, high throughput, no increase in chemical noise caused by the addition of cosolvent such as PEG/detergent, increased analyte size range and the use of multiple co-solvents.<sup>25</sup> SIC is a modified form of affinity chromatography where the protein is immobilized on the stationary phase and injected as the analyte.<sup>2,3,25</sup> Changes in protein-protein interactions are measured by changes in retention time and reflect changes in the colloidal stability of the protein.<sup>25</sup> Protein-protein self-interaction is mediated by a combination of the composition of the mobile phase and the protein's chemistry. SIC uses traditional high performance liquid chromatography (HPLC) instrumentation, which allows for automation, high throughput analysis and low sample consumption. The injected protein experiences attractive and repulsive interactions as it passes over the immobilized protein, which is reflected by changes in retention time. The retention time of the protein can be related to B by Equation 5.<sup>25</sup>

$$B_{22} = \left( \frac{N_A}{M^2} \right) \left( B_{HS} - \frac{k'}{\rho\phi} \right) \quad 5.$$

In Equation 5,  $N_A$  is Avogadro's number,  $M$  is the molecular weight of the protein,  $B_{HS}$  is the hard sphere (or excluded volume) contribution,  $\rho$  is the number of protein molecules per unit surface area,  $\phi$  is the phase ratio or the available surface area per stationary phase volume, and  $k'$  is the capacity (or retention) factor. The amount of protein immobilized on the surface and the available surface area of the particle, is used to calculate  $\rho$ , while  $\phi$  is determined by

Inverse Size Exclusion Chromatography (ISEC), Figure 1.4.<sup>25, 26</sup> The capacity factor,  $k'$  is given by Equation 6, where  $t_r$  is the retention time of protein and  $t_m$  is the retention time adjusted for size difference between the protein and acetone.

$$k' = \frac{t_r - t_m}{t_m} \quad 6.$$

The non-retained time,  $t_m$  is calculated by measuring the retention time of the protein and acetone on a column that contains no immobilized protein (referred

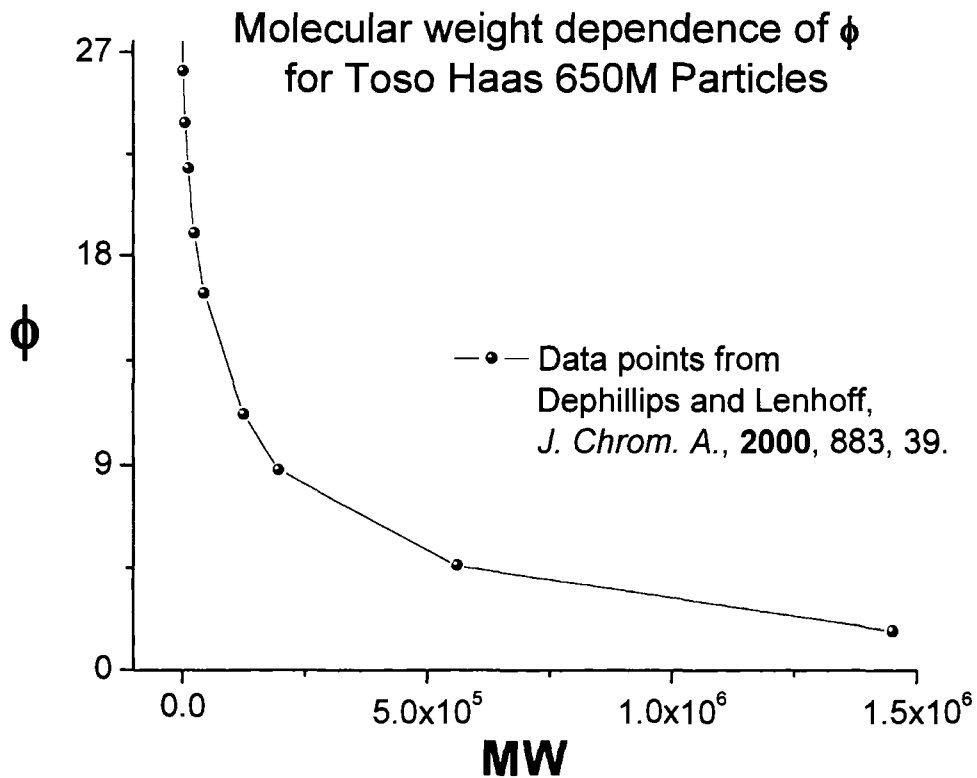


Figure 1.4. The amount of surface area of a particle available for protein immobilization.

to as a dead column).  $t_m$  is calculated from the ratio of the retention time of the protein ( $t_{\text{pro\_dead}}$ ) and acetone ( $t_{\text{ace\_dead}}$ ) measured on a dead column ( $t_{\text{pro\_dead}}/t_{\text{ace\_dead}}$ ) and multiplied by retention time of acetone ( $t_{\text{ace}}$ ) measured on a live column.<sup>25</sup> Measuring B for proteins in solution using SIC allows for the correlation of the effects of different solvent/co-solvent conditions in systems with SLS.

The excluded volume is determined from three different methods. If the protein has been crystallized or imaged by NMR, the excluded volume is determined by averaging the three axes to calculate a radius, which is then used to determine the excluded volume. Alternatively, dynamic light scattering (DLS) can be used to determine the excluded volume of the protein. Lastly, the molecular weight of the protein can be used to determine the spherical volume, Figure 1.5. From Equation 7, the excluded volume of a protein is calculated based on hard sphere geometry.

$$B_{HS} = 4V_m = 2/3\pi d^3 \quad 7.$$

$B_{HS}$  is the hard sphere (or excluded volume) contribution,  $V_M$  molecular volume and  $d$  is diameter of the protein.<sup>27</sup>

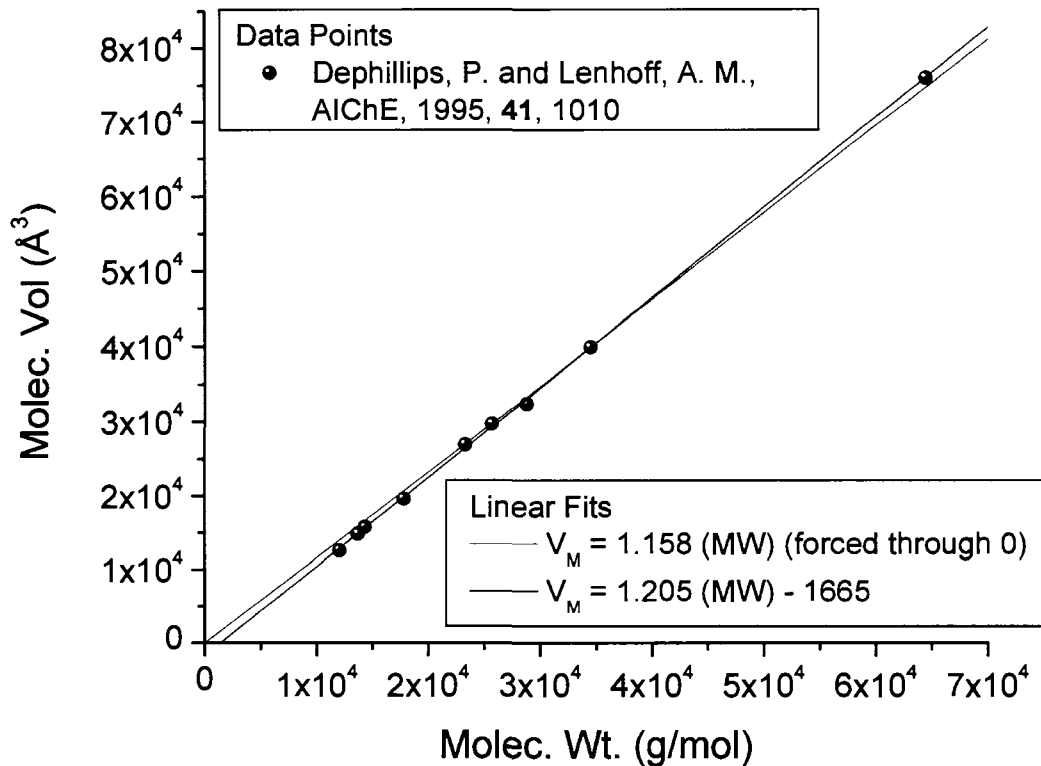


Figure 1.5. The empirical correlation between MW of protein and the corresponding molecular volume of the protein in solution.

**1.4.1 SIC for Membrane Proteins.** Typically membrane proteins are solubilized in aqueous solution for purpose of recovery and purification. When detergent is added at concentrations greater than the CMC to membrane proteins in an aqueous solution, a PDC is created where the hydrophobic tail of the detergent associates with hydrophobic area of the membrane protein. The addition of the detergent normally results in an increase in the excluded volume of the membrane.<sup>28</sup> The excluded volume term used to calculate B is changed to reflect

the size of the PDC, equation 8.

$$B = \left( \frac{NA}{M^2} \right) \left( B^{PDC} - \frac{k'}{\rho\phi} \right) \quad 8.$$

The difference in Equation 8 compared to Equation 2 is  $B^{PDC}$  the hard sphere (or excluded volume) contribution of the PDC.<sup>29</sup>

**1.5. Dissertation Summary.** Here, advancements in refining SIC for the measurement of B for proteins and peptides are presented. In the first example, the colloidal stability of two therapeutic proteins and a peptide were measured as function of salt and pH. Additionally, for the first time, B was measured for a wild type LB-005 and mutant LB-007 protein with increasing pH. SIC was able to detect changes in the colloidal stability of wild type and mutant protein, which differed in amino acid composition by only 3 residues. In the second example, a membrane protein, proteorhodopsin (pR), was used to measure the changes in B with increasing concentrations of detergent, PEG, varying solvent pH and mixed detergents system. The continual improvements in the SIC method have allowed for measurement of B of two additional membrane proteins, rhodobacter sphaeroides (RHO) and OmpX. Both membrane proteins were analyzed using less than 2 mg of protein. Finally, in an effort to reduce analysis time and protein consumption, monolithic columns were developed for SIC. The work presented in this document shows the broader use of SIC, for the measurement of colloidal stability of proteins and membrane proteins in solution.

## 1.6. References

1. Kumar, M., Silk-elastin protein polymer: A multifunctional active ingredient for skin care. *Journal of Cosmetic Science* **2005**, 56, (5), 352-353.
2. Payne, R. W.; Nayar, R.; Tarantino, R.; Del Terzo, S.; Moschera, J.; Di, J.; Heilman, D.; Bray, B.; Manning, M. C.; Henry, C. S., Second virial coefficient determination of a therapeutic peptide by self-interaction chromatography. *Biopolymers* **2006**, 84, (5), 527-533.
3. Valente, J. J.; Fryksdale, B. G.; Dale, D. A.; Gaertner, A. L.; Henry, C. S., Screening for physical stability of a *Pseudomonas* amylase using self-interaction chromatography. *Analytical Biochemistry* **2006**, 357, (1), 35-42.
4. Werner, R. G., Economic aspects of commercial manufacture of biopharmaceuticals. *Journal of Biotechnology* **2004**, 113, (1-3), 171-182.
5. Manning, M. C.; Patel, K.; Borchardt, R. T., Stability of Protein Pharmaceuticals. *Pharmaceutical Research* **1989**, 6, (11), 903-918.
6. Marx, V., Watching peptide drugs grow up. *Chemical & Engineering News* **2005**, 83, (11), 17-+.
7. Loll, P. J., Membrane protein structural biology: the high throughput challenge. *Journal of Structural Biology* **2003**, 142, (1), 144-153.
8. McNally, E. J., *Protein Formulation and Delivery*. AAI, INC.: Wilmington, North Carolina, 1999; Vol. 99.
9. Chi, E. Y.; Krishnan, S.; Randolph, T. W.; Carpenter, J. F., Physical stability of proteins in aqueous solution: Mechanism and driving forces in

- nonnative protein aggregation. *Pharmaceutical Research* **2003**, 20, (9), 1325-1336.
10. Wilson, W. W., Predicting Protein Crystallization from a Solution Property. *Acta Cryst.* **1994**, D50, 361-365.
  11. Neal, B. L.; Asthagiri, D.; Velev, O. D.; Lenhoff, A. M.; Kaler, E. W., Why is the osmotic second virial coefficient related to protein crystallization? *Journal of Crystal Growth* **1999**, 196, (2-4), 377-387.
  12. Wiener, M. C.; Snook, C. F., The development of membrane protein crystallization screens based upon detergent solution properties. *Journal of Crystal Growth* **2001**, 232, (1-4), 426-431.
  13. Sun, S. F., *Physical Chemistry of Macromolecules Basic Principles and Issues*. Second Edition ed.; John Wiley & Sons, Inc.: Hoboken, 2004; p 549.
  14. George, a.; Chiang, Y.; Guo, B.; Arabshahi, A.; Cai, Z.; Wilson, W. W., Second virial coefficient as predictor in protein crystal growth. *Macromolecular Crystallography, Pt A* **1997**, 276, 100-110.
  15. Guo, B.; Kao, S.; McDonald, H.; Asanov, A.; Combs, L. L.; Wilson, W. W., Correlation of second virial coefficients and solubilities useful in protein crystal growth. *Journal of Crystal Growth* **1999**, 196, (2-4), 424-433.
  16. Haas, C.; Drenth, J.; Wilson, W. W., Relation between the solubility of proteins in aqueous solutions and the second virial coefficient of the solution. *Journal of Physical Chemistry B* **1999**, 103, (14), 2808-2811.

17. Valente, J. J.; Payne, R. W.; Manning, M. C.; Wilson, W. W.; Henry, C. S., Colloidal behavior of proteins: Effects of the second virial coefficient on solubility, crystallization and aggregation of proteins in aqueous solution. *Current Pharmaceutical Biotechnology* **2005**, 6, (6), 427-436.
18. Valente, J. J.; Verma, K. S.; Manning, M. C.; Wilson, W. W.; Henry, C. S., Second virial coefficient studies of cosolvent-induced protein self-interaction. *Biophysical Journal* **2005**, 89, (6), 4211-4218.
19. Ho, J. G. S.; Middelberg, A. P. J.; Ramage, P.; Kocher, H. P., The likelihood of aggregation during protein renaturation can be assessed using the second virial coefficient. *Protein Science* **2003**, 12, (4), 708-716.
20. Krigbaum, W. R.; Flory, P. J., Statistical Mechanics of Dilute Polymer Solutions.4. Variation of the Osmotic 2<sup>nd</sup> Coefficient with Molecular Weight. *Journal of the American Chemical Society* **1953**, 75, (8), 1775-1784.
21. Miyaki, Y.; Einaga, Y.; Fujita, H., Excluded-Volume Effects in Dilute Polymer-Solutions.7. Very High Molecular-Weight Polystyrene in Benzene and Cyclohexane. *Macromolecules* **1978**, 11, (6), 1180-1186.
22. George, a.; Wilson, W. W., Predicting Protein Crystallization from a Dilute-Solution Property. *Acta Crystallographica Section D-Biological Crystallography* **1994**, 50, 361-365.
23. Wilson, W. W., Light scattering as a diagnostic for protein crystal growth - A practical approach. *Journal of Structural Biology* **2003**, 142, (1), 56-65.

24. Loll, P. J.; Hitscherich, C.; Aseyev, V.; Allaman, M.; Wiencek, J., Assessing micellar interaction and growth in detergent solutions used to crystallize integral membrane proteins. *Crystal Growth & Design* **2002**, *2*, (6), 533-539.
25. Tessier, P. M.; Lenhoff, A. M.; Sandler, S. I., Rapid measurement of protein osmotic second virial coefficients by self-interaction chromatography. *Biophysical Journal* **2002**, *82*, (3), 1620-1631.
26. DePhillips, P.; Lenhoff, a. M., Pore size distributions of cation-exchange adsorbents determined by inverse size-exclusion chromatography. *Journal of Chromatography A* **2000**, *883*, (1-2), 39-54.
27. Neal, B. L.; Lenhoff, a. M., Excluded-Volume Contribution to the Osmotic 2Nd Virial-Coefficient for Proteins. *Aiche Journal* **1995**, *41*, (4), 1010-1014.
28. Berger, B. W.; Gendron, C. M.; Lenhoff, A. M.; Kaler, E. W., Effects of additives on surfactant phase behavior relevant to bacteriorhodopsin crystallization. *Protein Science* **2006**, *15*, (12), 2682-2696.
29. Hitscherich, C.; Kaplan, J.; Allaman, M.; Wiencek, J.; Loll, P. J., Static light scattering studies of OmpF porin: Implications for integral membrane protein crystallization. *Protein Science* **2000**, *9*, (8), 1559-1566.

## 2. Therapeutic Agents

**2.1. Introduction.** In this chapter, the second virial coefficient ( $B$ ) was measured by SIC for two therapeutically important biomolecules, a peptide, enfuvirtide, and two single chain antibodies LB-005 and LB-007. SIC measurements for enfuvirtide and the antibodies required extensive method development that included new immobilization chemistries for SIC as well as optimization of the SIC method. These improvements allowed the first  $B$  values to be measured for a peptide. Conventional methods such as SLS do not have the ability to measure  $B$  of low molecular weight peptides, because of the lack of scattering caused by the peptide. Additionally, conventional methods are not practical to measure colloidal stability of mutants because of the large amount of protein consumed during analysis.

In the present work, SIC was used to measure  $B$  for enfuvirtide, a 36-amino acid therapeutic peptide with a molecular weight of 4.5 kDa, as a function of salt concentration, salt type and pH. Although it is well established that many peptides self-associate in aqueous solution, the ability to measure the extent of these interactions as a function of solution conditions remains elusive.<sup>1,2</sup> The physical parameter that best reflects the magnitude of self-interaction between macromolecules is  $B$ . There are a number of methods that can be used to determine  $B$ , including static light scattering (SLS), analytical ultracentrifugation, and membrane osmometry as discussed in Chapter 1.<sup>3-5</sup> These methods require

large amounts of material and can be quite time consuming. As a result, there has been little reported about B values for peptides. In fact, B values have been reported only once for a peptide by using dilution flow calorimetry.<sup>6</sup>

The ability to measure B as a function of solution conditions (pH, ionic strength, etc.) is critical for rationally controlling peptide behavior in aqueous solution. For example, it would be possible to increase the solubility of a given peptide by making B more positive (indicating more repulsive peptide-peptide interactions), as has been seen with a number of proteins.<sup>3,7,8</sup> In addition, there has been a growing need to develop peptide formulations at relatively high concentrations (> 100 mg/ml).<sup>9</sup> Higher concentrations allow for easier dosing and possible self-administration through subcutaneous injection. While this need has been most acute for monoclonal antibodies, there is a similar need for peptide therapeutics.

The second therapeutic agent analyzed was a single-chain (scFv) antibody fragment used to reduce the swelling and inflammation in joints caused by gout and arthritis. Currently there is no treatment for this problem, but it can be managed with nonsteroidal anti-inflammatory drugs such as ibuprofen. LB-005, a biological agent in early stage development has shown the ability to act as an anti-inflammatory. LB-005 is a fragment of an antibody, which contains parts of the heavy and light chain. The antibody-fragment has low solubility, on the scale of 0.5 mg/mL at pH 7. Therefore, the first approach was to adjust the solvent/co-solvent system to improve the colloidal stability of the protein in solution. The second approach was to modify the antibody by substituting two amino acids.

Thus new conditions were needed to achieve solubility above 10 mg/mL. B was used to measure changes in colloid stability of the antibody for both approaches.

The initially formulation screens focused on altering electrostatic interactions by adjusting pH and salt concentration. The formulation conditions were chosen based on the effects on the colloid stability of the protein; changing pH effects the electrostatic interactions. Additionally the concentration of a salt can increase or decrease the colloidal stability of the protein, by salting in and salting out the protein. Additional formulation screens examined the effects of sugars, which are excluded from the surface of the protein. The effects of changes in pH and salt on B have already been discussed in Chapter 1.

Enfuvirtide measurements were made for a variety of pH and ionic strength conditions and correlated with solubility and apparent molecular weight. This study demonstrates that it is possible to measure B for a peptide in a relatively rapid fashion, ultimately allowing one to screen formulations for those that will provide the greatest solubility. While the screening studies using B as the parameter for the antibody fragments provided quantitative data that allowed for the selection of a solvent/co-solvent system, which improved the solubility of LB-005 to be greater than 10 mg/mL. The SIC experiments on the mutant LB-007 showed the sensitivity of the method to detect changes in B related to changes in chemical composition of the protein. The data presented is the first time SIC has been used to screen a wild type and mutant of a protein to show different

magnitudes and trends in B. The data suggests that SIC can be used to screen mutant libraries for colloidal stability.

## **2.2. Materials and Methods**

**2.2.1. Chemicals and Reagents.** The following chemicals and materials were used as received for these experiments: potassium phosphate, hydrochloric acid, ethanolamine, sodium carbonate, sodium hydroxide, sodium chloride, sodium citrate, ammonium sulfate, sucrose, glycine and trehalose (Fisher).

Chromatography particles (Toyopearl AF-Tresyl-650M and Toyopearl AF-Amino-650M) were purchased from Supelco (Sigma-Aldrich). The coupling reagent (1-Ethyl-3-[3-dimethylaminopropyl]carbodiimide Hydrochloride) (EDC), N-hydroxysuccinimide (NHS), and the BCA colorimetric protein assay kit were purchased from Pierce. The capping reagent ethanolamine was purchased from (Aldrich). Enfuvirtide was supplied by Hoffmann-La Roche and used as received without further purification. Enfuvirtide has the sequence (CH<sub>3</sub>CO-YTSLIHSLIEESQNQQEKNEQELLELDKWASLWNWF-NH<sub>2</sub>). Legacy BioDesign LLC generously supplied the antibody fragments. All buffers were prepared using de-ionized water (18.1 Ω) purified using Milli-Q academic system.

**2.2.2. Enfuvirtide Sample Preparation.** Lyophilized enfuvirtide was dissolved in the experimental mobile phase in a 1.5 mL microcentrifuge tube. Enfuvirtide lowers the pH of the buffer so 0.5 M sodium hydroxide was used to adjust the pH to the desired value. Enfuvirtide samples were prepared daily.

**2.2.3. Enfuvirtide Column Preparation.** The preparation of the chromatography particles and peptide used 60 mM phosphate buffer (Sigma) adjusted to pH 7.5 with 1 M hydrochloric acid. In a clean 15 mL centrifuge tube, 0.3303 grams of tresyl particles were rinsed three times with 60 mM phosphate buffer. After each rinse the tube was centrifuged. 57 mg of enfuvirtide was weighed out and dissolved with 60 mM phosphate buffer to give a final concentration of 8 mg/mL. Enfuvirtide was then added to the washed tresyl particles. The mixture was agitated briefly and particles were allowed to settle. A 50  $\mu$ L sample was removed from the mixture, diluted to 600  $\mu$ L, and the absorbance measured at 280 nm to determine the initial peptide concentration. Measurements were performed to show that no measurable amount of peptide was immobilized during these first few seconds of particle/peptide contact (data not shown). After the first UV measurement, the peptide and particles were slowly mixed for 3 hours at room temperature (23°C). At the end of this time, a second UV measurement was performed following the same protocol as before to determine the amount of peptide remaining in solution and thereby indirectly the amount bound to the chromatography particles. After the final UV measurement, the mixture was rinsed with 60 mM phosphate buffer four times, 1 M ethanolamine (pH 8) was added, and the particles mixed overnight at room temperature. Ethanolamine was added to block the remaining unreactive groups. The remaining ethanolamine was removed by spinning down the particles in a microcentrifuge and discarding the supernatant. Finally, the particles were rinsed

four times with 60 mM phosphate buffer. The particles were stored in 60 mM phosphate buffer at 4° C before use and between runs. Coated particles were packed into a stainless steel 250 mm x 1 mm column and stored at 4° C when not in use. The stationary phase used for dead column experiments consisted of tresyl particles capped with ethanolamine. Packing consistency for both the live and dead columns were checked with acetone to verify that there were no significant voids present in the two columns (data not shown).

**2.2.4. Anti-Body Fragment Sequences.** The two mutants described in this study exhibit amino acid substitutions at two different sites and both have theoretical pI values near 7.8.<sup>10</sup> LB-005 differs from LB-007 by two amino acid substitutions of glycine to arginine at position 112 and phenylalanine to leucine at position 198.

**2.2.5. Anti-Body Fragment Sample Preparation.** LB-005 and LB-007 was thawed over night at 4°C and the liquid was clear when visually inspected. The pH of the LB-005 stock solution was adjusted to pH 5 using a Denver Instruments micro pH probe. LB-005 was concentrated using an Eppendorf mini spin plus and a protein concentrator with a 3 kDa membrane cutoff. 0.5 mL of the LB-005 was added to protein concentrator and centrifuged for eight minutes at 10,000 rpm. During the concentration process a UV spectrum was measured at 280 nm and 400 nm to monitor the protein concentration and the formation of aggregates.

**2.2.6. Anti-Body Fragment Column Preparation.** The preparation of the SIC stationary phase was identical for LB-005 and LB-007. The protein was dissolved in 0.1 M  $K_2HPO_4$  buffer (pH 7.5) adjusted with concentrated sodium hydroxide to the final pH. In a clean 1.5 mL eppendorf tube, 0.226 mL of AF-Amino-650M particles were rinsed three times with 0.1 M  $K_2HPO_4$  buffer (pH 7.5). After each rinsing, the tube was centrifuged and particles were allowed to settle. A protein concentrator with a 10 kDa cut-off was used to concentrate the protein, which had an initial concentration of 0.82 mg/mL. After concentrating, the final protein concentration was 3.25 mg/mL. Then, 1 mL of this solution was added to the washed amino particles. The mixture was agitated briefly and centrifuged for sixty seconds. A 50  $\mu$ L sample was removed from the mixture and diluted to 600  $\mu$ L, and the absorbance was measured at 280 nm to determine the protein concentration. After the UV measurement, 1.5 mg of 1-ethyl-3-(3-dimethylaminopropyl) carbodiimide (EDC) was added to the mixture and slowly mixed over night at room temperature. After this time period, a second UV measurement was performed to determine the amount of protein bound to the chromatography particles. After the second UV measurement, the chromatography particles were washed three times with 0.1 M  $K_2HPO_4$ , pH 7.5. After the final rinse, 1 M ethanolamine (pH 8) was added and slowly mixed with the particles for two hours at room temperature. The particles were centrifuged at 10,000 rpm and the supernatant was removed to remove the excess

ethanolamine. The particles were immediately packed into the SIC column using flexible PEEK tubing.

**2.2.7. LC System used for Enfuvirtide.** LC experiments were performed on a Varian LC system equipped with 9100 autosampler, 9012 ternary gradient pump and 9065 detector. The LC parameters used for the analysis of enfuvirtide are as follows, flow rate to 0.5 mL/min, 10  $\mu$ L injection and a detection wavelength of 280 nm. The parameters used for the analysis of enfuvirtide were determined during method development. The flow rate of 0.5mL/min was used for these experiments based on peak symmetry and the ability to detect the maximum change in retention time between low and high sodium chloride concentrations. The live column was equilibrated for one hour between experimental conditions to ensure that the immobilized peptide was in the same state as the mobile phase peptide. For each condition 3% (v/v) acetone was injected to check column integrity and as a non-retained marker. After analysis of acetone, four replicates of enfuvirtide were analyzed. This procedure was repeated for each mobile phase condition. The peak maximum was used to determine the retention time of acetone and enfuvirtide. Dead column experiments using the tresyl particles capped with ethanolamine followed the same procedures as the live column experiments. Dead column experiments were used to determine dead volume marker ( $t_m$ ) for the live column using a ratio of the retention time of the protein measured on the dead column ( $t_{pro\_dead}$ ) vs the retention time of acetone

measured on the dead column ( $t_{ace\_dead}$ ), according to previously published protocols.<sup>10</sup>

**2.2.8. LC System used for Antibody Fragment.** LC experiments were performed on a HP1050 system equipped with a HP1050 auto sampler, HP1050 ternary gradient pump and 1050 DAD detector for LB-005 and LB-007. The LC parameters used for the analysis of LB-005 and Lb-007 were as follows: flow rate to 0.1 mL/min, 1  $\mu$ L injection, and detection wavelengths of 280 nm. The LB-005 modified column was equilibrated for thirty minutes between conditions to ensure that the immobilized membrane protein was in the same state as the mobile phase protein. For each condition, 3% (v/v) acetone was injected three times as a non-retained marker to check column integrity, followed by six injections of pR.

Dead column experiments using the amino particles capped with 3-hydroxypropionic acid followed the same procedures as the live column experiments. Dead column experiments were used to determine dead volume marker ( $t_m$ ) for the live column using a ratio of the retention time of protein measured on the dead column ( $t_{pro\_dead}$ ), and the retention time of the acetone measured on the dead column ( $t_{ace\_dead}$ ), according to previously published protocols.<sup>11,12</sup>

**2.2.9. Molecular Weight for Enfuvirtide.** The molecular weight for Enfuvirtide was measured by Eli Lilly and company. Molecular weights were determined by

sedimentation studies using a Beckman Optima XL-A analytical ultracentrifuge with a sample temperature of 25° C. Six-channel cells (12 mm pathlength) were used with an An-60 Ti rotor operated at 250,00 rpm. The cell radii were scanned using 0.001 cm steps with detection at 308 nm. Data were analyzed using Beckman Origin software (version 4.1). Partial specific volumes ( $v_{\text{bar}} = 0.731$ ) and solvent density ( $\rho = 0.998$ ) were calculated using SEDNPERP software.

**2.2.10. Solubility Measurements for Enfuvirtide.** Solubility was measured by Eli Lilly and company. An appropriate mass of peptide was weighed and transferred to a 4 ml vial. Buffer (0.5 mL) was added and the sample was stirred for thirty minutes. The pH of each solution was adjusted, if needed, using sodium hydroxide or hydrochloric acid. After pH adjustment, the sample was stirred for an additional thirty minutes. In all cases, the peptide was in excess and never completely dissolved. After stirring, a 100  $\mu\text{L}$  aliquot was withdrawn from the supernatant and centrifuged for forty minutes at 12,500 rpm. The sample was then diluted 1000-fold and assayed for content by reverse phase HPLC. These experiments were performed in collaboration with Eli Lilly.

**2.2.11. Reverse Phase HPLC Method for Enfuvirtide.** The reverse phase method was performed by Lilly. The peptide content of a solution can be determined by reverse phase HPLC. The HPLC analysis was performed using an Agilent 1100 system with a Vydac C18 column (218TP54) with a 5  $\mu\text{m}$  particle size (300 Å pore size). The mobile phases were 0.1% trifluoroacetic acid (TFA) in

water (phase A) and 0.1% TFA in acetonitrile (phase B). The column temperature was 35 °C and the injection volume was 100 µl. The flow rate was 1.0 ml/min and detection was by UV absorbance at 215 nm. Mobile phase gradient started at 80% A and 20% B. At fifty minutes the gradient went to 49% A and 51% B, at fifty-one minutes it went to 34% A and 66% B, at fifty five minutes it went to 80% A and 20% B and at sixty minutes it went to 80% A and 20% B.

## **2.3. Results and Discussion**

**2.3.1. Enfuvirtide Chromatograms.** In previous studies, B values for proteins obtained by SIC correlated well with B determined by SLS.<sup>12-14</sup> With peptides, such a direct comparison is not possible because peptides do not scatter sufficient light. Consequently, independent verification of the results cannot be accomplished, as there are no established methods for measuring B for peptides. However, based upon studies with proteins, one can be confident that B values obtained from SIC are reliable. Consider typical SIC chromatograms for enfuvirtide, obtained as a function NaCl concentration, Figure 2.1. As with protein systems, the chromatograms display a progression to longer retention times and larger peak widths with increasing amounts of salt, indicating that the intermolecular forces are becoming more attractive. Therefore, the SIC behavior is consistent with what one would expect for salt effects on B for proteins.

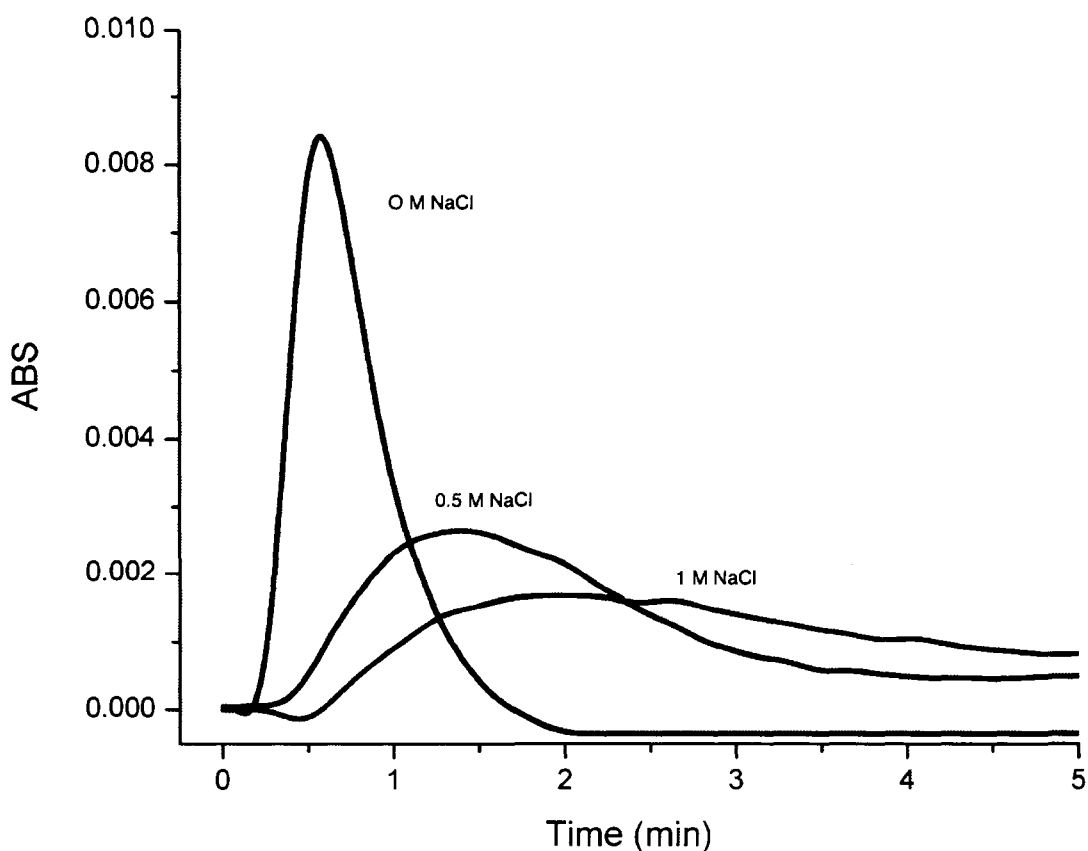


Figure 2.1. The effects of salt concentration on the SIC retention time, 0 M (Black), 0.5 M (Blue), 1 M (Red). Experimental conditions: pH 9, 20 mM sodium carbonate, injection volume 10  $\mu$ l, flow rate 0.1 mL/min.

**2.3.2. pH effects on the B of Enfuvirtide.** Figure 2.2 shows the effects of pH, ranging from 6 to 10, on the solubility of enfuvirtide as measured by traditional methods and B measured by SIC. In general, the peptide precipitates below pH 6 and rapidly chemically degrades at pH greater than 10. As the pH increases from 6 to 10, B for enfuvirtide increases correspondingly from  $-0.19 \times 10^{-4}$  to  $-0.05 \times 10^{-4}$  mol mL  $g^{-2}$ . Note that there is an abrupt increase in solubility from pH 6 to 7. Likewise, there is a marked increase (to more positive values) in B in the same pH range. Clearly, the increase in B mirrors the increase in solubility.

Peptide solubility is dependent on net charge, as electrostatics have the greatest impact on intermolecular interactions and are the longest range of interactions.<sup>15,17</sup> The net charge of peptide is affected by pH as side chains of various amino acids become protonated or deprotonated. Given the abrupt decrease in solubility from pH 7 to 6, it is most likely that this results from protonation of a His residue.

In general, the sign of B indicates whether the net interaction is attractive or repulsive, yet, absolute values for enfuvirtide are universally negative in this study. At first glance, this is unusual as negative B indicates net attractive forces between peptide molecules. In the case of proteins, this would indicate that aqueous solubility is low, but this is not the case for enfuvirtide.<sup>7,8</sup> Although solubility is optimal at positive B, relatively high solubility has been reported for proteins at slightly negative B.<sup>18</sup> Furthermore, at pH 10, the solubility of enfuvirtide is greater than 220 mg/mL, yet B is still slightly negative.

It is important to keep in mind that this is a peptide of significantly lower molecular weight than any protein previously studied by SIC (14,400 Da for lysozyme when compared to 4,000 Da for enfuvirtide). Since this is the first peptide to be examined by this method, one cannot determine if this is a typical range.

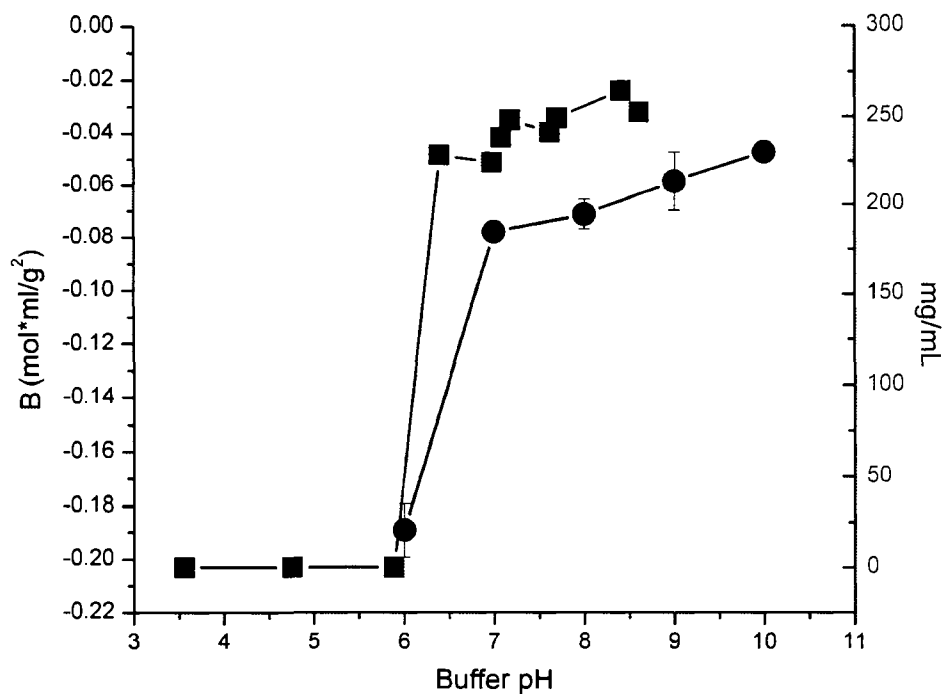


Figure 2.2. The effect of pH on solubility (RED) and B (BLUE) for enfuvirtide. Experimental conditions for SIC: All buffers contained 20 mM sodium carbonate, pH was adjusted with sodium chloride or hydrochloric acid, injection volume 10  $\mu$ l, flow rate 0.5 mL/min.

As stated before, it is not possible to verify these results by SLS methods due to insufficient scattering intensity nor have other methods been reported to provide accurate B values for peptides. All that can be said is that the scale of B is shifted to more negative values, probably reflecting the increased relative importance of specific side chain interactions. Clearly, what is more important than the absolute

value is the relative change in B. A shift to a more positive B indicates less overall attractive interactions, resulting in greater solubility.

The peptide having more negative B values than for proteins must have its origins in specific peptide-peptide interactions. Note that intermolecular interactions are dominated by three types of interactions: electrostatic forces, van der Waals or hydrophobic forces and excluded volume interactions.<sup>3,19</sup> Generally, electrostatic interactions dominate repulsive interactions, hydrophobic forces dominate attractive interactions and excluded volume interactions account for the fact that two molecules cannot occupy the same space at the same time.

Proteins show a much wider range of repulsive interactions (positive B) because they have the ability to fold to sequester hydrophobic residues from the surface, while peptides have only a limited ability to do so. The ability to fold these residues into the core of the protein results in an outer surface that is dominated by polarizable and ionic residues with only small hydrophobic patches spread across the protein surface. It is postulated that the negative B values obtained for enfuvirtide are the result of the high hydrophobic content of this peptide (5 Leu, 2 Ile, 2 Trp, 1 Phe, 1 Tyr out of 36 residues).

While a theoretical framework relating B to absolute solubility has been developed using thermodynamics, it is not useful for calculating solubility in solution because it requires information about the peptide crystal packing.<sup>9</sup> Furthermore, the solubility must be determined from a pure solid crystalline phase. Therefore, a direct quantitative conversion cannot be made between B

and the solubility of enfuvirtide. From a screening perspective, high pH leads to a marked increase of solubility. These results suggest that solubility optimization may be achieved by screening the pH ranges of maximum chemical stability for B values that are the most positive.

**2.3.3. The Effects of Salt on Enfuvirtide.** The effects of different NaCl concentrations (0 to 0.5 M NaCl) at pH 9 on B are shown in Figure 2.3. The abscissa shows the average molecular weight of the peptide as measured by ultracentrifugation, as well as B for enfuvirtide, as a function of NaCl concentration (up to 0.5 M). Overall, there is a steady decrease in B with increasing salt concentration. As B becomes more negative, the average molecular weight of the peptide increases. Both data sets indicate that, as the salt concentration increases, there is an increase in the attractive forces between the peptide molecules. While the increase in molecular weight does not necessarily demonstrate the presence of aggregates, it does indicate that there is a significant association. Recently, there have been reports of a correlation of B with aggregation propensity for proteins.<sup>20, 21</sup> This should not be surprising, if the initial step in aggregation is a colloidal association between peptide molecules.

A rapid decrease in B with increasing salt concentrations has been reported for a number of protein systems.<sup>8, 9, 22-25</sup> As the salt concentration increases, electrostatic repulsion is minimized. As a result, the attractive hydrophobic

regions of the peptide dominate the interaction causing the negative shift. At higher salt concentrations, there is often a nonmonotonic relationship, as excluded volume effects, solution nonideality, and direct ion binding effect begin to manifest themselves.<sup>17</sup> This can actually cause an increase in B, but usually only at salt concentrations well above 1 M. The actual magnitude of the effect also depends on the type of salt.<sup>24, 26</sup>

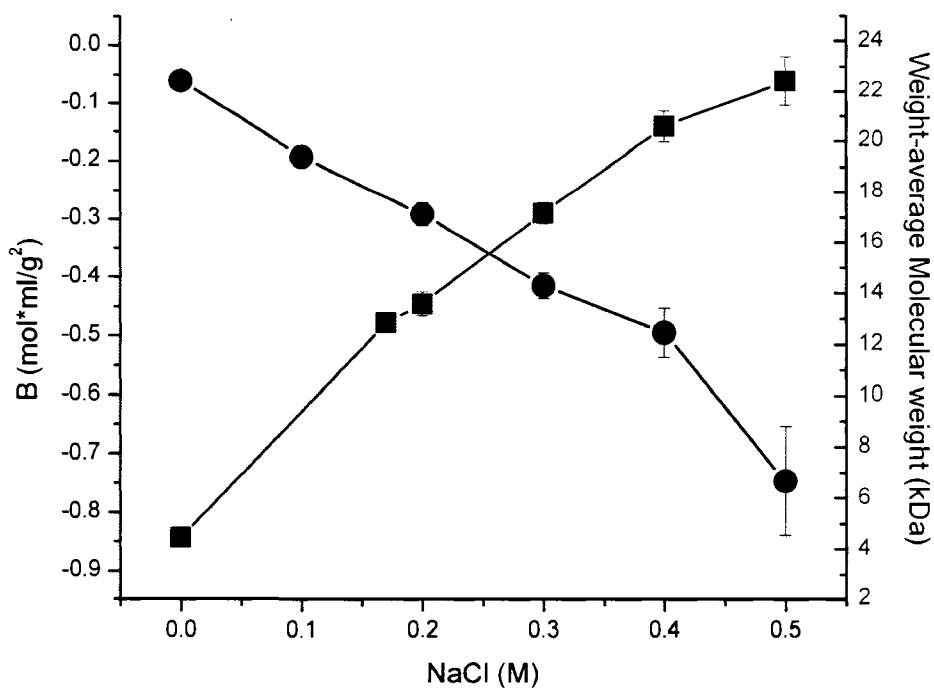


Figure 2.3. Salt dependence of B and the weight-averaged molecular weight of enfuvirtide. Experimental conditions: Buffers contained 20 mM sodium carbonate, injection volume 10  $\mu$ l, flow rate 0.5 mL/min, pH 9.

In order to verify this effect, two other salts were tested. Figure 2.4. shows the effects of sodium citrate and ammonium sulfate on B. These two salts were chosen based on the salts placement in the Hofmeister series, as both sodium citrate and ammonium sulfate are strongly hydrated kosmotropic anions, Figure 2.4.<sup>27</sup> B became significantly more negative upon the addition of 0.1 M of either salt. The effects of ammonium sulfate and sodium citrate on B are larger, relative to sodium chloride, consistent with their placement in the Hofmeister series. Similar effects of ammonium sulfate on lysozyme and albumin have been reported.<sup>23,8</sup>

In general, as the salt concentration increases, there is an increase in shielding of the electrostatic forces on the peptide that accounts for repulsive interactions causing an increase in the attractive hydrophobic interactions. As B becomes more negative, there is a decrease in solubility, at least according to previously published work on proteins.<sup>7-9,14, 24, 28</sup> The effects of salt type are typical of their placement in the Hofmeister series. Both citrate and sulfate are considered kosmotropic, generating a greater degree of order to water than NaCl. The increased order causes an unfavorable increase in the free energy of the solution. As a result, the peptide-peptide interactions become more attractive and B decreases.

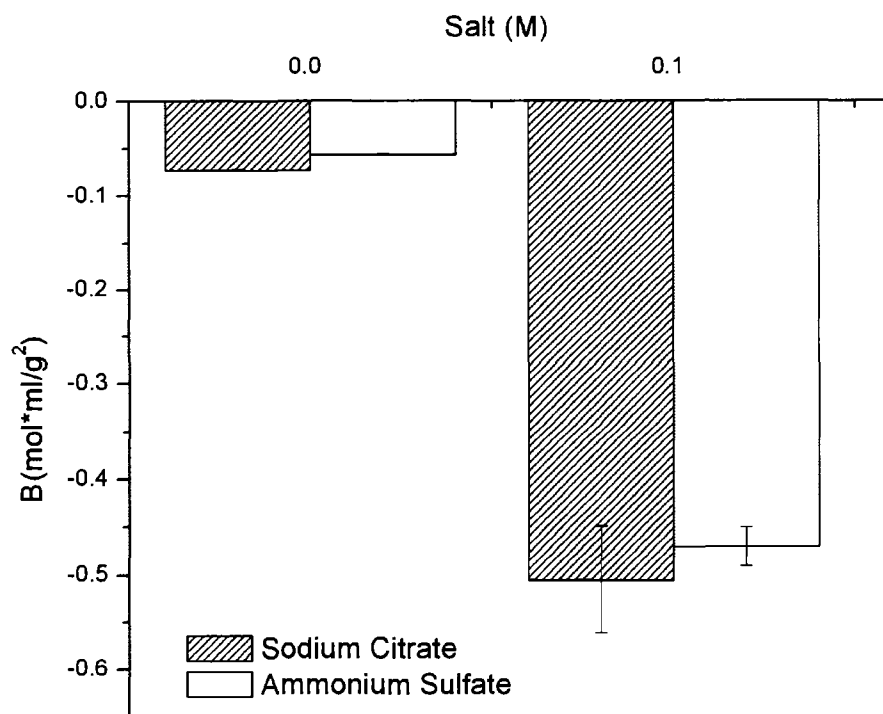


Figure 2.4. Effects of sodium citrate and ammonium sulfate on B. Experimental conditions: All buffers contained pH 9, 20 mM sodium carbonate, injection volume 10  $\mu$ l, flow rate 0.5 mL/min.

**2.3.4. Peptide concentration effects on B values of Enfuvirtide.** The effects of the different peptide concentrations at pH 9 were measured over a relatively wide concentration range (5-120 mg/mL), as shown in Figure 2.5. Typically, B is reported as independent of concentration unless there is a conformational change that alters the interactions.<sup>26</sup> In this study, varying the peptide concentration produced no statistically significant change in B between 5 and 80

mg/mL. At the highest peptide concentration tested (120 mg/mL), B is statistically different than at 80 mg/mL (based on the standard Student's t-test). One possible explanation is that the conformation of enfuvirtide is concentration-dependent. Concentration-dependent B values have not been reported with proteins, although no one has investigated such a large range of concentrations. A change in peptide conformation could also result in different peptide-peptide interactions, leading to different B values. Other mechanisms may also be contributing to the concentration dependence. For example, at these concentrations, one cannot rule out higher order effects, such as multi-body interactions, becoming important. The data suggest that each of these factors may be playing a role in the measurements of enfuvirtide. Other studies have reported a slight decrease in B with increasing protein concentration, indicating that higher order factors, such as nonideality, may be playing a significant role as concentrations exceed 10 mg/mL or more for proteins.<sup>23, 29</sup> The exact physical basis for these effects are yet to be determined.

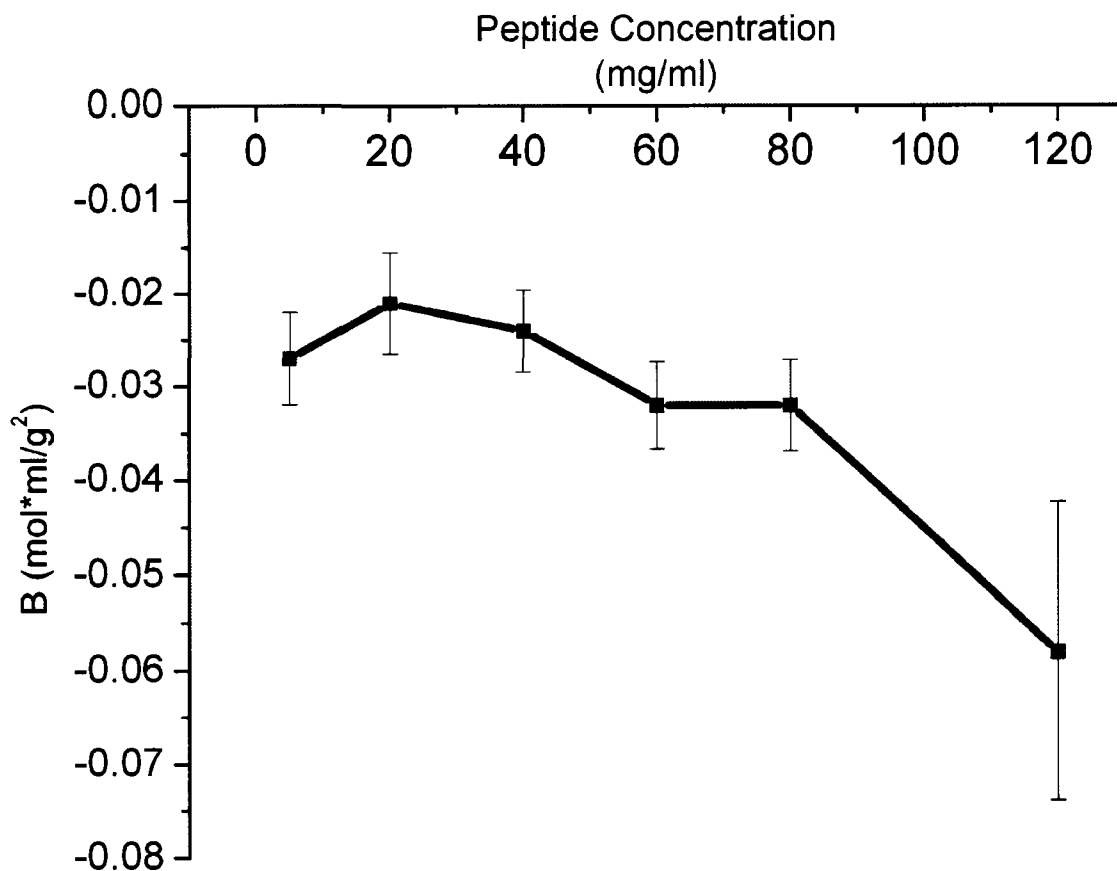


Figure 2.5. Effect of peptide concentration on the B values of enfuvirtide. Experimental conditions: Buffers contained pH 8, 20 mM sodium carbonate, injection volume 10  $\mu$ l, flow rate 0.5 mL/min.

**2.3.5. pH and NaCl Screens For LB-005.** The effects of pH and NaCl on the physical stability of LB-005 were measured by trending the magnitude and direction of B. The effects of pH and NaCl on B are showed as a surface plot in Figure 2.6. As pH increased from 3 to 7, at 0 M NaCl, B decreased from  $4 \times 10^{-4}$  to  $-25 \times 10^{-4}$  mol mL g<sup>-2</sup>). When NaCl was increased from 0 to 0.2 M at pH 7, B increased from  $-25 \times 10^{-4}$  to  $5 \times 10^{-4}$  mol mL g<sup>-2</sup>. Measuring pH affects on the

physical stability of proteins in solution can be challenging.<sup>21,30</sup> Figure 2.6 shows that SIC can trend the physical stability of a therapeutic protein with varying pH and salt, which is important in formulation development.<sup>21,30</sup>

Adjusting solvent pH affects the physical stability of a protein by changing long-range electrostatic interactions.<sup>27,31,32</sup> When the net charge of a protein approaches its isoelectric point (pI), colloidal stability is at minimum.<sup>27,31,32</sup> When the solvent pH approached the pI of 7.8 for LB-005, B was  $-25 \times 10^{-4} \text{ mol mL g}^{-2}$  at pH 7. At pH 3 an increase in repulsive electrostatic interactions was observed, which is represented by an increase in B to  $5 \times 10^{-4} \text{ mol mL g}^{-2}$ .<sup>33,34</sup> Protein solubility at pH 3 and 7 was measured at 30 and 1.5 mg/mL.<sup>3,20,34-36</sup> The relationship between B and solubility has been demonstrated, but not with a therapeutic protein.<sup>3,35</sup> Protein solubility was high at pH 3, but the pH buffer needs to be around the the pH of blood (7.4) for delivery.

The effects of NaCl on the physical stability of a protein is dependent on concentration.<sup>27</sup> For LB-005, as NaCl concentration increased, a salting in behavior was observed. Salting in occurs when the ions shield attractive electrostatic interactions and generally results in an increase in physical stability and increase in solubility.<sup>27</sup> The improvement in physical stability with the addition of NaCl is most pronounced at pH 7 where B changed  $30 \times 10^{-4} \text{ mol mL g}^{-2}$ ) from 0 to 0.2 M. The mechanism for salting in is highly dependent on the chemical and physical structure of the protein.

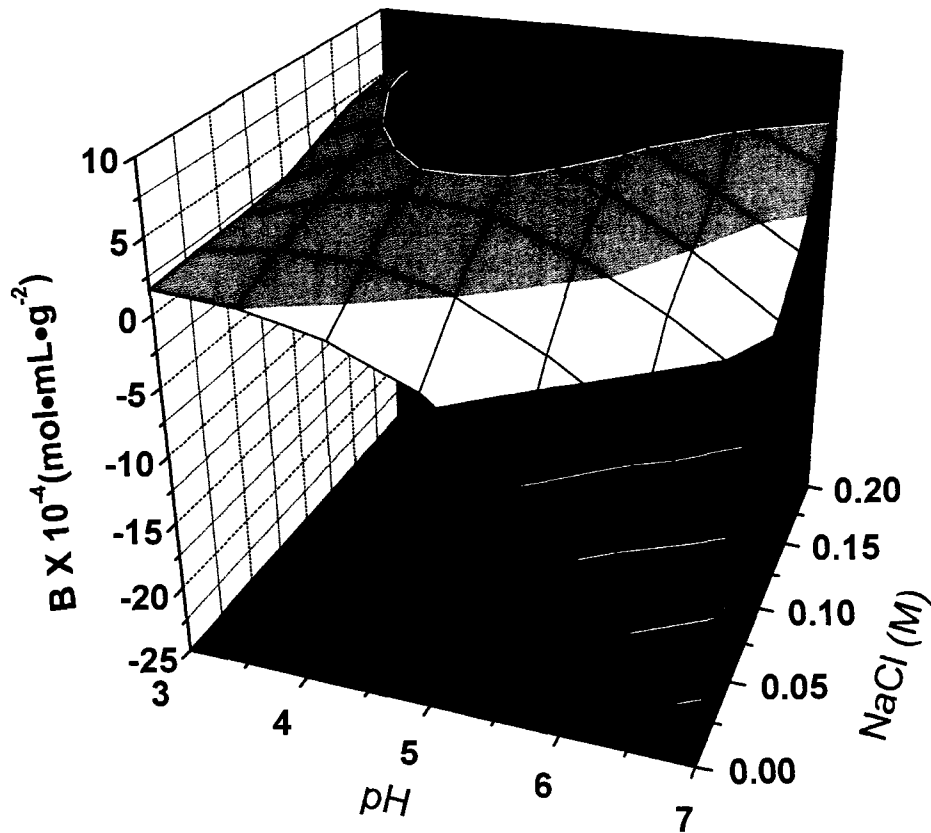


Figure 2.6. The effects of increasing the NaCl concentration from 0 to 0.20 M at pH 3, 5, and 7 on LB-005 virial coefficients. Instrument Settings: Mobile Phase: 10 mM  $\text{K}_2\text{HPO}_4$ , Flow Rate = 0.1 mL/min, injection volume 1  $\mu\text{L}$ , wavelength 280nm

**2.3.6. Sucrose, Glycine and Trehalose for LB-005.** The co-solvents sucrose, trehalose and glycine are sugars that are preferential excluded from the surface of the protein.<sup>21</sup> The colloidal stability of LB-005 was measured with  $B$ , when concentration of sucrose, trehalose and glycine changed for 5 to 10%, Figure

2.7. The change in B for 5% sucrose when compared to no sugar was  $10 \times 10^{-4}$  mol mL g<sup>-2</sup>), when concentration of sucrose was increased to 10% caused B increase to  $15 \times 10^{-4}$  mol mL g<sup>-2</sup>. For each sugar the change in B was greater at 10% compared to 5%.

Sugars preferably interact with water molecules decreasing their concentration around the protein surface. The interaction between the sucrose and protein backbone is thermodynamically unfavorable resulting in an increase in the chemical potential of the protein. The protein state with the less surface area therefore will be thermodynamically favored.<sup>37,38</sup> The water causes the hydrophobic groups to move inward causing energy of the unfolded protein to increase, resulting in improved physical stability.<sup>37,38</sup> The addition of sucrose causes the protein to become compact resulting in a decrease in surface area. The compact protein is more physical stable in solution. The increase in physical stability of the protein is reflected by an increase in B.<sup>12,35,39</sup>

**2.3.7. Comparing the Colloidal Stability of LB-005 to LB-007.** To further improve the solubility of LB-005, a series of point mutations in a small section of LB-005 were made, resulting in an increase in solubility for the mutant, LB-007 (data not shared by company). SIC was used to measure B at pH 5, 6 and 7 for LB-005 and LB-007, Figure 2.8. As the solvent pH increased from 5 to 7, B for LB-007 decreased from  $5 \times 10^{-4}$  to  $-5 \times 10^{-4}$  mol mL g<sup>-2</sup>, while LB-005 decreased from  $5 \times 10^{-4}$  to  $-30 \times 10^{-4}$  mol mL g<sup>-2</sup>. At pH 5 no difference in B was observed

when comparing LB-005 to LB-007. When the pH was increased to 7, the difference in B between LB-005 and LB-007 was  $-25 \times 10^{-4} \text{ mol mL g}^{-2}$ . There is clearly a difference in the physical stability of LB-005 and LB-007 between pH 6 and 7.

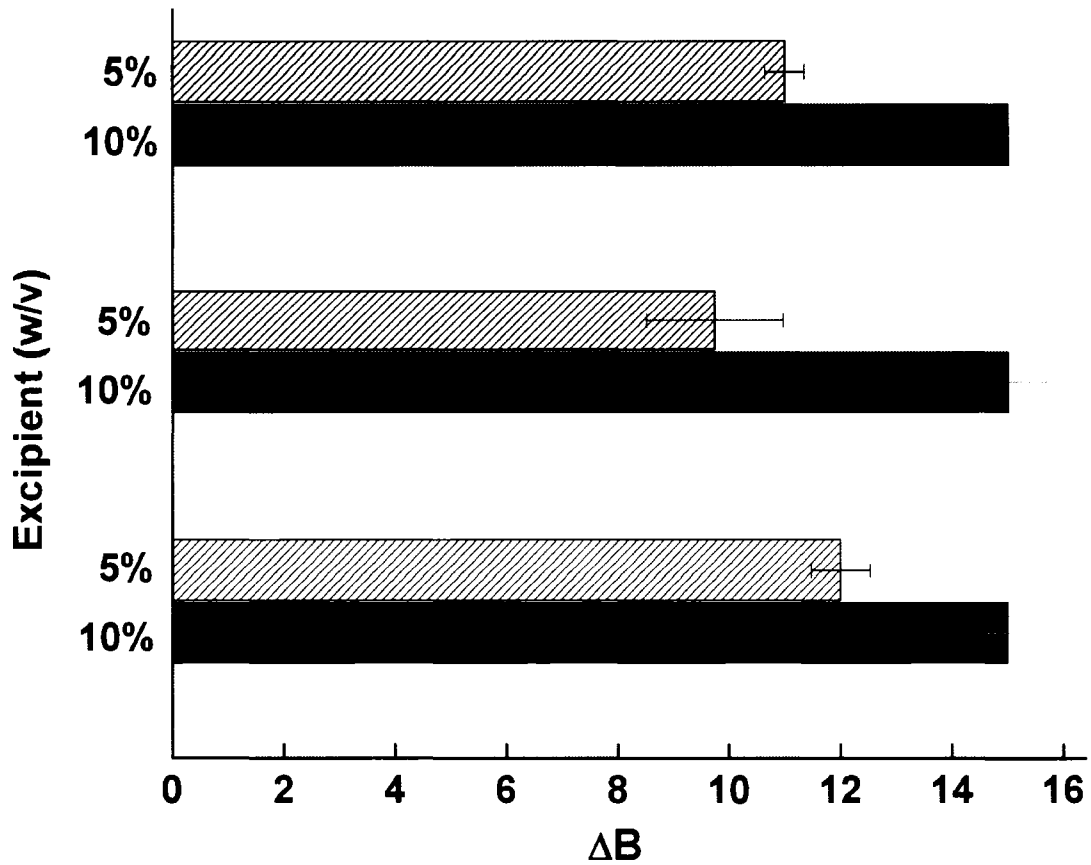
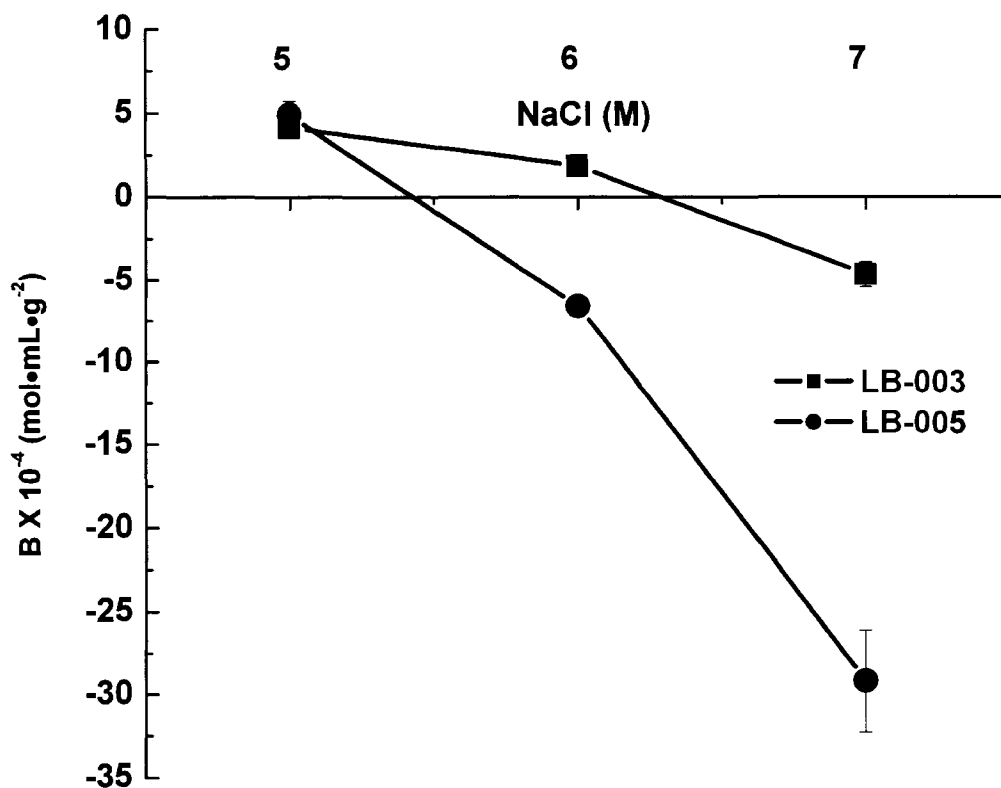


Figure 2.7. The change in B as an effect of sucrose (black), glycine (blue) and trehalose (red). Instrumental Settings: 10 mM  $\text{K}_2\text{HPO}_4$ , pH 7, flowrate= 0.1 mL/min, injection volume 1  $\mu\text{L}$ , wavelength 280 nm.



**Figure 2.8.** Comparing B for LB-005 to LB-007 at pH 5, 6 and 7. Instrumental settings: Mobile phase: 10 mM potassium phosphate, flow rate: 0.1 mL/min, injection volume 10  $\mu$ L, wavelength 280nm.

**2.3.8. Changes in Colloidal Stability of LB-007 with NaCl.** The effects of NaCl on the colloidal stability of LB-007 were measured. When no salt was present in the buffer B was  $-3 \times 10^{-4}$  mol mL g<sup>-2</sup>, indicating low colloidal stability, Figure 2.9. For LB-007 as the concentration of NaCl was increased, B changed increased

from  $-3 \times 10^{-4}$  to  $3.5 \times 10^{-4}$  mol mL  $g^{-2}$ . At 0.5 M NaCl, B was constant at  $3.5 \times 10^{-4}$  mol mL  $g^{-2}$ , at 1 M NaCl B decreased to  $2.5 \times 10^{-4}$  mol mL  $g^{-2}$ .

The data in Figure 2.9, shows two trends in B, salting in and salting out at lower salt concentrations, an increase in colloidal stability was observed and can generally be explained as the salt is ion pairing with charged amino acids. When the concentration of NaCl exceeded 0.5 M, a decrease in B was measured, known as a salting out effect, where the salt is shielding electrostatic effects, resulting in an increase in attractive interactions. The change in B for the LB-007 with increasing concentrations of NaCl agrees with effects of salt concentration on the colloidal stability of proteins.<sup>32</sup>

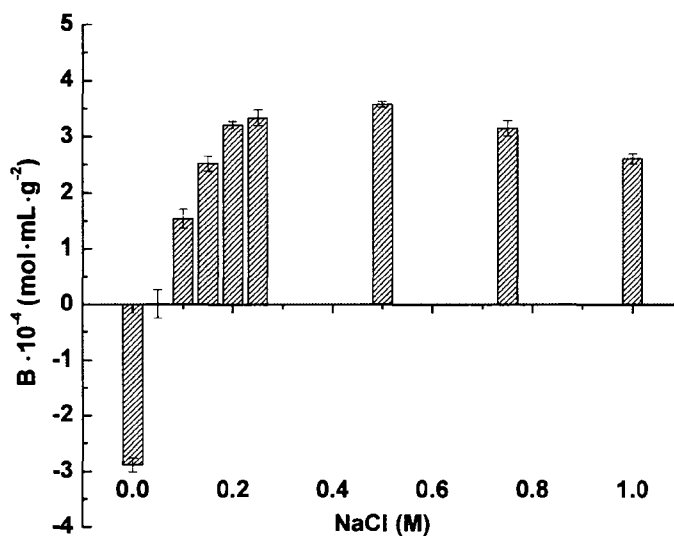


**Figure 2.9.** The effects of increasing NaCl concentration from 0 to 1 M at pH7 of LB-007. Instrumental settings: Mobile Phase: 10 mM  $K_2HPO_4$ , flowrate = 0.1 mL/min, injection volume 10  $\mu$ L, wavelength 280 nm

**2.4. Conclusion.** SIC was used to measure B as function of solution conditions for enfuvirtide. This represents the first detailed study of B values for a peptide. In this case, the solubility of enfuvirtide increases with an increase in pH from 6 to 10. Over this same range, B correlates well with solubility. Both solubility and B show a dramatic increase as the pH increases from 6 to 7, suggesting that protonation of His has a significant impact on intermolecular interactions. In addition, it was found that enfuvirtide solubility decreased with increasing salt concentration. Once again, B correlates well with apparent molecular weight an indication of aggregation. The ability to measure B of peptides by SIC allows one to pursue a rational and designed approach for assessing and optimizing the solubility of peptides. Furthermore, SIC analysis provides a better fundamental understanding of peptide self-interaction. The work described in this chapter is the first time that B values have been published for a peptide. Additionally, SIC was used successfully to pick a solvent/cosolvent system, which improved the solubility of a therapeutic protein, LB-005. Increasing the solubility of LB-005 allowed it to advance to the next stage of development, one step closer to a commercial product. For the first time SIC measured the effect of point mutations on the colloidal stability of a protein.

## **2.5. References**

1. McLaurin, J.; Yang, D. S.; Yip, C. M.; Fraser, P. E., Review: Modulating factors in amyloid-beta fibril formation. *Journal of Structural Biology* **2000**, 130, (2-3), 259-270.

2. Javadpour, M. M.; Barkley, M. D., Self-assembly of designed antimicrobial peptides in solution and micelles. *Biochemistry* **1997**, 36, (31), 9540-9549.
3. Guo, B.; Kao, S.; McDonald, H.; Asanov, A.; Combs, L. L.; Wilson, W. W., Correlation of second virial coefficients and solubilities useful in protein crystal growth. *Journal of Crystal Growth* **1999**, 196, (2-4), 424-433.
4. Kerns, E. H.; Di, L., Pharmaceutical profiling in drug discovery. *Drug Discovery Today* **2003**, 8, (7), 316-323.
5. Blasko, a.; Leahy-Dios, A.; Nelson, W. O.; Austin, S. A.; Killion, R. B.; Visor, G. C.; Massey, I. J., Revisiting the solubility concept of pharmaceutical compounds. *Monatshefte Fur Chemie* **2001**, 132, (7), 789-798.
6. Barone, G.; Delvecchio, P.; Giancola, C.; Notaro, G., Conformational Stability of Proteins and Peptide-Peptide Interactions in the Presence of Carbohydrates. *Thermochimica Acta* **1992**, 199, 189-196.
7. Haas, C.; Drenth, J.; Wilson, W. W., Relation between the solubility of proteins in aqueous solutions and the second virial coefficient of the solution. *Journal of Physical Chemistry B* **1999**, 103, (14), 2808-2811.
8. Demoruelle, K.; Guo, B.; Kao, S. M.; McDonald, H. M.; Nikic, D. B.; Holman, S. C.; Wilson, W. W., Correlation between the osmotic second virial coefficient and solubility for equine serum albumin and ovalbumin. *Acta Crystallographica Section D-Biological Crystallography* **2002**, 58, 1544-1548.

9. Shire, S. J.; Shahrokh, Z.; Liu, J., Challenges in the development of high protein concentration formulations. *Journal of Pharmaceutical Sciences* **2004**, 93, (6), 1390-1402.
10. Roque, A. C. A.; Lowe, C. R.; Taipa, M. A., Antibodies and genetically engineered related molecules: Production and purification. *Biotechnology Progress* **2004**, 20, (3), 639-654.
11. Payne, R. W.; Nayar, R.; Tarantino, R.; Del Terzo, S.; Moschera, J.; Di, J.; Heilman, D.; Bray, B.; Manning, M. C.; Henry, C. S., Second virial coefficient determination of a therapeutic peptide by self-interaction chromatography. *Biopolymers* **2006**, 84, (5), 527-533.
12. Valente, J. J.; Verma, K. S.; Manning, M. C.; Wilson, W. W.; Henry, C. S., Second virial coefficient studies of cosolvent-induced protein self-interaction. *Biophysical Journal* **2005**, 89, (6), 4211-4218.
13. Patro, S. Y.; Przybycien, T. M.; Isermann, H. P., Simulations of reversible protein-aggregate and crystal structure. *Abstracts of Papers of the American Chemical Society* **1996**, 211, 176-BIOT.
14. Teske, C. A.; Blanch, H. W.; Prausnitz, J. N., Measurement of lysozyme-lysozyme interactions with quantitative affinity chromatography. *Journal of Physical Chemistry B* **2004**, 108, (22), 7437-7444.
15. Kita, Y.; Arakawa, T.; Lin, T. Y.; Timasheff, S. N., Contribution of the Surface Free-Energy Perturbation to Protein Solvent Interactions. *Biochemistry* **1994**, 33, (50), 15178-15189.

16. Arakawa, T.; Bhat, R.; Timasheff, S. N., Preferential Interactions Determine Protein Solubility in 3-Component Solutions - the MgCl<sub>2</sub> System. *Biochemistry* **1990**, 29, (7), 1914-1923.
17. Bostrom, M.; Tavares, F. W.; Finet, S.; Skouri-Panet, F.; Tardieu, A.; Ninham, B. W., Why forces between proteins follow different Hofmeister series for pH above and below pI. *Biophysical Chemistry* **2005**, 117, (3), 217-224.
18. Ruppert, S.; Sandler, S. I.; Lenhoff, A. M., Correlation between the osmotic second virial coefficient and the solubility of proteins. *Biotechnology Progress* **2001**, 17, (1), 182-187.
19. Neal, B. L.; Lenhoff, a. M., Excluded-Volume Contribution to the Osmotic 2<sup>nd</sup> Virial-Coefficient for Proteins. *Aiche Journal* **1995**, 41, (4), 1010-1014.
20. Ho, J. G. S.; Middelberg, A. P. J.; Ramage, P.; Kocher, H. P., The likelihood of aggregation during protein renaturation can be assessed using the second virial coefficient. *Protein Science* **2003**, 12, (4), 708-716.
21. Chi, E. Y.; Krishnan, S.; Randolph, T. W.; Carpenter, J. F., Physical stability of proteins in aqueous solution: Mechanism and driving forces in nonnative protein aggregation. *Pharmaceutical Research* **2003**, 20, (9), 1325-1336.
22. Hitscherich, C.; Aseyev, V.; Wiencek, J.; Loll, P. J., Effects of PEG on detergent micelles: implications for the crystallization of integral membrane proteins. *Acta Crystallographica Section D-Biological Crystallography* **2001**, 57, 1020-1029.

23. Moon, Y. U.; Curtis, R. A.; Anderson, C. O.; Blanch, H. W.; Prausnitz, J. M., Protein-protein interactions in aqueous ammonium sulfate solutions. Lysozyme and bovine serum albumin (BSA). *Journal of Solution Chemistry* **2000**, 29, (8), 699-717.
24. Piazza, R.; Iacopini, S.; Galliano, M., BLGA protein solutions at high ionic strength: Vanishing attractive interactions and "frustrated" aggregation. *Europhysics Letters* **2002**, 59, (1), 149-154.
25. Benas, P.; Legrand, L.; Ries-Kautt, M., Strong and specific effects of cations on lysozyme chloride solubility. *Acta Crystallographica Section D-Biological Crystallography* **2002**, 58, 1582-1587.
26. Bevan, C. D.; Lloyd, R. S., A high-throughput screening method for the determination of aqueous drug solubility using laser nephelometry in microtiter plates. *Analytical Chemistry* **2000**, 72, (8), 1781-1787.
27. Curtis, R. A.; Ulrich, J.; Montaser, A.; Prausnitz, J. M.; Blanch, H. W., Protein-protein interactions in concentrated electrolyte solutions - Hofmeister-series effects. *Biotechnology and Bioengineering* **2002**, 79, (4), 367-380.
28. Ahamed, T.; Ottens, M.; van Dedem, G. W. K.; van der Wielen, L. A. M., Design of self-interaction chromatography as an analytical tool for predicting protein phase behavior. *Journal of Chromatography A* **2005**, 1089, (1-2), 111-124.

29. Tessier, P. M.; Lenhoff, A. M.; Sandler, S. I., Rapid measurement of protein osmotic second virial coefficients by self-interaction chromatography. *Biophysical Journal* **2002**, 82, (3), 1620-1631.
30. Manning, M. C.; Patel, K.; Borchardt, R. T., Stability of Protein Pharmaceuticals. *Pharmaceutical Research* **1989**, 6, (11), 903-918.
31. Curtis, R. A.; Lue, L., A molecular approach to bioseparations: Protein-protein and protein-salt interactions. *Chemical Engineering Science* **2006**, 61, (3), 907-923.
32. Curtis, R. A.; Montaser, A.; Prausnitz, J. M.; Blanch, H. W., Protein-protein and protein-salt interactions in aqueous protein solutions containing concentrated electrolytes (vol 57, pg 11, 1997). *Biotechnology and Bioengineering* **1998**, 58, (4), 451-451.
33. Schaink, H. M.; Smit, J. a. M., Determination of the osmotic second virial coefficient and the dimerization of beta-lactoglobulin in aqueous solutions with added salt at the isoelectric point. *Physical Chemistry Chemical Physics* **2000**, 2, (7), 1537-1541.
34. Shaw, K. L.; Grimsley, G. R.; Yakovlev, G. I.; Makarov, A. A.; Pace, C. N., The effect of net charge on the solubility, activity, and stability of ribonuclease Sa. *Protein Science* **2001**, 10, (6), 1206-1215.
35. Valente, J. J.; Payne, R. W.; Manning, M. C.; Wilson, W. W.; Henry, C. S., Colloidal behavior of proteins: Effects of the second virial coefficient on solubility, crystallization and aggregation of proteins in aqueous solution. *Current Pharmaceutical Biotechnology* **2005**, 6, (6), 427-436.

36. George, a.; Chiang, Y.; Guo, B.; Arabshahi, A.; Cai, Z.; Wilson, W. W.,  
Second virial coefficient as predictor in protein crystal growth.  
*Macromolecular Crystallography, Pt A* **1997**, 276, 100-110.
37. Timasheff, S. N., Protein hydration, thermodynamic binding, and  
preferential hydration. *Biochemistry* **2002**, 41, (46), 13473-13482.
38. Arakawa, T.; Timasheff, S. N., Theory of Protein Solubility. *Methods in  
Enzymology* **1985**, 114, 49-77.
39. Valente, J. J.; Fryksdale, B. G.; Dale, D. A.; Gaertner, A. L.; Henry, C. S.,  
Screening for physical stability of a Pseudomonas amylase using self-  
interaction chromatography. *Analytical Biochemistry* **2006**, 357, (1), 35-42.

### 3. Colloidal and Conformational Stability of Proteorhodopsin

**3.1. Introduction.** This chapter focuses on measuring  $B$  for a membrane protein, proteorhodopsin (pR), in different solvent/co-solvent systems. pR is a membrane protein found in marine bacteria and functions as proton pump in a manner that is analogous to the more common bacteriorhodopsin (bR).<sup>1</sup> Membrane proteins are critical biological elements that are responsible for signaling and transport of many materials across the cell membrane as well as being targets for approximately two-thirds of all therapeutic compounds. Further characterization of membrane protein structure and function is limited in part by the amount of material available for research. While the ability to express membrane proteins has improved through the development of better expression systems, the development of improved methods for recovery and purification has lagged. Extraction and purification of membrane proteins in aqueous solution requires detergent above the critical micelle concentration (CMC) and addition of co-solvents to stabilize a protein-detergent complexes (PDC).<sup>2-5</sup> Adjusting detergent type and concentration along with the solvent/co-solvent systems to improve the colloidal stability of PDC is critical for extracting membrane proteins and improving purification yield.<sup>6</sup> Because of the large number of commercially available of detergents and co-solvents, determining solution compositions that maximize colloidal stability of PDC can be a difficult process.<sup>7-10,4,11,12,13</sup> A of number groups have screened detergents for the purpose of selecting solvent/co-solvent systems for crystallization and membrane protein

extraction.<sup>7-10,4,11,12,13</sup> The drawbacks to these detergent screens is that the data is generally qualitative, it requires large amounts of sample, and frequently suffers from low throughput.<sup>8,14</sup> An alternative approach would be to quantitatively measure  $\zeta$ , a known predictor of colloidal stability. Static light scattering is not practical for membrane proteins because of the chemical noise caused by polymeric additives and detergent micelles.<sup>2,15-17</sup>

**3.2. Conformational Stability of pR.** Changes in the tertiary and quaternary structure of the membrane protein in this chapter are referred to as conformational stability and are impacted by the detergent structure among other effects.<sup>18-20</sup> When membrane proteins start to denature from the native state the conformational stability decreases.<sup>19</sup> Bacteriorhodopsin (bR) is a homologue to pR and its conformation is dependent on the detergent type and concentration.<sup>21, 22</sup> Ionic detergents, such as SDS, contain a permanent charge on the head group but causes bR to denature as measured by the detachment of the retinal.<sup>23</sup> Non-ionic detergents contain an uncharged hydrophilic head groups and a hydrophobic tail and have been shown to stabilize the conformation of membrane proteins.<sup>6, 24, 25</sup> Additionally, studies have shown changes in the enzymatic activity of the membrane protein,  $\text{Ca}^{+2}$ -ATPase in the presence of different detergent types and concentrations.<sup>21</sup> For the current set of experiments the conformational stability of pR was measured by the maximum absorbance of the attached retinal in different detergents and buffers.

**3.3. Colloidal Stability of a Membrane Protein.** The colloidal stability of soluble proteins has been quantified in different solvent/co-solvent systems by measuring the osmotic second virial coefficient (B).<sup>4,9,10,26</sup> For soluble proteins B can be described as a two-body interaction in which the protein can interact with another protein or solvent molecule.<sup>26-29</sup> When protein-protein interactions are favored, colloidal stability decreases corresponding to a decrease in solubility.<sup>26-29</sup> When protein-solvent interactions are favored, colloid stability increases corresponding to an increase in solubility.<sup>26-29</sup> For a membrane protein colloidal stability is more complicated because of the hydrophilic and hydrophobic regions of the analyte.<sup>6,9,30-32</sup> The exposed hydrophobic groups of the membrane protein increase the free energy cost, causing aggregation aqueous solutions.<sup>6,9,30-32</sup> To prevent aggregation and denaturing the membrane protein in aqueous solutions the addition of a detergent is vital.<sup>33-35</sup> The detergent molecules contain both polar and nonpolar regions of molecule and the detergent associates with hydrophobic area of the membrane protein shielding it from the solvent.<sup>33-35</sup> To maximize the colloidal stability of the membrane protein, the concentration of the detergent needs to meet or exceed the CMC, creating a protein-detergent-complex (PDC).<sup>33-35</sup> Previous studies with membrane proteins have correlated B with colloidal stability of the PDC.<sup>2,9</sup> Measuring B for membrane proteins is problematic because presence of the detergent in the buffer.<sup>2,9</sup>

An alternative approach to measuring B is SIC, which has the advantages of low protein consumption, shorter analysis time and the ability to make measurements in complex buffer systems. B was measured by SIC for proteorhodopsin (pR) a membrane protein, presented here. Determination of B as a function of surfactant type and co-solvent concentration for pR was used to measure changes in colloidal stability. Additional screening studies using salts measured the change in B using pR as a model membrane protein. In all cases, SIC was capable of measuring B for pR in complex buffer systems. This paper demonstrates the utility of SIC for measuring changes in the physical stability of proteorhodopsin (pR) in different detergent solvent/co-solvent systems. Two forms of pR were analyzed, a wild type and a slow cycle mutant, as a function of varying detergent concentration and addition of co-solvents. The results demonstrate SIC can be used as an alternative approach for screening solvent/co-solvent systems to improve the colloidal stability of PDCs.

### **3.4. Materials and Methods**

**3.4.1. Chemical and Reagents.** The following chemicals and materials were used as received: potassium phosphate, potassium iodide, hydrochloric acid, sodium carbonate, sodium hydroxide, sodium chloride and TRIS (Fisher, USA). 2-(N-Morpholino)Ethanesulfonic Acid, Monohydrate (MES) was purchased from Acros Organics. 3-hydropropionic acid was purchased from TCI. Monohydrate 3-hydropropionic acid was purchased from TCI. Chromatography particles (Toyopearl AF-Amino-650M) were purchased from Supelco. The coupling

reagent (1-Ethyl-3-[3-dimethylaminopropyl]carbodiimide Hydrochloride) (EDC), N-hydroxysuccinimide (NHS), and the BCA colorimetric protein assay kit were purchased from Pierce. The detergent n-dodecyl- $\beta$ -D-malroside (DDM) was purchased from Sigma. Tween 20, CHAPS and evans blue were purchased from Sigma. The dye used for measuring CMC of the mixed detergent systems was evans blue purchased from Sigma. Proteorhodopsin was generously supplied by Gencor and used as received without further purification. Peek tubing and frits were purchased from Unchurch (USA). BCA colorimetric assay was purchased from Pierce (USA). All buffers were prepared with 18.1 M $\Omega$  from Millipore-Q Academic.

**3.4.2. pR Purification of pR Wild Type and Slow Cycle Mutant.** pR was generically altered with a His tag for purifying the membrane protein using a Ni-affinity column. To begin 26 grams of intact cells were removed from a -14°C refrigerator, dissolved in 50 mM Hepes, 100mM KCl, pH 8.2, 2% DDM and slowly stirred at room temperature. After the cells were added to buffer, the samples were homogenized by glass hand homogenizer or using a french press. A french press is used to break the cell membrane walls by passing the cell through a narrow opening at high pressure. The homogenized samples were then divided into 50 mL centrifuge tubes and centrifuged at 10 x 1000 rpm for 20 minutes. The supernatant which contained the pR, as indicated by the red color, was removed and transferred into 20 mL centrifuge tubes. The samples were then placed in an ultra-centrifuge and were centrifuged at 50,000 rpm for 30 minutes. The pellets at

the bottom of the centrifuge tubes were combined and dissolved in 50 mM  $K_2HPO_4$ , pH 8.2, 100 mM KCl, and 0.05% DDM.

In the first purification step the dissolved pR was added to the Ni-affinity particles and agitated at 40°C in an incubator for 4 hours, after which the light blue particles turned red and were washed in a funnel with the buffer used to dissolve pR. The washing step was repeated until the wash buffer remained clear. The pR attached to Ni-affinity particles was removed by washing with a buffer supplemented with 400 mM imidazole. The pR was then dialyzed with 30,000 MW dialysis tubing in 50 mM  $K_2HPO_4$ , pH 8.2, 100 mM KCl and 0.05% DDM overnight at room temperature.

The pR from the first purification step was further purified on Ni-Affinity column with a 86 mL volume attached to BioCad 700 with fraction collector and Biocad vision workstation. The instrumental setting are as follows; sample load 100 mL, elution gradient 20 mM imidazol to 400 mM imidazol over 15 column volumes, fraction collector set to 9 mL, detector set to 280 and 450 nM. Fractions were collected from one-third of the peak on both sides and combined. The pR was then dialyzed with 30,000 MW dialysis tubing in 50 mM  $K_2HPO_4$ , pH 8.2, 100mM KCl and 0.05% DDM overnight at room temperature.

The diluted pR was then concentrated using a membrane with a size cut off of 30,000 MW under nitrogen at 4°C. The concentrated protein was then aliquated

and stored at room temperature. Genecor purified the slow cycle mutant while Robert Payne purified the wild type.

#### **3.4.3. Photocycling Proteorhodopsin in Solution.** An Agilent 8453

spectroscopy system was used to measure the change in absorbance when pR was photocycled in conditions varying from pH 2 to 12. pR was dissolved and diluted in 20 mM TRIS, 0.1% DDM while varying buffer pH. The blank absorbance spectrum was measured for the buffer from 200 to 700 nm. pR was transferred to a 0.5 mL quartz cuvet and excited by a 520 nm light source, while the spectrum was collected from 200 to 700 nm. The sample was then excited by 472nm light source and the spectrum from 200 to 700nm was repeated for each condition.

#### **3.4.4. Photocycling Proteorhodopsin on the Stationary Phase.** Photocycling proteorhodopsin on the stationary phase was determined by changes in the particles color. Proteorhodopsin immobilized on the stationary phase was photocycled using two diodes with emitting wavelengths of 520nm, and 472 nm. The immobilized proteorhodopsin was photocycled at pH 12. The immobilized proteorhodopsin was then exposed to 520 nm, causing a change in particle color. Next, the particles were excited by a 472 nm light source returning them to their original color. This was repeated with each new batch of immobilized pR to verify structural integrity of the membrane.

**3.4.5. Sodium Dodecyl Sulfate Polyacrylamide Gel Electrophoresis (SDS-Page).** pR was diluted with water 1X, 5X and 10X and added to a 1 to 1 fraction with LDS sample buffer. The LDS buffer used for SDS-page contained 60 uL of water, 40 uL of reducing agent and 100  $\mu$ L of LDS 4X solution. The samples were heated to 45°C for 45 minutes in a hot water bath. 10  $\mu$ L of each dilution was loaded onto a 4% to 12% TRIS-BIS gel. The power supply was set to a constant voltage of 200 V for 30 min.

The gel was removed, washed with water, and fixed for 30 minutes in 12% TCA, 3.5% sulfosalicylic acid. The gel was once more washed with water and stained over night in 0.1% coomassie R-250 blue, 40% ethanol, 10% acetic acid and microwave at high or 20 minutes. The stain was removed with 10% ethanol and 7.5% acetic acid over two hours.

**3.4.6. Size Exclusion Chromatography (SEC).** SEC data was collected on HP1050 equipped with a HP1050 quardary pump, a HP1050 autosampler and a HP1050 photo diarray using a phenomenex biosep-SEC-S 3000 with the following dimensions 300 x 7.80 mm. The column was equilibrated with mobile phase composed of 0.1 M  $\text{Na}_2\text{HPO}_4$  at pH 7.3. The sample was dissolved in the same mobile phase. The instrumental conditions used for all SEC runs are as follows, flowrate 1mL/min, injection volume 10 uL and wavelength recorded at 280 and 500nm.

**3.4.7. Bicinchoninic Acid (BCA).** The BCA procedure outlined by Pierce was followed for the calibration curve and sample measurements.<sup>36</sup> The following changes were made; first the particles were removed and allowed to settle in the pipette tip to determine particle volume. The particles were added to the working reagent and diluted to a finale volume of 0.1 mL. The sample, blank and unmodified particles were prepared and the protein concentration was measured.<sup>36,37</sup>

**3.4.8. Column Preparation.** The preparation of chromatography particles for immobilization of pR was performed in coupling buffer composed of 0.02 M MES, 0.1% (w/v) DDM, pH 6. In an eppendorf tube, AF-Amino-650M particles were rinsed three times with coupling buffer. After each rinse the tube was centrifuged and supernatant was removed. pR (~8mg/mL) was added to the washed particles. After the addition of protein, 60 mg of EDC and 3 mg NHS were added slowly to the mixture and gently mixed overnight at 22°C using a shaker plate. After protein coupling, the amino particles were rinsed three times with coupling buffer. After the third rinse, the particles were washed with 0.5 M 3-hydroxypropionic acid (HPA) at pH 6 and 60 mg EDC was added followed by overnight mixing.<sup>38</sup> HPA was added to block any remaining reactive functional sites. The particles were then washed with coupling buffer to remove HPA and EDC. The immobilized protein was slurry packed into FEP tubing with an inner diameter of 0.062" and the end of the tube was capped with a 2 μM frit-in-a ferrule. Coupling of pR to the amino particles resulted in the particles turning a

light purple color. The amount of protein immobilized onto the amino particles was quantified using a BCA colorimetric assay.<sup>36</sup> The immobilized pR was photocycled by exposing the particles to 520 and 472 nm using appropriate wavelength light emitting diodes at pH 12, resulting in a color change. Immobilized pR was photobleached when exposed to 520 nm, indicating that the immobilized pR was in a native conformation.

**3.4.9. LC System.** LC experiments were performed on a HP1050 system equipped with a HP1050 auto sampler, a HP1050 ternary gradient pump and a 1050 DAD detector. The LC parameters used for the analysis of proteorhodopsin are as follows: flow rate to 0.1 mL/min, 3  $\mu$ L injection, and detection wavelengths of 280 and 550 nm. The pR-modified column was equilibrated for 40 min between conditions to ensure that the immobilized membrane protein was in the same state as the mobile phase protein. For each condition, 3% (v/v) acetone was injected three times as a non-retained marker to check column integrity, followed by six injections of pR.

Dead column measurements were made to determine the retention time of protein on an unmodified column. Dead column experiments followed the same procedures as the live column experiments using amino particles capped with HPA. The experiments were used to determine dead volume marker ( $t_m$ ) for the live column using a ratio of the retention time of protein measured on the dead

column ( $t_{\text{pro\_dead}}$ ), and the retention time of the acetone measured on the dead column ( $t_{\text{ace\_dead}}$ ), according to previously published protocols.<sup>26,39</sup>

**3.4.10. Small Scale SIC Instrument.** Small-Scale LC experiments were performed using a Harvard syringe pump (PHD 4400), rheodyne 0.5  $\mu\text{L}$  manual injector and SSI 500 detector UV/Vis. The LC parameters used for the analysis of pR are as follows, flow rate (varied)  $\mu\text{L}/\text{min}$ , 0.5  $\mu\text{L}$  injection and wavelength set to 280 nm. Data was collected using National Instruments USB 6009 and Labview 8. All chromatograms were analyzed using Origin version 8. The Labview program was written for the purpose of data collection for the small scale SIC. For each experimental condition, 3% (v/v) acetone was injected as a non-retained marker, to check column integrity and adjust for solvent viscosity. For each condition the column was equilibrated for 30 mins, after which acetone and pR were injected.

**3.4.11. Dye Absorption Method.** CMC of the detergent for each screen condition were measured by monitoring changes in the max absorbance of dye, Evans Blue. The max absorbance of the dye changes when interacting with the detergent micelle as compared to the aqueous environment. The stock solution of Evans Blue was dissolved in 20 mM MES, 50mM NaCl, pH 7 for a final concentration of 0.1 M. For each condition 5  $\mu\text{L}$  of  $1 \times 10^{-6}$  M of dye was added to 1 mL of solution. The mixture was equilibrated for 12 hours at room

temperature. After sample equilibration the spectrum was collected on a Cary 500 uV/vis spectrometer from 300 to 800 nm.

#### **3.4.12. Measuring Conformational Changes in pR.** Changes in pR

conformation were measured by changes in the absorbance of the retinal at each screening condition. For each screening experimental condition 0.005mL of pR was added to 1 mL of buffer and allowed to equilibrate over night at room temperature. After equilibration the sample was scanned from 250 to 650 nm. The data was then analyzed using Origin version 8.

### **3.5. Results and Discussion.**

**3.5.1. SEC results for pR.** The slow cycle mutant pR was run on a SEC column to measure the purity of the sample supplied by Genecor, Figure 3.1.1. Data was collected for two wavelengths 280 and 500 nm, which is the absorbance of the phenylalanine, tryptophan, tyrosine and the attached retinal. The SEC data shows a peak at 1.7 minutes for pR, which absorbs of 280 nm and 500 nm. The identify of the second peak at 3 minutes for absorbance at 280 nm, is not known. The SEC data shows the sample supplied by Genecor contains pR.

SDS-Page gel was used to determine the purity of the wild type protein, Figure 3.1.2. Two lanes were loaded with wild type protein, in lane 1 a 1:1 dilution of protein was loaded and in the second lane 1:10 dilution was used. In the first lane, the high molecular weight band is aggregated wild type pR and the second

band is the denatured subunit of the wild type pR. SDS-page Gel and the SEC data indicate that pR is present in the sample.

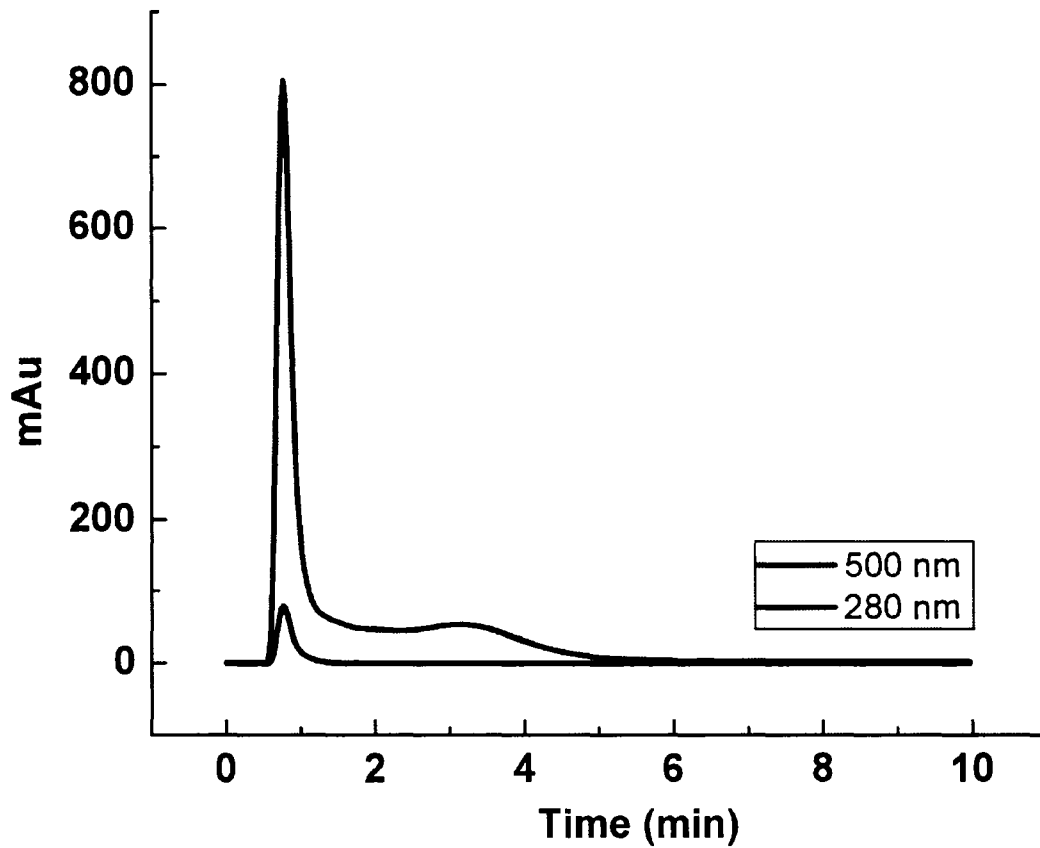


Figure 3.1.1. pR injected on to SEC column to determine sample purity.

Experimental Conditions: Mobile phase was composed of 0.1 M  $\text{Na}_2\text{HPO}_4$  at pH 7.3, injector volume 10uL, flowrate of 1 mL/min and wavelength set to 280 and 500nm.

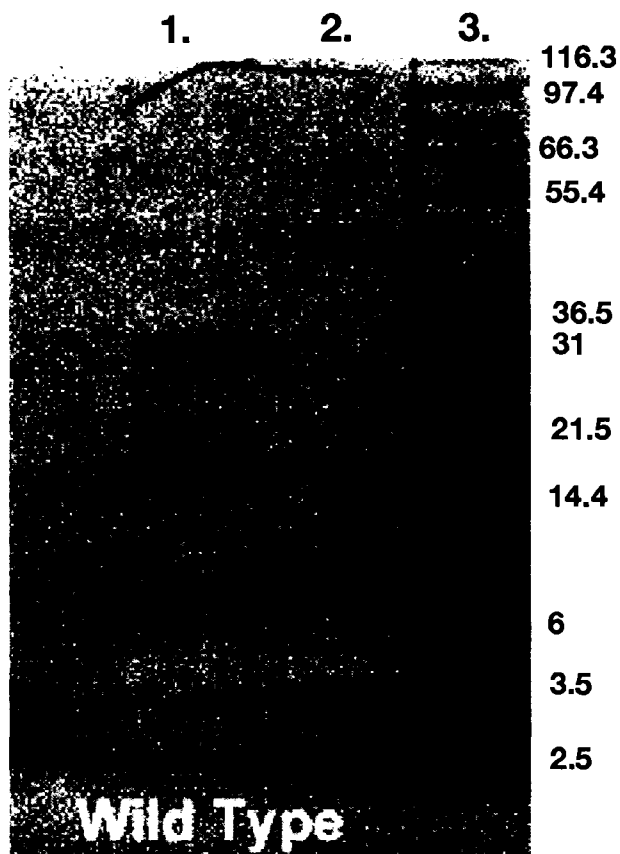


Figure 3.1.2. SDS Page Gel using a Novex 4-12% Bis –Tris Gel w/MES of dialyzed wild type pR. Wild type pR in lane 1 is 1  $\mu$ L wild type pR and lane 2 is 1:10 dilution of wild type pR with deionized water. Lane 3 is the mW standard measured in kDa.

**3.5.2. Photocycling of Proteorhodopsin Immobilized on the Stationary Phase.** Photocycling of pR is caused by changes in the conformation of the retinal in the center of the pR and is dependent the conformation of the protein. pR was immobilized on to the stationary phase and pH 7 buffer was added to the left edge of the particles, while pH 12 buffer was added to the right edge, Figure

3.1.3. When the immobilized pR was exposed to 472 nm the immobilized protein changed color in pH 12 buffer, caused by the change in retinal conformation. The protein was then exposed to 520 nm light, resulting in a return to the original conformation of the retinal, indicated by red color of the particles. The ability to photocycle immobilized pR suggests the protein is in its native conformation.

**3.5.3. Photocycling of Proteorhodopsin in the mobile phase.** Additionally, pR was photocycled in the solution to check the basic buffer conditions did not effect the conformation of pR. Photocycling causes a shift in the absorbance profile of proteorhodopsin, which was measured by Agilent 8453 spectroscopy system. The peak height of proteorhodopsin changed when exposed to 520nm and 404 nm, Figure 3.1.4. The solution was then exposed to 472 nm causing the absorbance maximum to return to 528nm, Figure 3.1.4. Below pH 9 no change in the absorbance maximum of the solution was observed when exposed to 520nm.

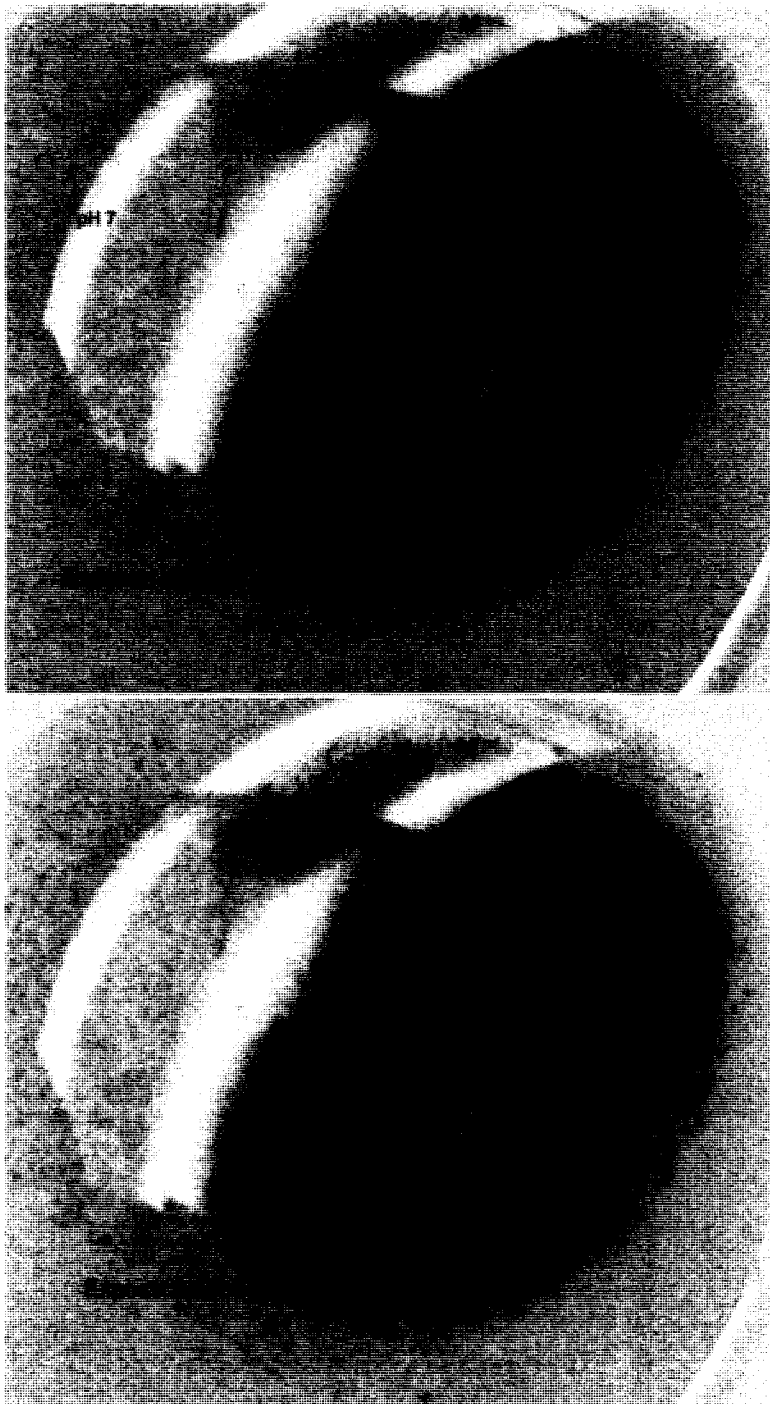


Figure 3.1.3. Photocycling immobilization of pR at pH 7 and pH 12. Buffer conditions 20 mM MES in 0.1% DDM.

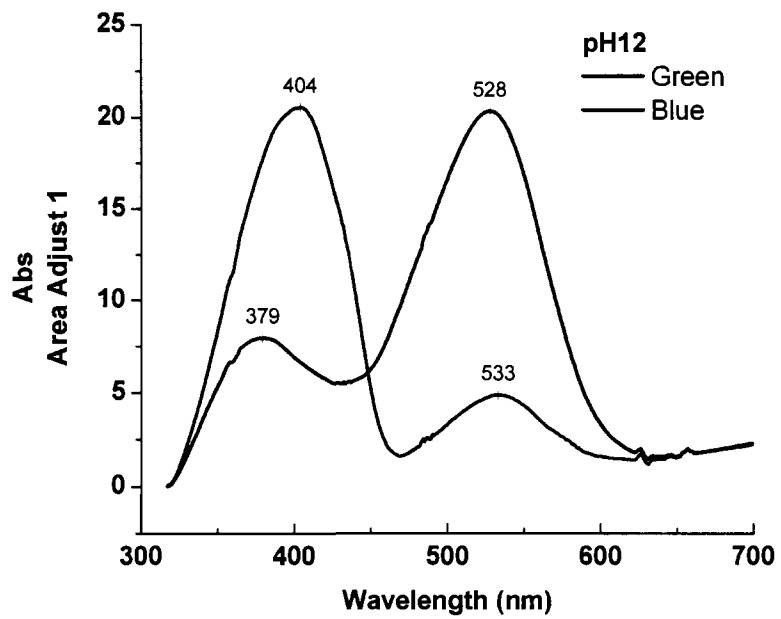
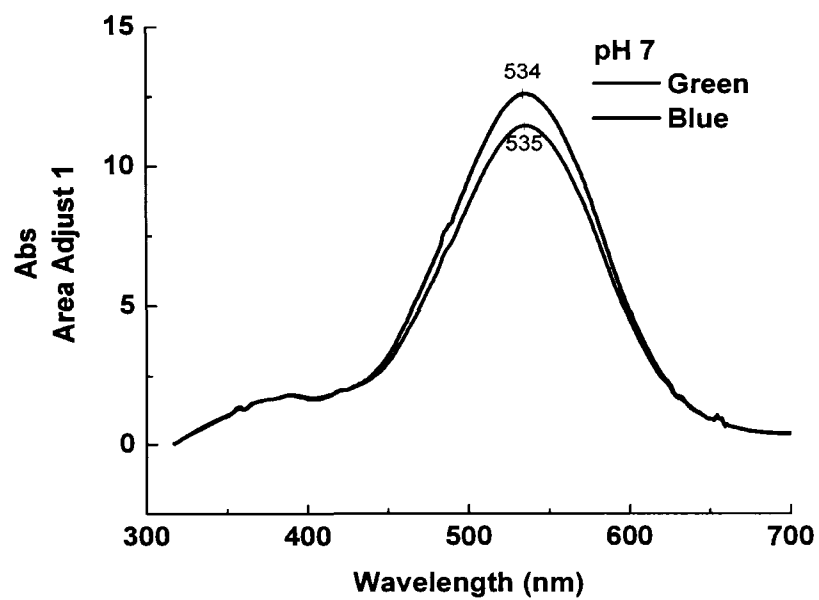


Figure 3.1.4. Photocycling of proteorhodopsin in solution at pH 12 and 7. Buffer 20mM TRIS, 0.03% DMS

**3.5.4. Concentration Dependence of Detergent.** The effects of detergent are concentration dependent; below the CMC the physical stability of the PDC is at a minimum, while above the CMC, the PDC is more stable.<sup>34</sup> The effect of detergent concentration on B was analyzed using SIC, Figure 3.1.5. Concentrations of DDM (CMC = 0.04%) were increased from 0.03% to 0.10% (w/v) while keeping the solvent/cosolvent system constant at pH 7, 20 mM MES.<sup>40</sup> When the concentration of DDM was below the CMC, B for the wild type and mutant pR were  $-2.4 (\pm 1.0) \times 10^{-4} \text{ mol mL g}^{-2}$  and  $-2.3 (\pm 0.07) \times 10^{-4} \text{ mol mL g}^{-2}$  respectively, indicating low physical stability. When the DDM concentration exceeded 0.04%, B increased and remained constant for the wild type  $1.08 (\pm 0.07) \times 10^{-4} \text{ mol mL g}^{-2}$  and for the mutant  $1.14 (\pm 0.1) \times 10^{-4} \text{ mol mL g}^{-2}$ . Trends in B both types of pR indicate an increase in physical stability with increasing concentrations of DDM. The trends in B agree with current theories of detergent concentration effects on membrane protein stability in aqueous solutions.<sup>34</sup> At DDM concentrations below the CMC, hydrophobic interactions are dominating the colloidal stability of PDC. When the DDM is above the CMC, surfactant-surfactant interactions are dominating colloidal stability.

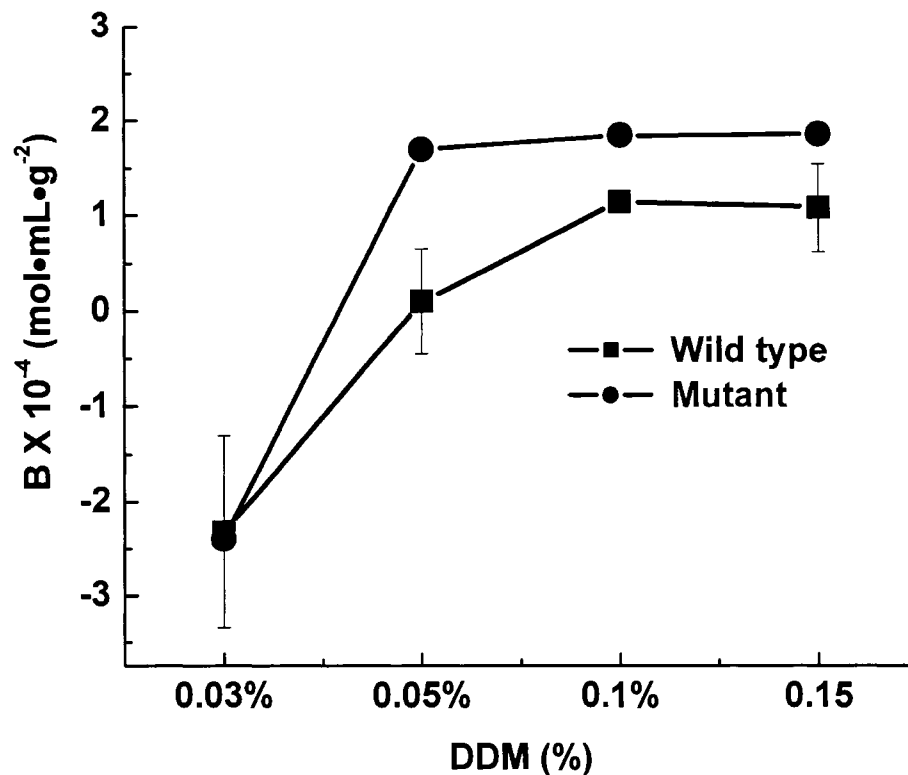


Figure 3.1.5. Measuring the change in magnitude and direction of B with increasing % of DDM. SIC conditions: Mobile phase: 20 mM MES, pH 7, flow rate: 0.1 mL/min, injection volume 1  $\mu\text{L}$ , wavelength 520 nm.

**3.5.5. Effects of pH.** The effects of pH on the physical stability of the PDC were measured by varying the solvent pH and % DDM for wild type and slow cycle mutant, Figure 3.1.6. For the slow cycle mutant, as pH increased from 3 to 8, B was between -5 to -3 ( $\pm 0.14$ )  $\times 10^{-4} \text{ mol mL g}^{-2}$  for DDM concentrations 0.03% and 0.04%. When solvent pH exceeded pH 8, B increased and fluctuated

between 0.5 and  $3 (\pm 0.14) \times 10^{-4} \text{ mol mL g}^{-2}$ , indicating the colloidal stability of the protein had been reached. When the concentration of DDM exceeded the CMC, no pH trend was observed and B values were between 0.5 to  $2 (\pm 0.07) \times 10^{-4} \text{ mol mL g}^{-2}$ . B was positive for pH 9 and 10 for the wild type pR, Figure 3.1.6. Unlike the slow cycle mutant, all DDM concentrations showed a similar trend in B between pH 7 and 10. Changing solvent conditions such as pH effected the physical stability of the PDC and the detergent micelles.<sup>15</sup> The size of the detergent micelle can be effect by changes in pH. Changes in the size of the PDC could prevent short-range attractive interactions, causing an increase in B.<sup>2,4,41</sup>

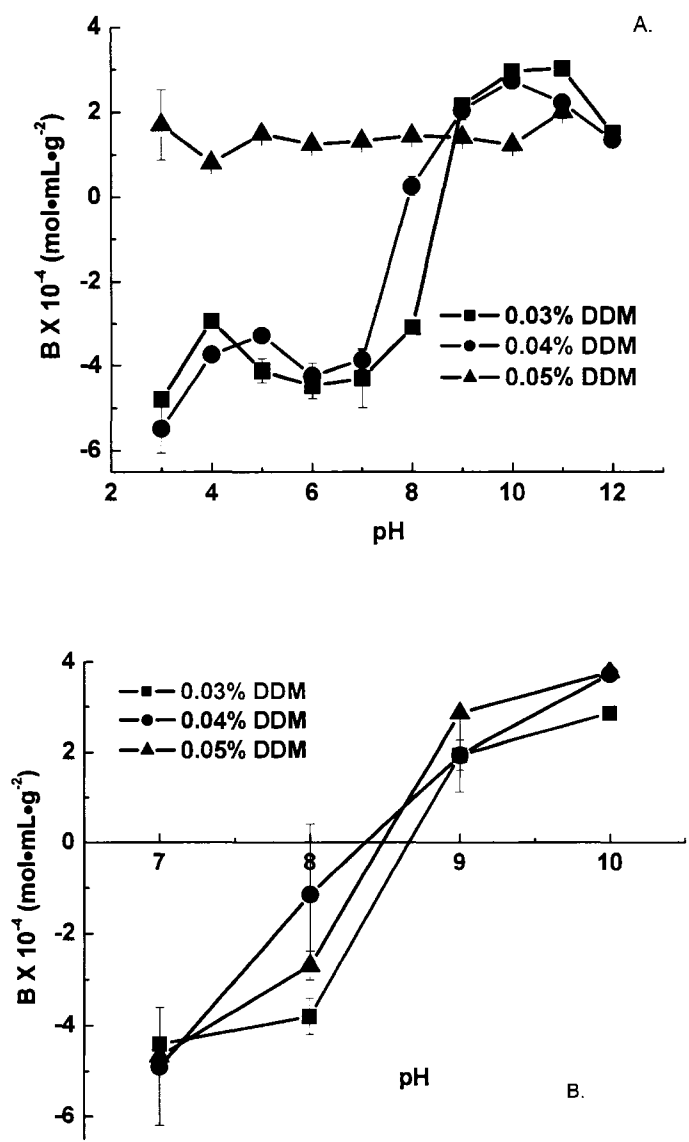


Figure 3.1.6. B was measured for mutant pR (A) and wild type pR (B) at various pH and detergent concentration using SIC Instrumental conditions: Mobile phase: 20mM TRIS, flow rate: 0.1 mL/min, injection volume 1  $\mu\text{L}$ , wavelength 520nm.

**3.5.6. Effects of Salt.** Salt type and concentration have a profound effect on the physical stability of proteins and membrane proteins. B of the PDC for the wild type and slow cycle mutant was analyzed at increasing concentrations of NaCl and K<sub>2</sub>HPO<sub>4</sub>, Figure 3.1.7. Changes in the physical stability for the slow cycle with increasing concentrations of NaCl from 0 M to 1.5 M resulted in a decrease in B from 3.5 (±0.01) to 1 (± 2.0) x (10<sup>-4</sup> x mol x mL x g<sup>-2</sup>), Figure 3.1.7. A similar trend in B was observed for increasing concentrations of K<sub>2</sub>HPO<sub>4</sub> from 0 M to 1.5 M, where B decreased from 5 (± 0.01) to 0.75 (± 0.01) x (10<sup>-4</sup> x mol x mL x g<sup>-2</sup>). The change in colloidal stability of the wild type pR was observed when the concentrations of both salts increased, reflected by an increase in B from -4 ± 5.7 X 10<sup>-4</sup> mol mL g<sup>-2</sup> to -0.1 ± 3.7 X 10<sup>-4</sup> mol mL g<sup>-2</sup> for NaCl and +1.5 ± 2.0 X 10<sup>-4</sup> mol mL g<sup>-2</sup> for K<sub>2</sub>HPO<sub>4</sub>, Figure 3.1.7.

The salt effects on the physical stability of a protein or PDC are dependent on the placement of the salt in the Hofmeister series, the salt concentration and the presence of detergent.<sup>2,4,11 41, 42</sup> Opposite trends in B were observed for the wild type and slow cycle mutant with increasing concentrations of salt. For the slow cycle mutant, a decrease in B was measured with increasing concentrations of both NaCl and K<sub>2</sub>HPO<sub>4</sub>. With other detergent systems, increasing salt concentrations increases the size and shape of the PDC, resulting in a change in physical stability.<sup>2,4,11,41,42</sup> When comparing the trends in magnitude and direction of B for both forms of pR,

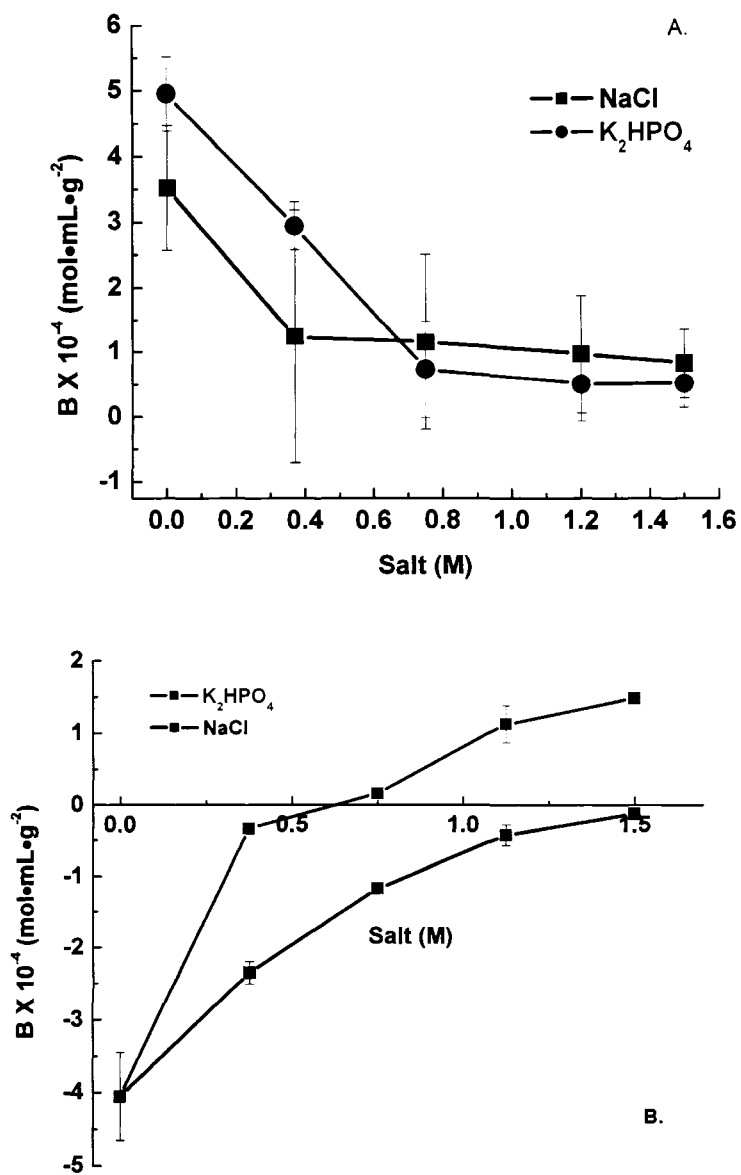


Figure 3.1.7. B measurements for mutant (A) and wild-type pR (B) at various concentrations of NaCl and K<sub>2</sub>HPO<sub>4</sub> using SIC. Instrumental conditions: mobile phase pH 9, 20 mM MES, flow rate 0.1 mL/min, injection volume 1  $\mu$ L, wavelength 520 nm.

what is apparent is that trends in the physical stability are dominated by PDC and not the salt.

**3.5.7. Denaturing pR with SDS.** The conformational stability of pR was measured by measuring the absorbance of the retinal.<sup>23</sup> pR in its native conformation absorbs at 280 nm and 531 nm in pH 7, 20 mM MES, 0.05% DDM, Figure 3.1.8.<sup>23</sup> The amino acids Phe, Tyr and Trp absorb at 280 nm, the attached retinal absorbs at 531 nm, while the free retinal absorbs at 381 nm. pR denatures as the concentration of SDS increased from 0 to 10 mM, causing a loss of red color, Figure 3.1.9, shown by the decrease in absorption at 531 nm. For pR as the concentration of SDS increased from 0 to 10 mM the absorbance at 531 nm decreased from 0.2 to 0 AU, while the absorbance of 381 nm increased from 0 to 0.15 abs, Figure 3.1.9. For the attached retinal a decrease in absorbance at 531 nm was observed in 5mM of SDS, Figure 3.1.8. shows pR is completely denatured. The change in intensity of the retinal at 531 and 381 nm as membrane protein denatures is also observed with bR.

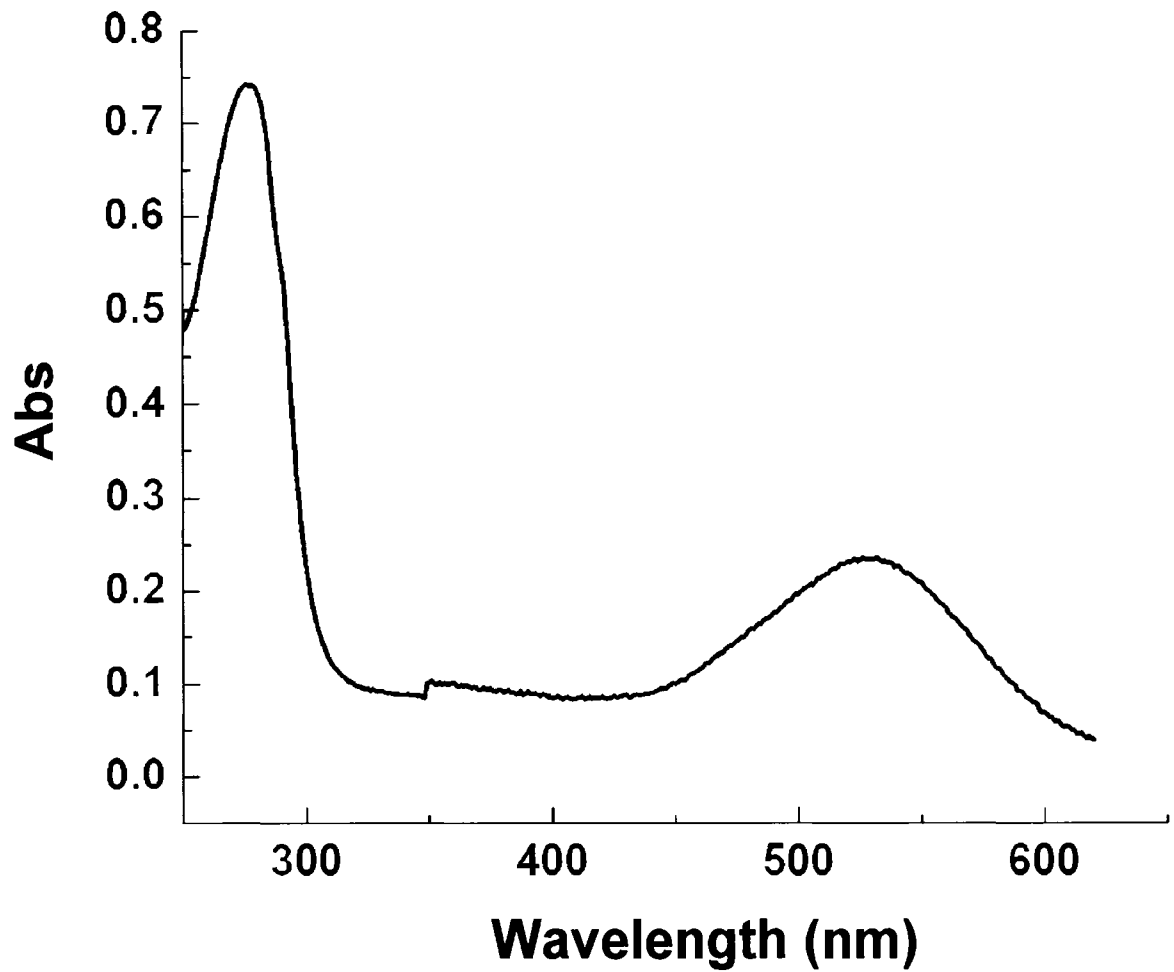


Figure 3.1.8. pR in its native conformation absorbs at 280 nm and 531 nm in pH 7, 20 mM MES, 0.05% DDM (A). As the concentration of SDS increases from 0 to 10mM, pR loses its native conformation by the change in color.

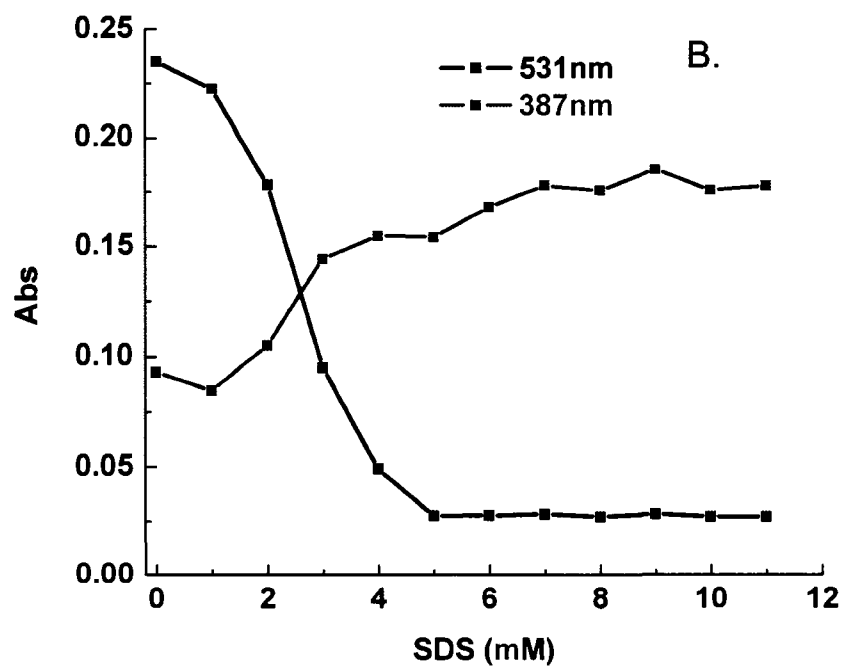
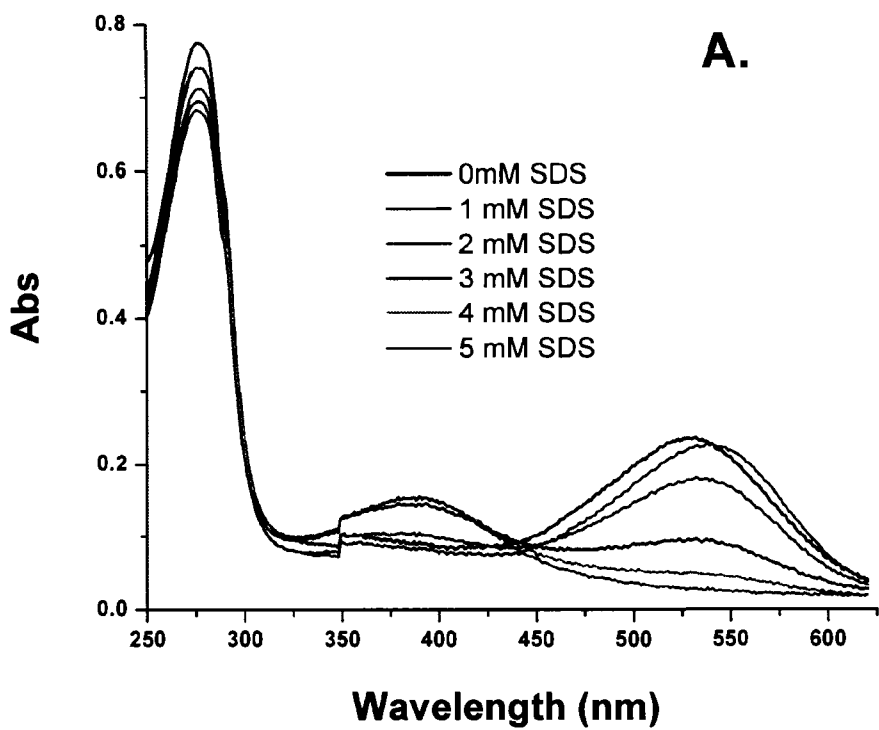


Figure 3.1.9. The spectrum of PR denaturing (A) and trending the absorbance of 531 and 387 nm (B) in pH 7, 20 mM MES, 0.05% DDM (A).

**3.5.8. Conformational Stability of pR.** Changes in the native structure of pR for each screening condition were monitored by measuring the absorbance of the retinal at 531 and 381 nm.<sup>23</sup> The data collected for the absorbance at 531 nm for each screening condition is presented as a contour plot, Figure 3.1.10. In the first screening study, the absorbance at 531 nm was measured for concentrations of Tween 20 and DDM ranging from 0.08 to 0.34 mM and 0.00 to 0.09 mM respectively, Figure 3.1.10.A. Two lines that represent the CMC of the detergents divide the contour plot; the horizontal line is the CMC of Tween 20 (0.06 mM) and the vertical line is the CMC of DDM (0.17 mM). The contour plot shows three areas of significant change at 531 nm. Absorbance of 531 nm is at a minimum in the lower left corner of the contour plot where the concentration of the DDM is below the CMC. The second minimum at 531 nm is on the right hand side of the contour plot when DDM is above the CMC and Tween 20 is below the CMC. Lastly, there is a maximum when Tween-20 is above the CMC at all concentrations of DDM. The conformation of pR was measured in the presence of increasing concentration of CHAPS, Tween 20, and DDM as shown in Figure 3.1.10 B and C. No significant change in the absorbance at 531 nm was measured for either system. The absorbance of the retinal fluctuated between 0.07 to 0.09 AU, Figure 3.1.10 B and C.

Both the detergent type and concentration can affect conformational stability of pR. When two nonionic detergents are mixed the conformational stability is dependent on detergent concentration. When the concentration of Tween 20 is

below the CMC, stability of the pR is dependent on the concentration of DDM. If concentration of DDM is below the CMC, not enough detergent molecules are available to stabilize the membrane protein by shielding the hydrophobic area from the solvent. The data shows when DDM is above the CMC and Tween 20 is below the CMC, the membrane protein is not completely stabilized. This might be due to Tween 20 preventing the DDM from completely covering the hydrophobic area of the membrane protein by steric effects. For a zwitterionic versus nonionic systems the zwitterionic detergent dominates the conformational stability of pR.

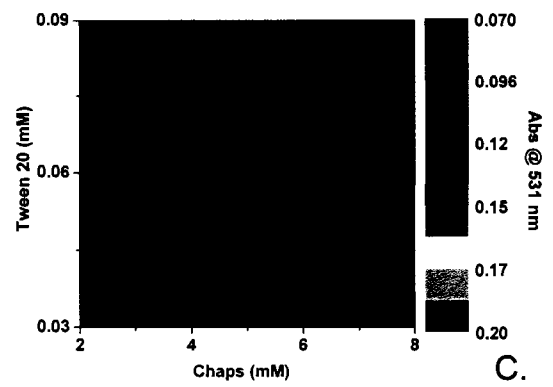
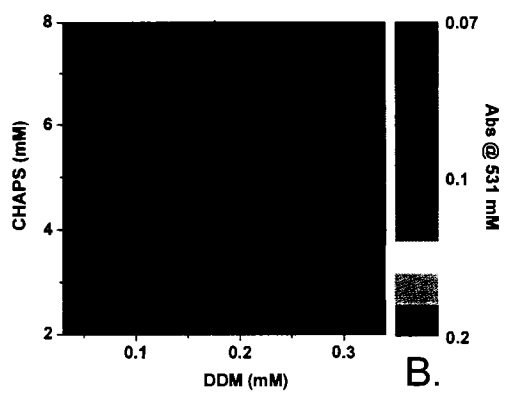
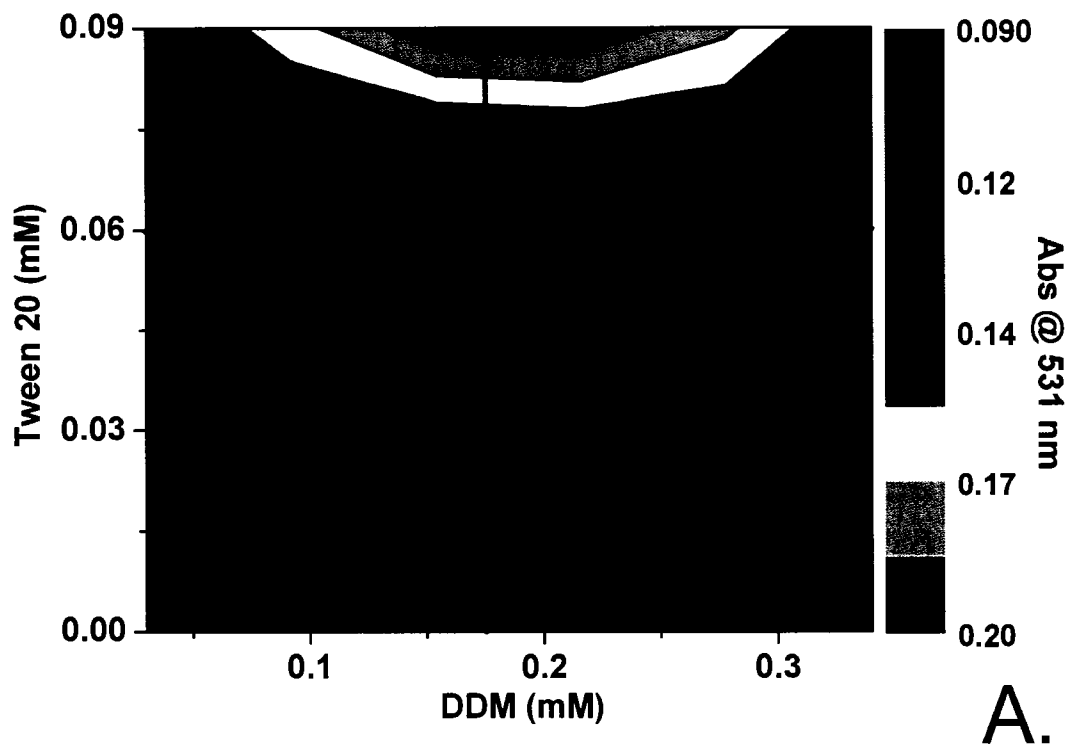


Figure 3.1.10. Conformational Stability of pR measured by changes of the retinal absorbance at 531 nm, (A) DDM vs tween 20, DDM vs Chaps (B) and Chaps vs Tween 20 (C) in pH 7 and 20 mM MES.

**3.5.9. Measuring B for Mixed Detergent Systems.** The effects of a mixed detergent system on the colloidal stability of pR were evaluated by SIC. Figure 3.1.11. shows the contour plot of B for pR in three different detergent mixtures DDM, Tween 20 and CHAPS, at pH 7 and 20 mM MES. The first screening experiment measured B at different concentrations of DDM (0.30 to 0.37 mM) without Tween 20 and CHAPS present in the buffer system, Figure 3.1.11.A. The data shows an improvement in the colloidal stability of pR with increasing DDM concentrations from 0.08 to 0.37 mM. B increased from  $-26$  to  $4.6 \times 10^{-4} \text{ mol mL g}^{-2}$ , under the same conditions similar to past experiments, Figure 3.1.5. When Tween 20 was added to the buffer with DDM, B values fluctuated between  $-3.0$  to  $+0.7 \times 10^{-4} \text{ mol mL g}^{-2}$ . In Figure 3.1.11B and C, the addition of CHAPS versus DDM and Tween 20 resulted in no significant change in B, which stayed in the range between  $-3$  to  $0.7 \times 10^{-4} \text{ mol mL g}^{-2}$ . When pR is in the presence of a two different detergents, B does not significantly change when the concentration of either detergent is below the CMC.

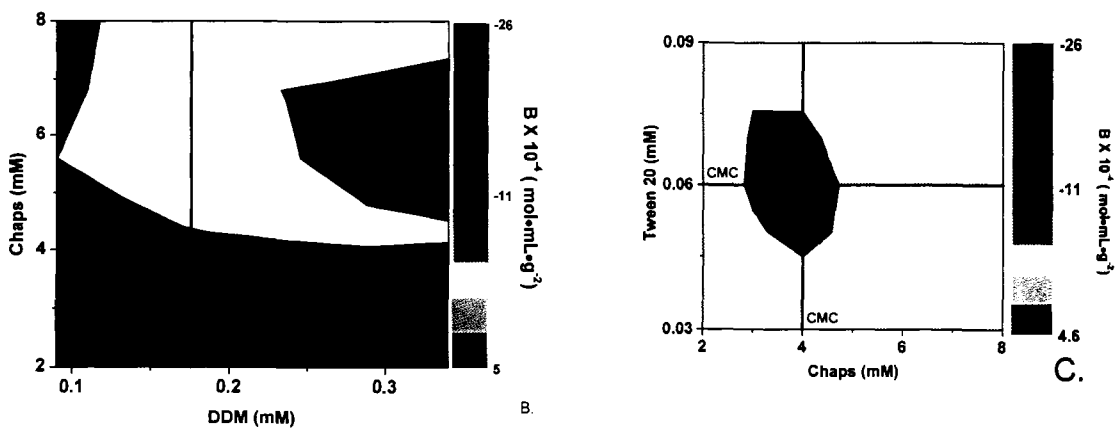
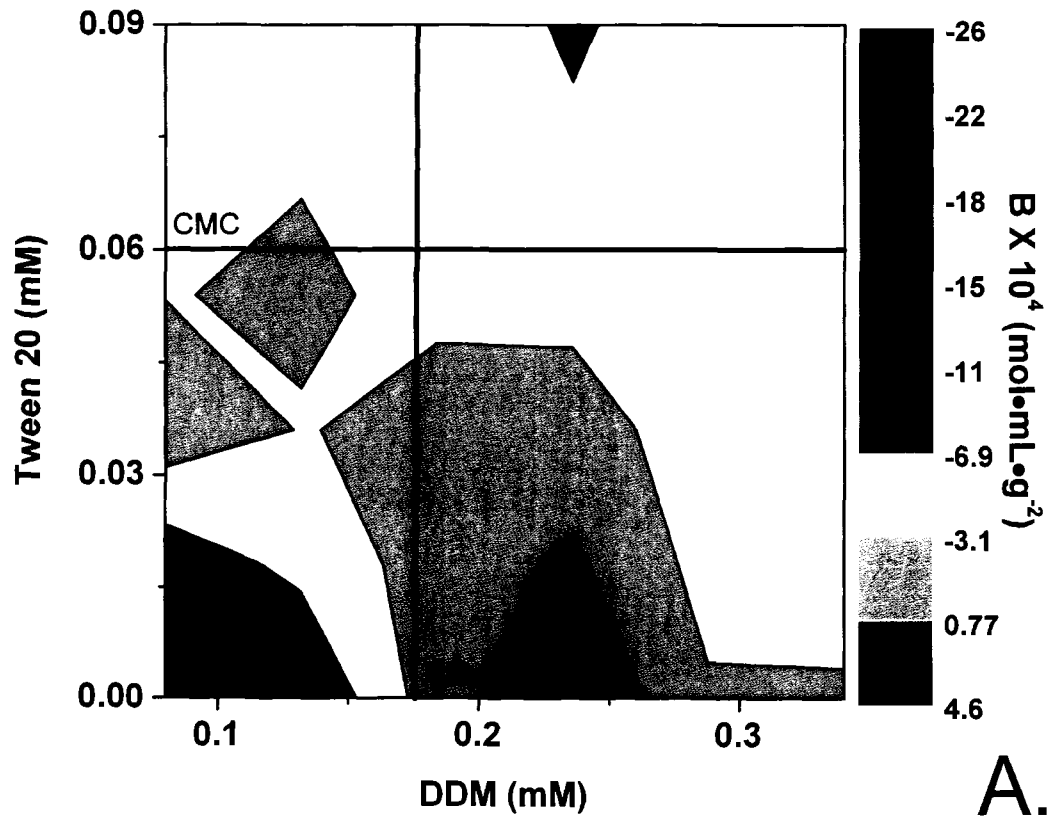


Figure 3.1.11. Colloidal Stability of pR measured by changes in B, (A) DDM vs Tween 20, DDM vs Chaps (B) and Chaps vs Tween 20 (C) in pH 7 and 20 mM MES.

**3.5.10. Detecting Detergent Micelles.** Previous studies have demonstrated the correlation between improved colloidal stability of membrane proteins and presence of detergent micelles.<sup>43-47</sup> Data shows that colloidal stability of a membrane protein is achieved when the concentration of the detergent is greater than the CMC.<sup>6, 24, 25</sup> Detergent micelles are formed when the concentration of the detergent exceeds the CMC. CMC can be altered by the presence of additives (salt, pH, organic and lipids) and temperature. For this reason the presence of the micelles was measured for each experimental conditions. Detergent CMC is measured by two methods. The first method measures changes in the concentration of detergent monomer by changes in surface tension and solution conductivity.<sup>43-47</sup> The second method detects the presence of micelles in solution by light scattering and/or dye adsorption.<sup>43-47</sup> Here, the dye absorption was used for detecting micelles at each condition.

Dye absorption detects the micelles by shifts in  $\lambda_{\max}$  of the dye in the visible range. When the concentration of detergent is below the CMC,  $\lambda_{\max}$  would be similar to the absorbance of the dye dissolved in the aqueous solution. When the concentration of the detergent is greater than CMC, the dye is absorbed into the hydrophobic core of the micelles causing a shift in  $\lambda_{\max}$  to longer wavelengths. The shifted  $\lambda_{\max}$  would be similar to the absorbance of the dye dissolved in the hydrocarbon solvent. The dye used to detect the micelles in a two detergent system was Evans Blue, Figure 3.1.12. Figure 3.1.12. shows the shift in  $\lambda_{\max}$  of Evans Blue when the concentration of the three detergents were twice as high

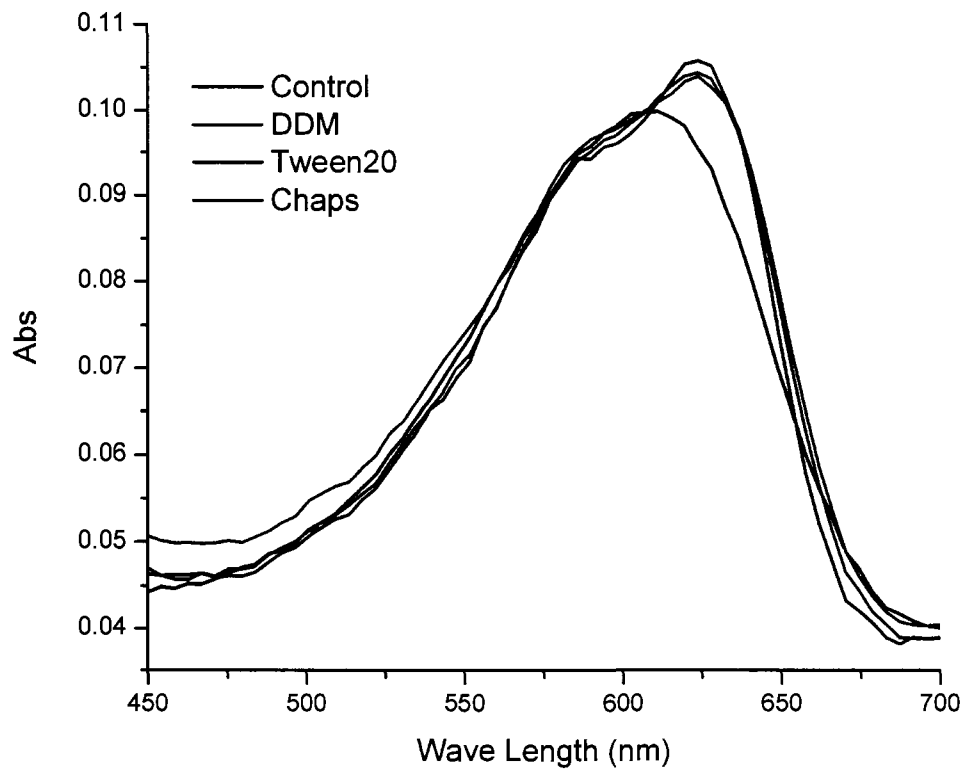


Figure 3.1.12. Evans Blue shift in wavelength maximum caused by the presence of the micelles at pH 7, 20 mM MES.

as the CMC. The control for the experiment was the dye dissolved in pH 7, 20 mM MES containing no detergent with a measured  $\lambda_{\max}$  of 614 nm. When the dye was dissolved in the three detergents above the CMC the  $\lambda_{\max}$  shifted to 628 nm, indicating the presence of micelles.

Evans Blue at a concentration of  $1 \times 10^{-5}$  M was added to each screening condition and samples were allowed to equilibrate for 24 hours. Following equilibration, the spectrum was collected from 450 to 700 nm and  $\lambda_{\max}$  was determined. The shift in the  $\lambda_{\max}$  for the DDM vs Tween 20 is shown in Figure 3.1.13.A. The contour plot indicates the presence of the micelles above 0.2 mM DDM and 0.06 mM Tween 20. At 0.03 DDM and no Tween 20 no micelles are detected which is in agreement with reported value of DDM CMC of 0.17 mM. Figure 3.1.13. B shows the change in  $\lambda_{\max}$  for DDM vs CHAPS, the wavelength is above the control, indicating the presence of the micelles. While  $\lambda_{\max}$  for Tween 20 vs CHAPS indicates that no micelles are in solution below the CMC of the both detergents.

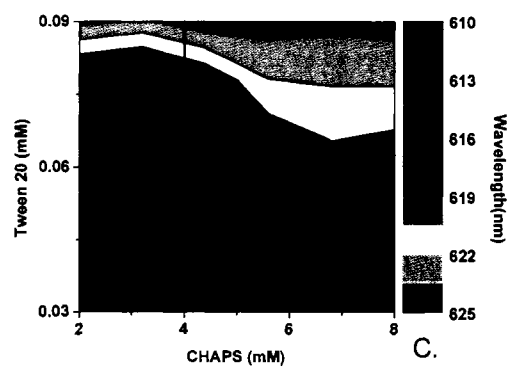
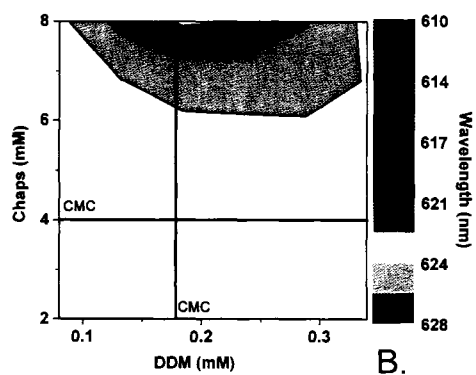
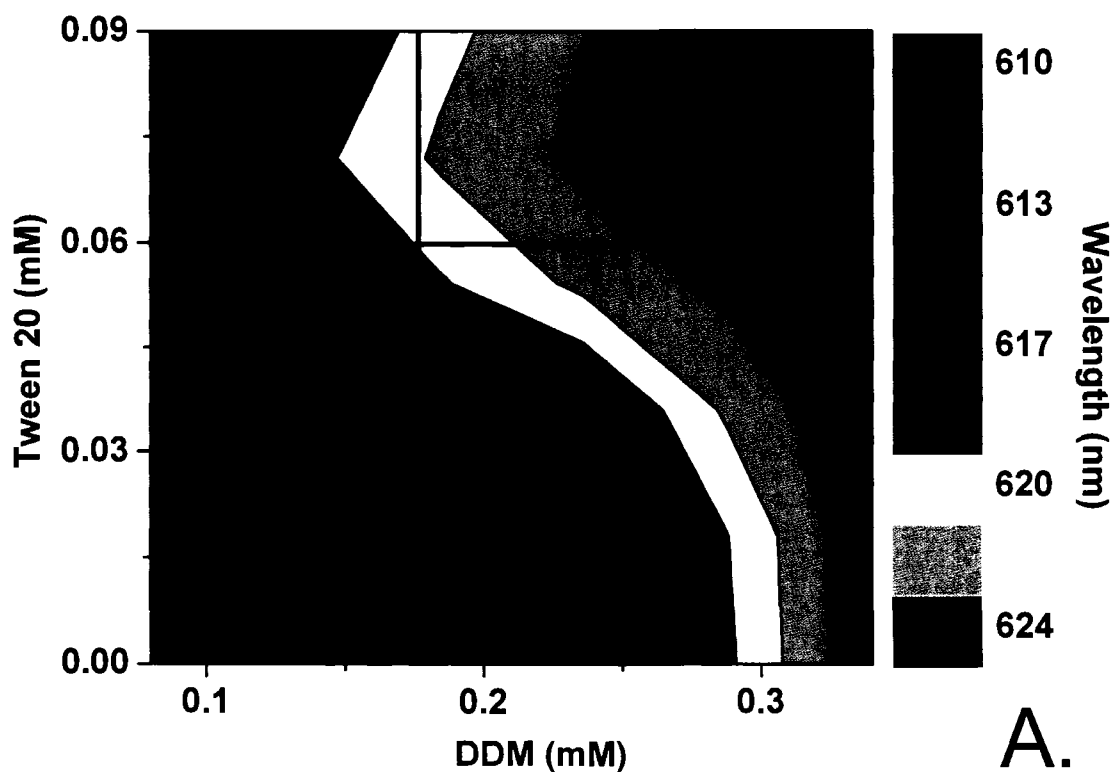


Figure 3.1.13. Shifts in wavelength caused by formation of Micelles, (A) DDM vs Tween 20, DDM vs Chaps (B) and Chaps vs Tween 20 (C) in pH 7 and 20 mM MES.

**3.6.1. Conclusion.** B was used to measure changes in the direction and magnitude of the physical stability of pR while varying co-solvent type and concentration. The data presented here indicates the physical stability of pR is dependent on the membrane protein, pH, and detergent type. Additionally, for the first time SIC was used to measure the difference between a mutant and a wild type of a membrane protein. The data presented in this paper shows the importance of the solvent system on physical stability of PDC. Using SIC to measure the changes in B for membrane proteins is an alternative to current methods used for screening solvent-cosolvent systems and could help to maximize physical stability for improved yields during purification.

This chapter demonstrated the affects of a two detergent system on the conformational and colloidal stability of pR. The detergents chosen for these screening experiments were based on the differences in detergent head group and length of the hydrophobic tail. DDM is a mild detergent used to extract pR from the cell membrane and is commonly used in biology because of its ability to stabilize the conformation of a membrane protein. Tween 20 an nonionic detergent has been used to stabilize the bR and other membrane proteins.<sup>48</sup> The two systems investigated were nonionic verses nonionic and nonionic verses zwitterionic where the conformational and colloidal stability were measured by UV and SIC. The data sets show little agreement between changes in colloidal and conformational stability for Tween 20 vs DDM. Comparing the colloidal and CMC pf pR the data sets agree with effects of detergent concentration for tween

20 vs DDM. Below the CMC of both detergents the colloidal stability is at a minimum, when the concentration exceeds the CMC of either detergent, causes an increase in the protein-solvent interactions. Changing detergent concentration does not effect conformational and colloidal stability of the pR when CHAPS was added.

### 3.7. References.

1. Beja, O.; Spudich, E. N.; Spudich, J. L.; Leclerc, M.; DeLong, E. F., Proteorhodopsin phototrophy in the ocean. *Nature* **2001**, 411, (6839), 786-789.
2. Loll, P. J.; Allaman, M.; Wiencek, J., Assessing the role of detergent-detergent interactions in membrane protein crystallization. *Journal of Crystal Growth* **2001**, 232, (1-4), 432-438.
3. Garavito, R. M.; Picot, D.; Loll, P. J., Strategies for crystallizing membrane proteins. *Journal of Bioenergetics and Biomembranes* **1996**, 28, (1), 13-27.
4. Berger, B. W.; Gendron, C. M.; Robinson, C. R.; Kaler, E. W.; Lenhoff, A. M., The role of protein and surfactant interactions in membrane-protein crystallization. *Acta Crystallographica Section D-Biological Crystallography* **2005**, 61, 724-730.
5. Columbus, L.; Lipfert, J.; Klock, H.; Millett, I.; Doniach, S.; Lesley, S. A., Expression, purification, and characterization of *Thermotoga maritima*

- membrane proteins for structure determination. *Protein Science* **2006**, 15, (5), 961-975.
6. Garavito, R. M.; Ferguson-Miller, S., Detergents as tools in membrane biochemistry. *Journal of Biological Chemistry* **2001**, 276, (35), 32403-32406.
  7. Niegowski, D.; Hedren, M.; Nordlund, P.; Eshaghi, S., A simple strategy towards membrane protein purification and crystallization. *International Journal of Biological Macromolecules* **2006**, 39, (1-3), 83-87.
  8. Eshaghi, S.; Hedren, M.; Nasser, M. I. A.; Hammarberg, T.; Thornell, A.; Nordlund, P., An efficient strategy for high-throughput expression screening of recombinant integral membrane proteins. *Protein Science* **2005**, 14, (3), 676-683.
  9. Loll, P. J., Membrane protein structural biology: the high throughput challenge. *Journal of Structural Biology* **2003**, 142, (1), 144-153.
  10. Wilson, W. W., Light scattering as a diagnostic for protein crystal growth - A practical approach. *Journal of Structural Biology* **2003**, 142, (1), 56-65.
  11. Berger, B. W.; Garcia, R. Y.; Lenhoff, A. M.; Kaler, E. W.; Robinson, C. R., Relating surfactant properties to activity and solubilization of the human adenosine A(3) receptor. *Biophysical Journal* **2005**, 89, (1), 452-464.
  12. Ko, J. S.; Oh, S. W.; Kim, K. W.; Nakashima, N.; Nagadome, S.; Sugihara, G., Blending effects on adsorption and micellization of different membrane protein solubilizers: A thermodynamic study on three mixed systems of

- CHAPS with MEGA-8,-9 and-10 in pH 7.2 phosphate buffer solution. *Colloids and Surfaces B-Biointerfaces* **2005**, 45, (2), 90-103.
13. Wiener, M. C.; Snook, C. F., The development of membrane protein crystallization screens based upon detergent solution properties. *Journal of Crystal Growth* **2001**, 232, (1-4), 426-431.
  14. Lesley, Expression, Purification and Characterization of Thermotoga Maritima Membrane Proteins for Structural Determination. **2007**.
  15. Loll, P. J.; Hitscherich, C.; Aseyev, V.; Allaman, M.; Wiencek, J., Assessing micellar interaction and growth in detergent solutions used to crystallize integral membrane proteins. *Crystal Growth & Design* **2002**, 2, (6), 533-539.
  16. Hitscherich, C.; Aseyev, V.; Wiencek, J.; Loll, P. J., Effects of PEG on detergent micelles: implications for the crystallization of integral membrane proteins. *Acta Crystallographica Section D-Biological Crystallography* **2001**, 57, 1020-1029.
  17. Hitscherich, C.; Kaplan, J.; Allaman, M.; Wiencek, J.; Loll, P. J., Static light scattering studies of OmpF porin: Implications for integral membrane protein crystallization. *Protein Science* **2000**, 9, (8), 1559-1566.
  18. Manning, M. C.; Patel, K.; Borchardt, R. T., Stability of Protein Pharmaceuticals. *Pharmaceutical Research* **1989**, 6, (11), 903-918.
  19. Chi, E. Y.; Krishnan, S.; Randolph, T. W.; Carpenter, J. F., Physical stability of proteins in aqueous solution: Mechanism and driving forces in

- nonnative protein aggregation. *Pharmaceutical Research* **2003**, 20, (9), 1325-1336.
20. Stowell, M. H. B.; Rees, D. C., Structure and Stability of Membrane-Proteins. *Advances in Protein Chemistry, Vol 46* **1995**, 46, 279-311.
21. Lund, S.; Orłowski, S.; Deforesta, B.; Champeil, P.; Lemaire, M.; Moller, J. V., Detergent Structure and Associated Lipid as Determinants in the Stabilization of Solubilized Ca<sup>2+</sup>-Atpase from Sarcoplasmic-Reticulum. *Journal of Biological Chemistry* **1989**, 264, (9), 4907-4915.
22. Delrio, E.; Gonzalezmanas, J. M.; Gurtubay, J. I. G.; Goni, F. M., On the Mechanism of Bacteriorhodopsin Solubilization by Surfactants. *Archives of Biochemistry and Biophysics* **1991**, 291, (2), 300-306.
23. LAM, E.; Packer, L., Non-Ionic Detergent Effects on Spectroscopic Characteristics and the Photocycle of Bacteriorhodopsin in Purple Membranes. *Archives of Biochemistry and Biophysics* **1983**, 221, (2), 557-564.
24. Jones, M. N., Surfactants in membrane solubilisation. *International Journal of Pharmaceutics* **1999**, 177, (2), 137-159.
25. Gohon, Y.; Popot, J. L., Membrane protein-surfactant complexes. *Current Opinion in Colloid & Interface Science* **2003**, 8, (1), 15-22.
26. Valente, J. J.; Payne, R. W.; Manning, M. C.; Wilson, W. W.; Henry, C. S., Colloidal behavior of proteins: Effects of the second virial coefficient on solubility, crystallization and aggregation of proteins in aqueous solution. *Current Pharmaceutical Biotechnology* **2005**, 6, (6), 427-436.

27. Haas, C.; Drenth, J.; Wilson, W. W., Relation between the solubility of proteins in aqueous solutions and the second virial coefficient of the solution. *Journal of Physical Chemistry B* **1999**, 103, (14), 2808-2811.
28. Guo, B.; Kao, S.; McDonald, H.; Asanov, A.; Combs, L. L.; Wilson, W. W., Correlation of second virial coefficients and solubilities useful in protein crystal growth. *Journal of Crystal Growth* **1999**, 196, (2-4), 424-433.
29. George, a.; Wilson, W. W., Predicting Protein Crystallization from a Dilute-Solution Property. *Acta Crystallographica Section D-Biological Crystallography* **1994**, 50, 361-365.
30. Fernandez, C.; Hilty, C.; Wider, G.; Wuthrich, K., Lipid-protein interactions in DHPC micelles containing the integral membrane protein OmpX investigated by NMR spectroscopy. *Proceedings of the National Academy of Sciences of the United States of America* **2002**, 99, (21), 13533-13537.
31. Odahara, T., Stability and solubility of integral membrane proteins from photosynthetic bacteria solubilized in different detergents. *Biochimica Et Biophysica Acta-Biomembranes* **2004**, 1660, (1-2), 80-92.
32. Tanford, C.; Reynolds, J. a., Characterization of Membrane Proteins in Detergent Solutions. *Biochimica Et Biophysica Acta* **1976**, 457, (2), 133-170.
33. Lundstrom, K., Structural genomics on membrane proteins: Mini review. *Combinatorial Chemistry & High Throughput Screening* **2004**, 7, (5), 431-439.

34. Seddon, A. A.; Curnow, P.; Booth, P. J., Membrane proteins, lipids and detergents: not just a soap opera. *Biochimica Et Biophysica Acta-Biomembranes* **2004**, 1666, (1-2), 105-117.
35. Prive, G. G., Detergents for the stabilization and crystallization of membrane proteins. *Methods* **2007**, 41, (4), 388-397.
36. Plant, a. L.; Locasciobrown, L.; Haller, W.; Durst, R. a., Immobilization of Binding-Proteins on Nonporous Supports - Comparison of Protein Loading, Activity, and Stability. *Applied Biochemistry and Biotechnology* **1991**, 30, (1), 83-98.
37. Smith, P. K.; Krohn, R. I.; Hermanson, G. T.; Mallia, a. K.; Gartner, F. H.; Provenzano, M. D.; Fujimoto, E. K.; Goeke, N. M.; Olson, B. J.; Klenk, D. C., Measurement of Protein Using Bicinchoninic Acid. *Analytical Biochemistry* **1985**, 150, (1), 76-85.
38. Berger, B.; Gendron, C.; Stant, M.; Kaler, E.; Robinson, C.; Lenhoff, A., Exploring the roles of protein and surfactant interactions in membrane protein crystallization. *Biophysical Journal* **2004**, 86, (1), 97A-97A.
39. Valente, J. J.; Verma, K. S.; Manning, M. C.; Wilson, W. W.; Henry, C. S., Second virial coefficient studies of cosolvent-induced protein self-interaction. *Biophysical Journal* **2005**, 89, (6), 4211-4218.
40. Sivals, U.; Tjerneld, F., Mechanisms of phase behaviour and protein partitioning in detergent/polymer aqueous two-phase systems for purification of integral membrane proteins. *Biochimica Et Biophysica Acta-General Subjects* **2000**, 1474, (2), 133-146.

41. Bianco, C.; Schneider, C. S.; Lenhoff, A. M.; Kaler, E. W., Surfactant effects on the unfolding of a beta-barrel integral membrane protein. *Biophysical Journal* **2007**, 4A-4A.
42. Curtis, R. A.; Lue, L., A molecular approach to bioseparations: Protein-protein and protein-salt interactions. *Chemical Engineering Science* **2006**, 61, (3), 907-923.
43. Suzuki, H., Determination of Critical Micelle Concentration of Surfactant by Ultraviolet Absorption Spectra. *Journal of the American Oil Chemists Society* **1970**, 47, (8), 273-&.
44. Corrin, M. L.; Harkins, W. D., Determination of the Critical Concentration for Micelle Formation in Solutions of Colloidal Electrolytes by the Spectral Change of a Dye. *Journal of the American Chemical Society* **1947**, 69, (3), 679-683.
45. Garcia, M. E. D.; Sanzmedel, a., Dye Surfactant Interactions - a Review. *Talanta* **1986**, 33, (3), 255-264.
46. Anacker, E. W., Modeling Dye Surfactant Interactions. *Journal of Colloid and Interface Science* **1994**, 164, (1), 54-62.
47. Cabral, J. P. S.; Smith, a. R. W., Determination of the Critical Micelle Concentration of Dodecylguanidine Monoacetate (Dodine). *Journal of Colloid and Interface Science* **1992**, 149, (1), 27-33.
48. Dencher, N. a.; Heyn, M. P., Formation and Properties of Bacteriorhodopsin Monomers in Nonionic Detergents Octyl-Beta-Glucoside and Triton X-100. *Febs Letters* **1978**, 96, (2), 322-326.

## 4. Small Scale SIC

**4.1. Introduction.** This chapter discusses miniaturization of the SIC method from conventional scale columns to miniaturized columns, for the purpose of decreasing protein consumption to less than 1 mg of protein. By shortening the column the amount of protein consumed is decreased, allowing B measurements to be performed on proteins on early stage therapeutic proteins, peptides and membrane proteins. Additionally, the cost of co-solvents used for SIC screening studies can prohibit the measurement of B, especially when co-solvents are biological detergents used for stabilizing membrane proteins.

This chapter presents data that was collected in our work to miniaturize the SIC column. The small scale system that was assembled could accurately pump less than 30  $\mu\text{L}/\text{min}$  and inject volumes of 0.5  $\mu\text{L}$  reproducibly. The new system made it possible to accurately measure changes in magnitude and direction of B for lysozyme using a miniaturized SIC column with a volume less than 0.1  $\mu\text{L}$ . When comparing the magnitude and direction of B for lysozyme generated on conventional scale SIC and SLS to a miniaturized SIC column, no significant difference between the data sets were observed. The development of the miniaturized SIC column, small scale instrumentation and accompanying software made it possible to measure B as discussed Chapters 3 and 5.

### 4.2. Methods and Materials

**4.2.1. Reagents and Chemicals.** The following chemicals and materials were used as received for these experiments: hydrochloric acid, ethanolamine, sodium hydroxide, sodium chloride, and sodium acetate (Fisher). Chromatography particles (Toyopearl AF-Formyl-650M) were purchased from Supelco (Sigma-Aldrich). Sodium cyanoborohydride and ethanolamine were purchased from Sigma-Aldrich. The amount of protein immobilized on the particles was measured by BCA and supplied by Pierce. Lysozyme was used as received from Sigma with no additional purification.

**4.2.2. Column Preparation.** Lysozyme was immobilized onto chromatography particles in coupling buffer composed of 0.1 M  $K_2HPO_4$  pH 7.5 adjusted with concentrated sodium hydroxide. In a clean 1.5 mL eppendorf tube, 250  $\mu$ L of AF-Formyl-650M particles were rinsed three times with 0.1 M  $K_2HPO_4$  pH 7.5 buffer. After each rinsing the tube was centrifuged and particles were allowed to settle. Lysozyme (8mg/mL) was added to the washed particles along with 10 mg of sodium cyanoborohydride and the mixture was agitated over night at 22°C. After protein immobilization the particles were rinsed three times with coupling buffer, followed by the addition 1 M ethanolamine and 10 mg of sodium cyanoborohydride. The mixture was then agitated for 4 hours at 22°C. Ethanolamine was removed by three rinses of coupling buffer and the particles were stored at 4°C in coupling buffer. The amount of protein immobilized onto the AF-Formyl-650M particles was quantified using the BCA method as discussed previously.

**4.2.3. Column Construction.** The conventional scale column was constructed from PEEK tubing with an inner diameter (ID) of 1.0 mm x 10 to 20 cm and capped with a 2  $\mu\text{m}$  frit. The miniaturized SIC column was composed of FEP tube with an ID of 0.75 mm x 5 cm and capped with a 2  $\mu\text{m}$  frit.

**4.2.4. Measuring Protein Concentration by BCA.** The BCA procedure outlined by Pierce was followed for the calibration curve and sample measurements. The following changes were made, the particles are removed and allowed to settle in the pipette tip to determine particle volume. The particles were added to the working reagent and diluted to 0.1 mL. The sample, blank, and unmodified, particles were prepared and the protein concentration was measured.

**4.2.5. Conventional Scale LC.** LC experiments were performed on a HP1050 system equipped with a HP1050 auto sampler, HP1050 ternary gradient pump and 1050 DAD detector. Parameters used for detection of lysozyme are as follows: flow rate and injection volume varied for each experiment and detection wavelength was set to 280 nm. The lysozyme-modified column was equilibrated for 30 min between conditions to ensure that the immobilized protein was in the same state as the mobile phase protein. For each condition, 3% (v/v) acetone was injected three times as a non-retained marker to check column integrity, followed by four injections of lysozyme.

Dead column experiments using AF-Formyl-650M particles capped with ethanolamine followed the same procedures as the live column experiments. Dead column experiments were used to determine dead volume marker ( $t_m$ ) for the live column using a ratio of the retention time of protein measured on the dead column ( $t_{pro\_dead}$ ), and the retention time of the acetone measured on the dead column ( $t_{ace\_dead}$ ), according to previously published protocols.<sup>3</sup>

**4.2.6. Small Scale LC.** LC experiments were performed using a Harvard syringe pump (PHD 4400), rheodyne 0.5  $\mu$ L manual injector and a SSI 500 UV/Vis detector. The LC parameters used for the analysis of lysozyme were flow rate 20  $\mu$ L/min, 0.5  $\mu$ L injection and wavelength set to 280 nm. Data was collected using National Instruments USB 6009 and Labview 8. The chromatographic data was processed and analyzed using Origin version 8, example of a data set is shown in Figure 4.1.1. Labview 8 was programmed for the purpose of data collection for the small scale SIC experiments. The Labview 8 program was used to monitor the voltage from the UV/VIS and resistance from a magnetic sensor attached to the arm of the manual injector. The change in the resistance from the magnetic sensor signals the injection of the sample on to the column.

The lysozyme column was equilibrated for 20 minutes between conditions and pR was equilibrated for 40 minutes. To check column integrity and adjust for solvent viscosity 3% acetone was injected as a non-retained marker. After the

analysis of acetone, three to six replicates of protein were injected for each experimental condition.

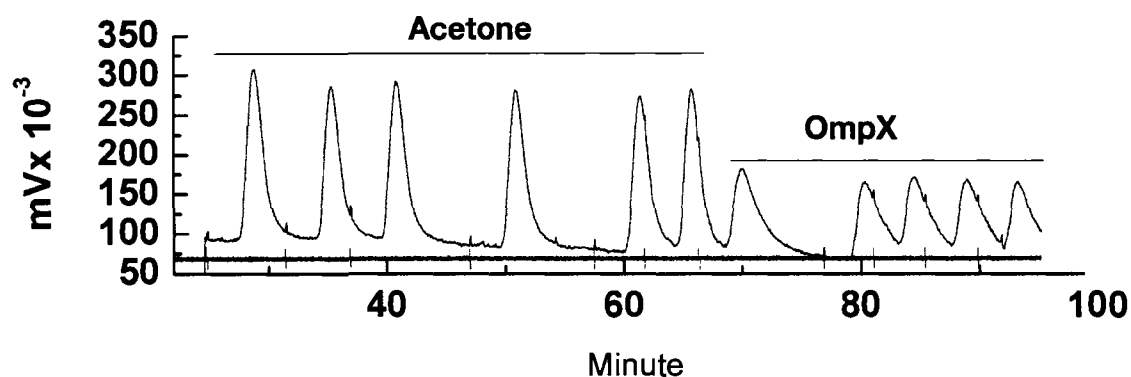


**Figure 4.1.1.** Example of chromatogram collected off of the small scale SIC, black line is UV data of acetone and OmpX, red line is 2<sup>nd</sup> derivative of the signal from injector where a negative inflection indicates sample injection.

### 4.3. Results and Discussion

**4.3.1. Effects of Flowrate on B.** The first set of experiments was to characterize the effects of flow on B at repulsive and attractive conditions using the conventional SIC column. On a standard HPLC, B was measured for lysozyme at different concentrations of NaCl ranging from 0 to 1 M, while increasing the flowrate from 0.1 to 0.4 mL/min, Figure 4.1.2. When no NaCl was added to the buffer, B values fluctuated around  $5.2 \times 10^{-4}$  mL mol g<sup>-2</sup> as the flow rate increased. At 0.5 M NaCl, the magnitude of B increased with increasing flow rate, beginning at  $-11 \times 10^{-4}$  mL mol g<sup>-2</sup> for 0.1 mL/min and increased to  $-9 \times 10^{-4}$  mol mL g<sup>-2</sup> for 0.4 mL/min. When the concentration of NaCl was increased to 1 M the magnitude of B increased with increasing flow rate starting at  $-35 \times 10^{-4}$  mol mL g<sup>-2</sup> for 0.1 mL/min and ending at  $-30 \times 10^{-4}$  mol mL g<sup>-2</sup> for 0.4 mL/min. As shown

in previous chapters, the magnitude of B decreased with increasing NaCl concentrations.

The parameters used for this experiment were based on commonly performed SIC experiments, using a conventional SIC column.<sup>1-3</sup> The SIC column length typically used in the lab was 33 cm and the column is commonly packed with 350  $\mu\text{L}$  of particles. The flow rates for this experiment were based on past SIC experiments and Lenhoff's original SIC paper.<sup>4, 5</sup> A limitation of the stationary phase used for the SIC method is when the backpressure exceeds 1000 psi the polymer particles will deform, resulting in unsymmetrical acetone peaks.

Therefore, a flow rate of less than 0.1 mL/min was used to minimize backpressure. When examining Figure 4.1.2, the data set shows that NaCl has a larger effect on the magnitude of B than flowrate for this column length and volume. While the effects of flow rate on B using a conventional scale column is only apparent at salt concentrations greater than 1M for NaCl.

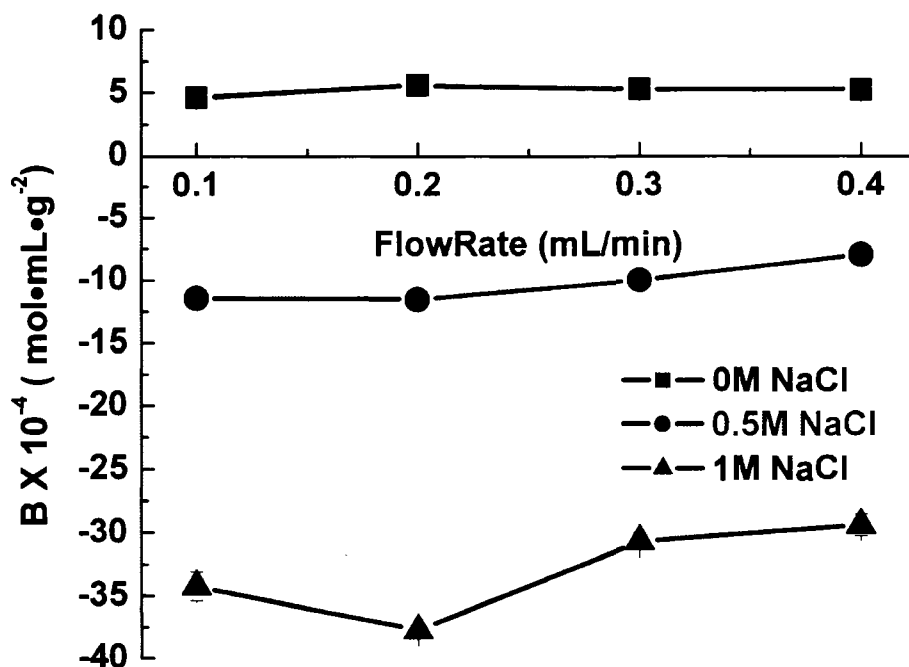


Figure 4.1.2. Effects of flowrate and NaCl concentration on B. Experimental Conditions: column length 33 cm, buffer conditions pH 4.5, 0.1 M acetic acid, injection volume 10  $\mu$ L, detector 280 nm.

**4.3.2. Column Length.** In the previous section flowrate had a small effect on B at 1 M NaCl, here we investigate the effect of column length on B is investigated. The miniaturized SIC column has a decreased volume of stationary phase, causing a decrease in the amount of protein available on the column for two body interactions. To determine the effects of a decreased stationary phase volume and column length the same column was used for this experiment and was shortened for each condition. This was done to insure the coupling density for the

column was held constant at 12 mg/mL. Three different column lengths were analyzed to model the performance of a miniaturized SIC column.

The effects of decreasing column length are shown for lysozyme at increasing concentrations of NaCl from 0 to 1 M, Figure 4.1.3. When no NaCl was present in the buffer, B was measured at  $5 \times 10^{-4} \text{ mol mL g}^{-2}$  for each column length. As the column length was increased from 8.5 to 33 cm, the magnitude of B decreased from 0 to  $-10 \times 10^{-4} \text{ mol mL g}^{-2}$ . When examining the magnitude of B for the three column lengths, the difference in B was the greatest at 1 M NaCl. In this case as the column length increased from 8.5 to 33 cm, the value of B measured decreased from  $-10 \times 10^{-4}$  to  $-30 \times 10^{-4} \text{ mL mol g}^{-2}$ . At concentrations of NaCl equal or greater than 0.5 M the magnitude of B was dependent on column length. The data shows a correlation between column length and the change in magnitude of B.

SIC needs to be sensitive enough to measure changes in the magnitude to determine the direction of two body interactions. For the SIC, method magnitude is dependent on the average of all two body interactions as the protein plug elutes through the column. The average number of two body interactions that occur as the protein plug elutes through the column decreases as the column length is shortened, causing the change in magnitude of B to decrease. This is demonstrated by comparing the B values measured for a column of 33 cm to 16

cm. Additionally, the change in B as the column decreases appears to be non-linear.

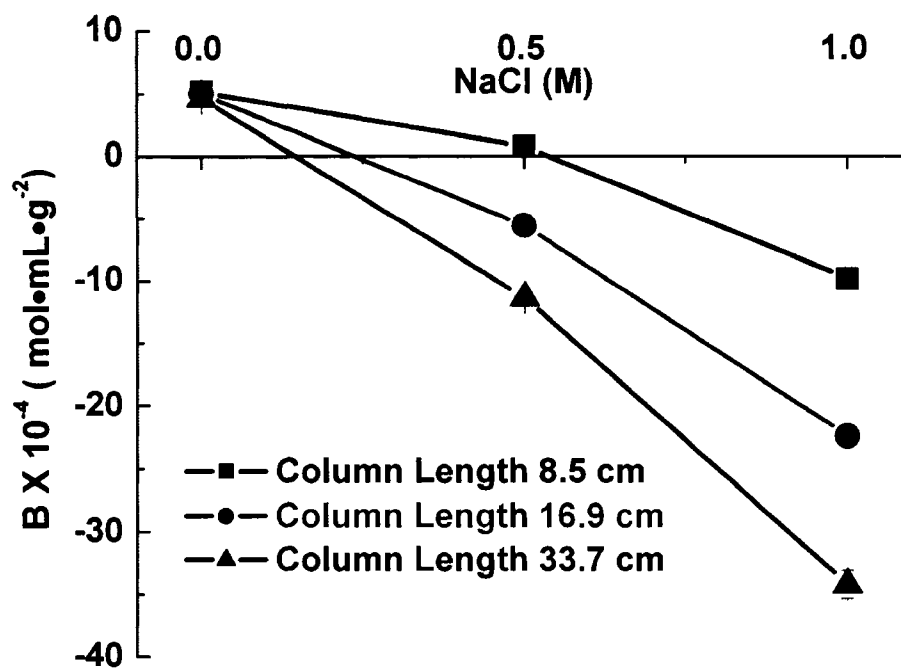


Figure 4.1.3. Effects of decreasing column length on B. Experimental conditions: flow rate: 0.1 mL/min. Buffer conditions: pH 4.5, NaCl 0, 0.5 and 1 M, 0.1 M acetic acid, injection volume 10  $\mu$ L, detector 280 nm.

**4.3.3. Effects of Flowrate on  $V_0$ .** For SIC miniaturization the effects of column length and flowrate on  $V_0$  need further characterization. The dead column experiments were designed to prevent the protein from interacting with stationary phase, by modifying the stationary phase and adding 5% NaCl.  $V_0$  corrects for the size difference between the protein and acetone. The lysozyme peak will always come off before the acetone peak represented by the  $V_0$  being less than 1.

$V_0$  was characterized as column length was decreased from 28.5 to 8.5 cm and flowrate was increased from 0.1 to 0.4 mL, Figure 4.1.4. Decreasing the column length, caused  $V_0$  to decrease in all cases. The 8.5 cm column experienced the sharpest drop in the  $V_0$  from 0.97 to 0.88 as flow rate increased from 0.1 to 0.4 mL/min. While the 16.8 and 28.5 cm columns had comparable changes in  $V_0$  from 0.92 to 0.98 when the flow rate was increased. The data in Figure 4.1.4 shows that column length and flow rate have a small impact on the  $V_0$  of lysozyme, unlike the live column in previous section. The data shows that  $V_0$  values are not significantly affected by changes in column length.

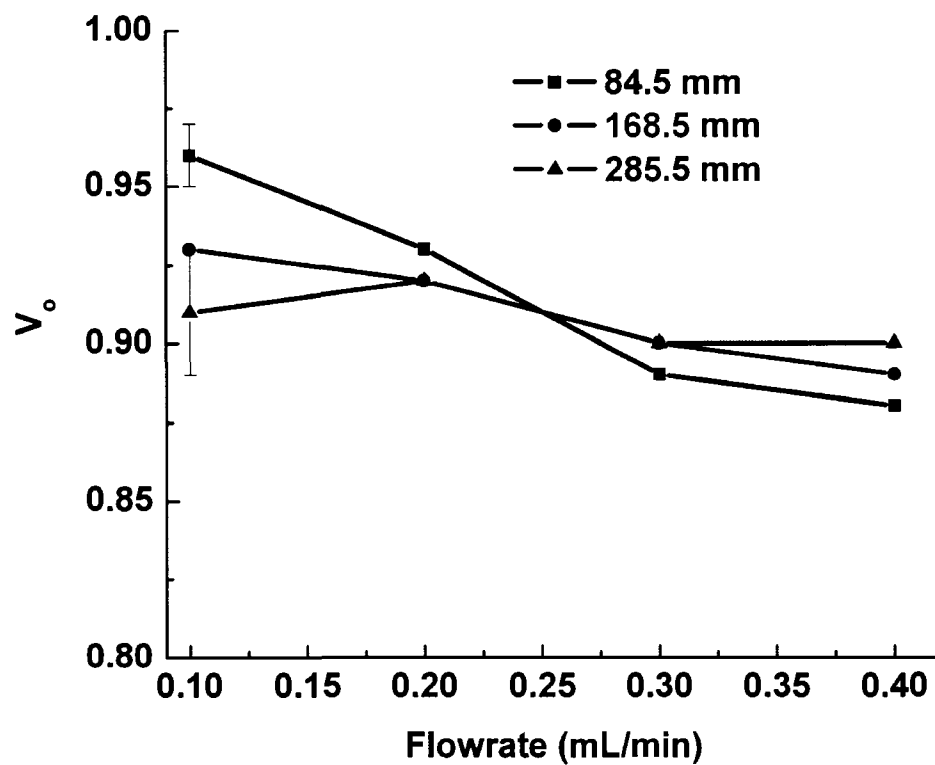


Figure 4.1.4. Effects of flow rate and column length on  $V_o$ . Experimental conditions: pH 4.5, 0.1 M acetic acid, Injection volume 10  $\mu$ L, wavelength 280 nm.

**4.3.4. Effects of Injection Volume.** The effect of increasing injection volume on B, is protein dependent. For example, the injection volume of lysozyme has an effect on the magnitude of B, when greater than 20  $\mu\text{L}$ . B was measured for lysozyme as the injection volume increased from 1 to 64  $\mu\text{L}$  shown in figure 4.1.5. When injection volume was less than 20  $\mu\text{L}$ , no significant change in B was observed. When the injection volume was greater than 20  $\mu\text{L}$ , B decreases  $2 \times (10^{-4} \times \text{mol} \times \text{g}^{-2})$  to  $-0.5 \times (10^{-4} \times \text{mol} \times \text{g}^{-2})$ . Figure 4.1.5 is representative of the chromatograms collected when the injection volume was increased from 8 to 64  $\mu\text{L}$ . As the injection volume of lysozyme increased, the protein peak max shifted to longer migration times. When comparing peak symmetry of 8 to 64  $\mu\text{L}$ , more peak tailing is observed at 64  $\mu\text{L}$ . The increase in peak tailing of lysozyme at high injection volumes is an indicator of an overloaded column. The data shows that injection volume lowers B at high injection volume due to column saturation. Therefore, the size of the miniaturized column needs to be taken into account to prevent overloading the column.

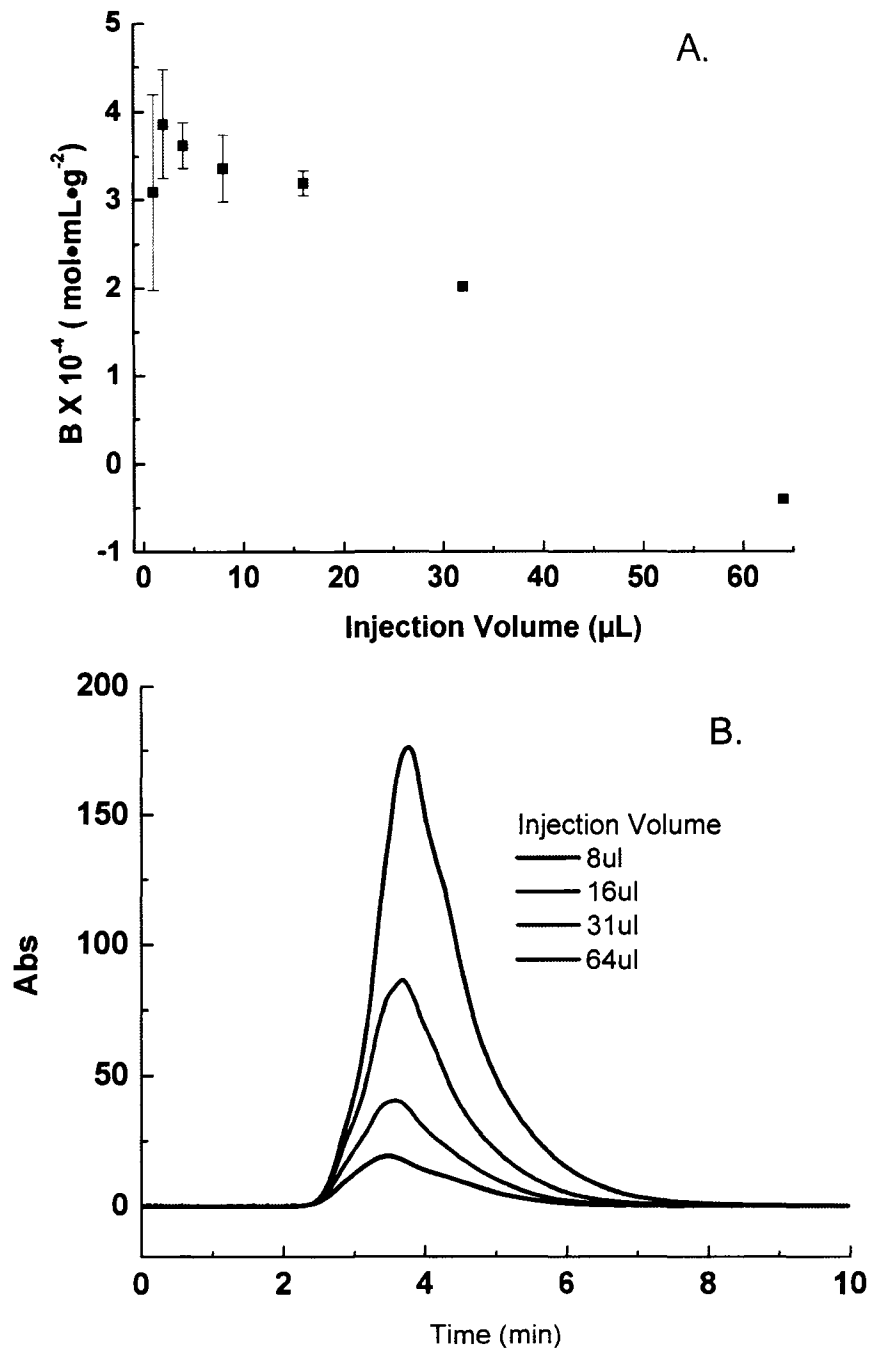


Figure 4.1.5. Effects of increasing injection volume on B (A) and chromatograms (B) Experimental conditions: flow rate: 0.1 mL/min. Buffer conditions. pH 4.5, 0.1M acetic acid, detector 280 nm.

**4.3.5. Miniaturized SIC Column.** These experiments show the use of the miniaturized SIC column to measure the change in B for lysozyme at different concentrations of NaCl. Figure 4.1.6 (A), shows the change in magnitude of lysozyme at 0, 0.2, 0.4 and 0.5 M NaCl. Lysozyme chromatograms showing the effects of increasing NaCl concentration are shown in Figure 4.1.6 (B). Lysozyme peaks are shifted to the left as the concentration of NaCl is increased, indicating attractive interactions. B decreased to negative values when NaCl concentration increased from 0 to 1 M, starting at  $5 \times (10^{-4} \times \text{mol} \times \text{mL} \times \text{g}^{-2})$  to  $-15 \times (10^{-4} \times \text{mol} \times \text{mL} \times \text{g}^{-2})$ . The standard deviation for each salt condition is comparable to the conventional scale experiment. Additionally, the data shows the small scale SIC instrument is comparable to standard HPLC, in terms of flow stability and injection volume reproducibility. The 5 cm column was able to detect changes in B as NaCl concentration was increased.

**4.5. Conclusions.** The data shown in this chapter demonstrates that decreasing the size of the column does not affect the direction or trend in B for lysozyme. Additionally, when B values measured by the small scale SIC were compared to the SLS or concentration scale SIC no difference was observed.

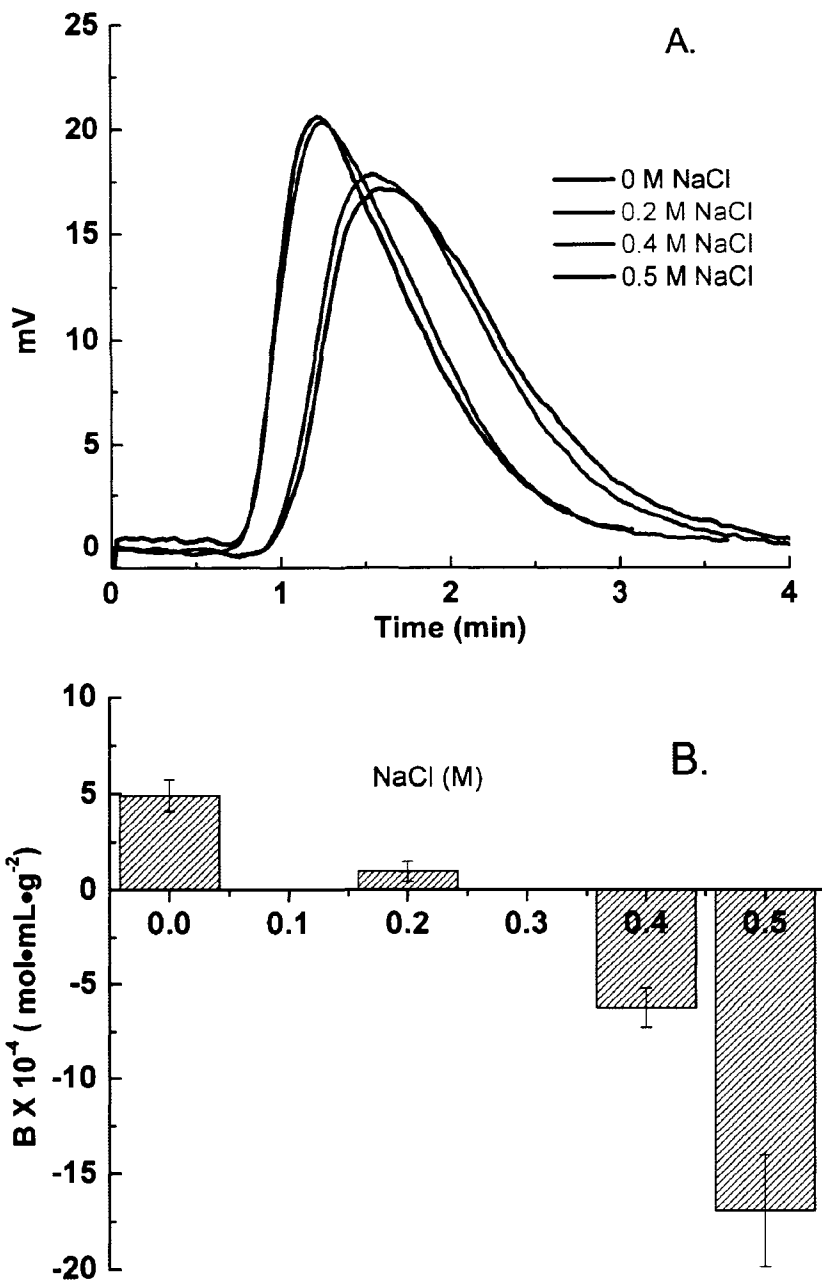


Figure 4.1.6. Chromatograms of lysozyme with increasing NaCl concentration, using a small scale SIC column. Instrumental settings: Mobile phase 0.1 M acetic acid, pH 7, injection volume 0.5  $\mu\text{L}$ , wavelength 280 nm.

#### 4.6. References.

1. Valente, J. J.; Verma, K. S.; Manning, M. C.; Wilson, W. W.; Henry, C. S., Second virial coefficient studies of cosolvent-induced protein self-interaction. *Biophysical Journal* **2005**, 89, (6), 4211-4218.
2. Valente, J. J.; Payne, R. W.; Manning, M. C.; Wilson, W. W.; Henry, C. S., Colloidal behavior of proteins: Effects of the second virial coefficient on solubility, crystallization and aggregation of proteins in aqueous solution. *Current Pharmaceutical Biotechnology* **2005**, 6, (6), 427-436.
3. Payne, R. W.; Nayar, R.; Tarantino, R.; Del Terzo, S.; Moschera, J.; Di, J.; Heilman, D.; Bray, B.; Manning, M. C.; Henry, C. S., Second virial coefficient determination of a therapeutic peptide by self-interaction chromatography. *Biopolymers* **2006**, 84, (5), 527-533.
4. Tessier, P. M.; Vandrey, S. D.; Berger, B. W.; Pazhianur, R.; Sandler, S. I.; Lenhoff, A. M., Self-interaction chromatography: a novel screening method for rational protein crystallization. *Acta Crystallographica Section D-Biological Crystallography* **2002**, 58, 1531-1535.
5. Tessier, P. M.; Lenhoff, A. M.; Sandler, S. I., Rapid measurement of protein osmotic second virial coefficients by self-interaction chromatography. *Biophysical Journal* **2002**, 82, (3), 1620-1631.

## 5. OmpX and Photosynthetic Reaction Center

**5.1. Introduction.** This chapter discusses measuring B by small scale SIC for two membrane proteins, photosynthetic reaction center RHO and OmpX. These membrane proteins are difficult to grow, extract from the membrane and purify, resulting in less than 0.5 mg of available material for OmpX and 200  $\mu$ L for RHO.<sup>1-3</sup> B values measured for RHO demonstrate that ability of small scale SIC, described in chapter 4, to perform limited screening studies using less than 200  $\mu$ g of sample. For OmpX, B was measured in a complex co-solvent/detergent system used for crystallization, the data clearly showed changes in B expected for this type of buffer system. These studies are important because they show the ability of small scale SIC to measure B in a complex co-solvent/detergent system and using less than 200  $\mu$ L of sample, which is important because of the low yields for many early stage development proteins.

RHO is a part of the large super family of G-protein-coupled receptor located at the outer segments of the retinal rod photoreceptor.<sup>4</sup> When RHO absorbs light, it changes in conformation to an activated intermediate. This change in conformation activates G-protein, which is a crucial step in phototransduction cascade.<sup>4, 5</sup> The tertiary structure of RHO is composed of  $\alpha$ -helices and  $\beta$ -sheets, Figure 5.1. The functional characteristics are semi dependent on the type of detergent; in Figure 5.1 different detergents are stabilizing the conformation of RHO.<sup>2, 5</sup> The amount of RHO used for the screening study totaled less than 200

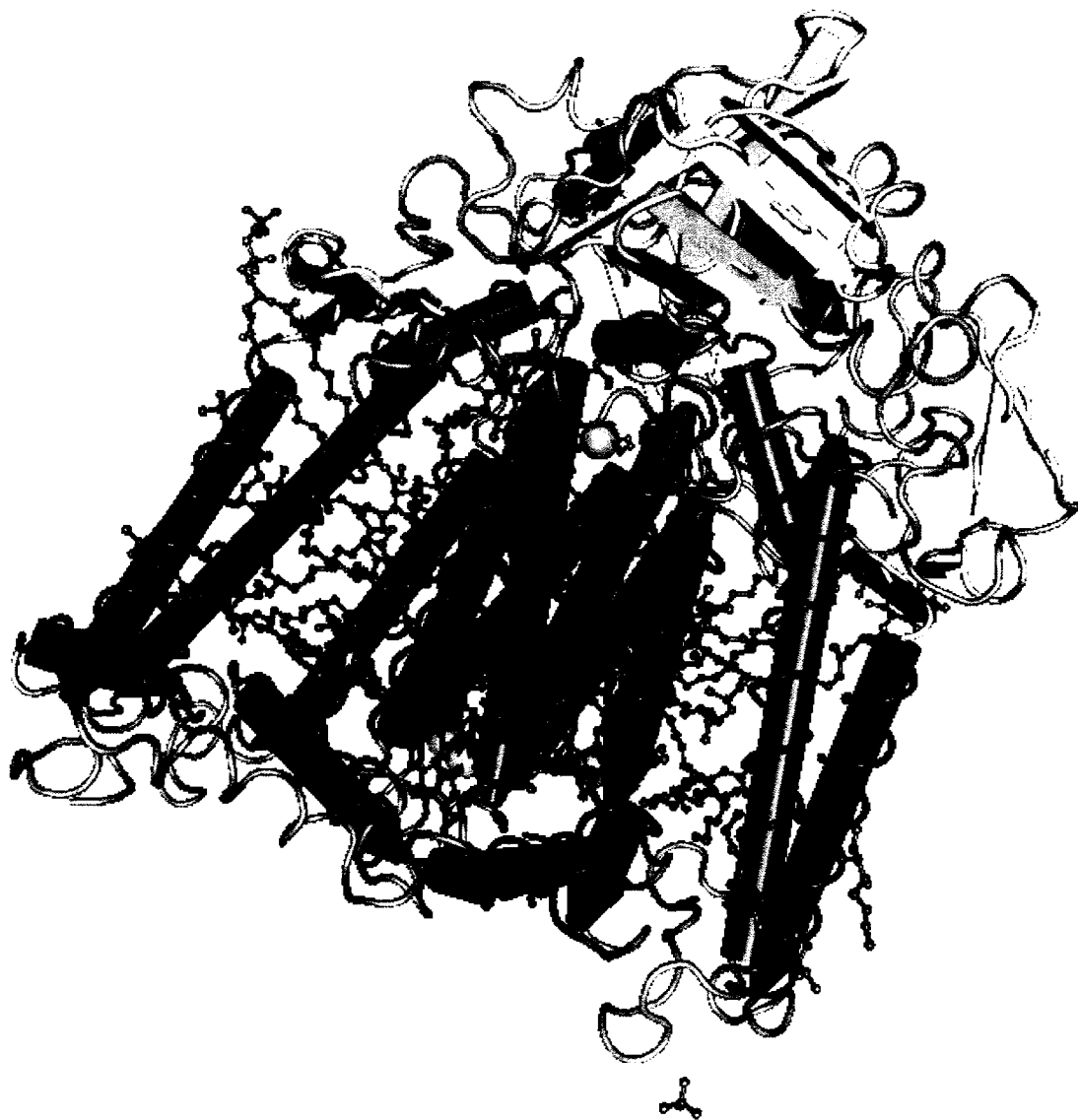


Figure 5.1.1. RHO crystallized by sitting drop setup at room temperature in the following buffer conditions, 3.5% heptano-1,2,3-triol, 0.1% lauryl dimethylamine oxide, 2.0% dioxane, and 0.75 M potassium phosphate, pH 7.4.<sup>5</sup>

$\mu\text{L}$ , which included protein immobilization and SIC measurements. Two co-solvents, PEG above 12.5% and  $\text{K}_2\text{HPO}_4$  above 0.4 M used in the crystallization buffer.<sup>6-8</sup> Both of these co-solvents caused an increase in attractive protein-protein interactions, resulting increase in negative B. The decrease in B measured for RHO with increasing concentration of  $\text{K}_2\text{HPO}_4$  and PEG agree with the theory of protein solubility for soluble proteins.

OmpX is a membrane protein that is part of the defense mechanism against the human immune system for gram-negative bacteria.<sup>9, 10</sup> NMR and X-ray diffraction have been used to determine the structure of OmpX, providing important information about mechanisms of virulence.<sup>11</sup> The function of OmpX is to adhere to proteins on the membrane of the target cell.<sup>9, 12</sup> OmpX is composed of 6- $\beta$ -sheets forming a  $\beta$  barrel, Figure 5.1.2.<sup>13</sup> The buffer used to crystallize OMPX by the hanging drop method was composed of a mixture of different co-solvents and concentrations.<sup>13</sup> The co-solvents were added so that weak protein-protein interactions were favored, allowing for enough time for the protein-detergent complex to form an ordered structure. SIC was used to quantitatively measure changes in colloidal stability for the addition of co-solvent. Additionally, the effects of co-solvent used to crystallize OmpX were examined by measuring changes in B. The results of the experiments demonstrate that SIC was able to measure the change in B with a complex solvent/co-solvent system and was able to detect changes in the physical stability of OmpX.



Figure 5.1.2. The structure of OmpX from *Escherichia coli*, crystallized in 30% (v/v) 2-propanol, 20% (v/v) glycerol, 0.2 M CaCl<sub>2</sub> and 0.1 M sodium acetate, pH 4.6

In many cases, a membrane protein is extracted by one type of detergent and purified by another detergent.<sup>1, 3, 14-17</sup> These two detergent systems are important for purification and crystallization of membrane proteins. The effects of a mixed detergent system on the colloidal stability of membrane proteins is difficult to determine by SLS because of scattering caused by the micelles and limited amount of sample. The effects of the simple detergent system on the physical stability of the membrane have not been explored beyond a qualitative approach, which only determines the presence of the membrane protein after extraction process.<sup>18, 19</sup> The above reasons small scale SIC was used to measure B for a mixture of glycerol and E<sub>8</sub>C<sub>4</sub>. The work with OMPX demonstrates a change in B for membrane protein a complex co-solvent/detergent system. Additionally, the work demonstrates that SIC is capable of measuring changes in B of a membrane protein in a mixed detergent system using less than 200  $\mu$ L.

## **5.2. Materials and Methods.**

**5.2.2. Chemical and Reagents.** The following chemicals and materials were used as received: potassium phosphate, hydrochloric acid, sodium carbonate, sodium hydroxide and MES (Fisher, USA). 3-hydropropionic acid was purchased from TCI. Chromatography particles (Toyopearl AF-Amino-650M) were

purchased from Supelco. PEG 4,000 was purchased from J.F. Baker Chemical Co. USA. N,N-Dimethyldodecylamine N-oxide (LDAO) was the detergent used for coupling experiments and was purchased from Sigma USA with a purity of >99%. Tetraethylene glycol monoethyl ether (C<sub>8</sub>E<sub>4</sub>) and glycerol. 3-hydroxypropanoic acid was purchased from TCI. PEG 4,000 was purchased from J.F. Baker Chemical Co. The coupling reagent (1-Ethyl-3-(3-dimethylaminopropyl)carbodiimide Hydrochloride) (EDC), N-hydroxysuccinimide (NHS), and the BCA colorimetric protein assay kit were purchased from Pierce. RHO was supplied by Dr. Delucas from UAB and was used as received without further purification. OMPX was supplied by Dr. Patrick Loll (Drexell University) and was used as received without further purification. All buffers were prepared with 18 M $\Omega$  water from Millipore-Q Academic.

**5.2.3. Column Preparation.** The preparation of amino chromatography particles for immobilization of RHO was performed in 0.02 M MES, 6% LDAO, pH 6 adjusted with concentrated sodium hydroxide. In a clean 1 mL eppendorf tube, 50  $\mu$ L of 5 mg/mL of RHO was diluted to 300  $\mu$ L in coupling buffer and added to 100  $\mu$ L of AF-Amino-650M particles. With the addition of RHO, 30 mg of EDC and 1.5 mg NHS were added to the mixture and slowly mixed over night at 22°C. After membrane protein immobilization the particles turned brown, the same color of soluble RHO, Figure 5.1.3.

**5.2.4. Column Preparation.** The preparation of amino chromatography particles for immobilization of OmpX was performed in 0.02 M MES, 0.6% C<sub>8</sub>E<sub>4</sub>, pH 6 adjusted with concentrated sodium hydroxide. In a clean 1 mL eppendorf tube, 0.05 mL of AF-Amino-650M particles were rinsed three times with coupling buffer. After each rinse, the tube was centrifuged and the supernatant was removed. 0.10 mL of OmpX was diluted to 0.25mL with coupling buffer and added to the washed amino particles. After the addition of OmpX, 30 mg of EDC and 1.5 mg NHS were added to the mixture and slowly mixed overnight at room temperature. After coupling, the particles were rinsed three times in coupling buffer and stored at 4°C.

**5.2.5. Small Scale SIC.** LC experiments were performed using a Harvard syringe pump (PHD 4400), Rheodyne 0.5  $\mu$ L manual injector and SSI 500 UV/Vis detector. The LC parameters used for the analysis of RHO are as follows: flow rate 60  $\mu$ L/min, 0.5  $\mu$ L injection and wavelength set to 280 nm. The data was collected using National Instruments USB 6009, Labview 8 and analyzed using Origin version 8. For each experimental condition 3% (v/v) acetone was injected as a non-retained marker, to check column integrity and adjust for solvent viscosity. After the analysis of acetone, three to six replicates of protein were injected.



Figure 5.1.3. RHO immobilized on amino particles after washing with coupling buffer. Coupling buffer contained 0.02 M MES, 6% LDAO at pH 6.

**5.2.6. Bicinchoninic Acid (BCA).** The BCA procedure outlined by Pierce was followed for the calibration curve and sample measurements. The following changes were made to the Pierce protocol: first the particles were removed and allowed to settle in the pipette tip to determine particle volume. The particles were added to the working reagent and diluted to 0.1 mL. The sample, blank and unmodified particles were prepared and the protein concentration was measured.<sup>20, 21</sup>

### **5.3. Results and Discussion.**

**5.3.1. Effects of  $K_2HPO_4$ .** The effects of different  $K_2HPO_4$  concentrations (0 to 0.8 M) at pH 6, 0.02 M MES and 6% LDAO are shown in Figure 5.1.3. The elution time of RHO at the different concentrations of  $K_2HPO_4$  did not change with increasing salt concentrations, with an average elution time around 0.9 min. Changes were observed in peak area of the different salt concentrations and the peak symmetry. At 0 M  $K_2HPO_4$  the elution peak of RHO is symmetric with slight tailing and peak max at -6 mV. When the concentration of the salt was increased from 0 to 0.8 M, the symmetry of the peak decreased with significant tailing and a shoulder to the right of the peak. Additionally, the peak height of the elution peak of RHO decreased from -6 mV to 0 mv with increasing height.

The decrease in peak height at peak max, decrease of peak symmetry and increase in peak tailing, indicates an increase in attractive protein-protein interactions. The same change in elution peak height and symmetry was

observed with enfuvirtide, Figure 5.1.4.<sup>22</sup> No change in magnitude or direction of B was observed for RHO at different  $K_2HPO_4$  concentrations.

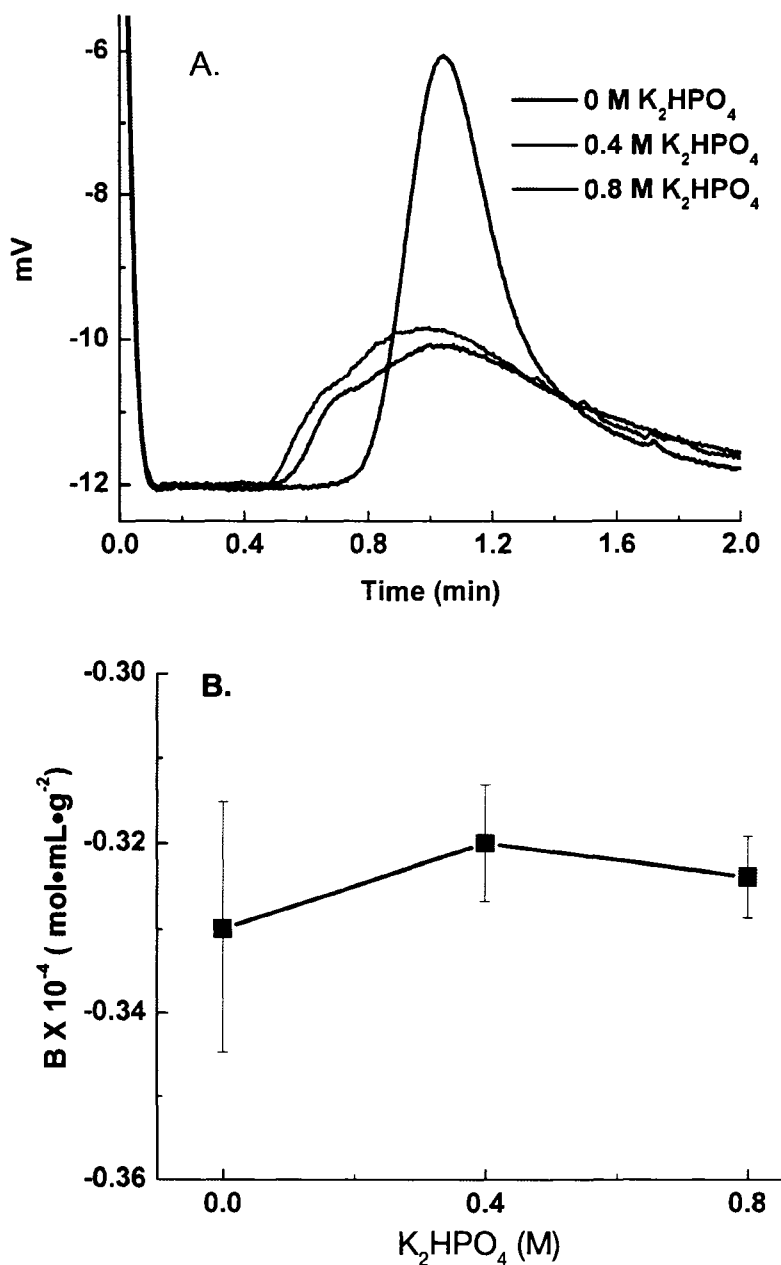


Figure 5.1.4. The effects of different  $K_2HPO_4$  concentrations (0 to 0.8 M) on the B values (A) and peak symmetry (B) on RHO. Buffer conditions: pH 6, 0.02 M MES and 6% LDAO Instrumental Settings flow rate: 60  $\mu\text{L}/\text{min}$ , injection volume 0.5  $\mu\text{L}$ , wavelength 280nm.

**5.3.2. Effects of PEG.** PEG is a common co-solvent used to crystallize soluble and membrane proteins. The effects of different PEG concentrations (0 and 12%) at pH 6, 0.02 M MES and 6% LDAO are shown in figure 5.1.5. The difference in elution time is clearly observed when the run buffer contained 12.5% PEG as seen in Figure 5.1.4. At 0% PEG, B was at  $-3.7 \times 10^{-4} \text{ mol mL g}^{-2}$ , when PEG was increased to 12.5% B was at  $-6.64 \times 10^{-4} \text{ mol mL g}^{-2}$ , Figure 5.1.5. Other accounts of PEG vs B have shown similar trend, as the concentration of PEG increases B has decreased.<sup>6,7</sup>

The effects of different PEG concentrations (0 to 30%) at pH 8.5. 0.5% C<sub>8</sub>E<sub>4</sub>, 20 mM TRIS-HCL, 20 mM NaCl are shown in Figure 5.1.6. At 0% PEG, B was  $-4.0 \times 10^{-4} \text{ mol mL g}^{-2}$ , when PEG was increased from 0 to 30%, B decreased to  $-2.0 \times 10^{-4} \text{ mol mL g}^{-2}$ , Figure 5.2.2. The screening experiment was performed to determine if the instrumental setup was sensitive enough to detect changes in B, PEG was used because of its effects it has been used to crystallize membrane proteins. The decrease in B, with increasing PEG concentration increases indicates that PDC-PDC interactions are favored, in agreement with previous results for PDC.<sup>6</sup> The data indicates that the instrumental set up was capable of measuring changes in B.

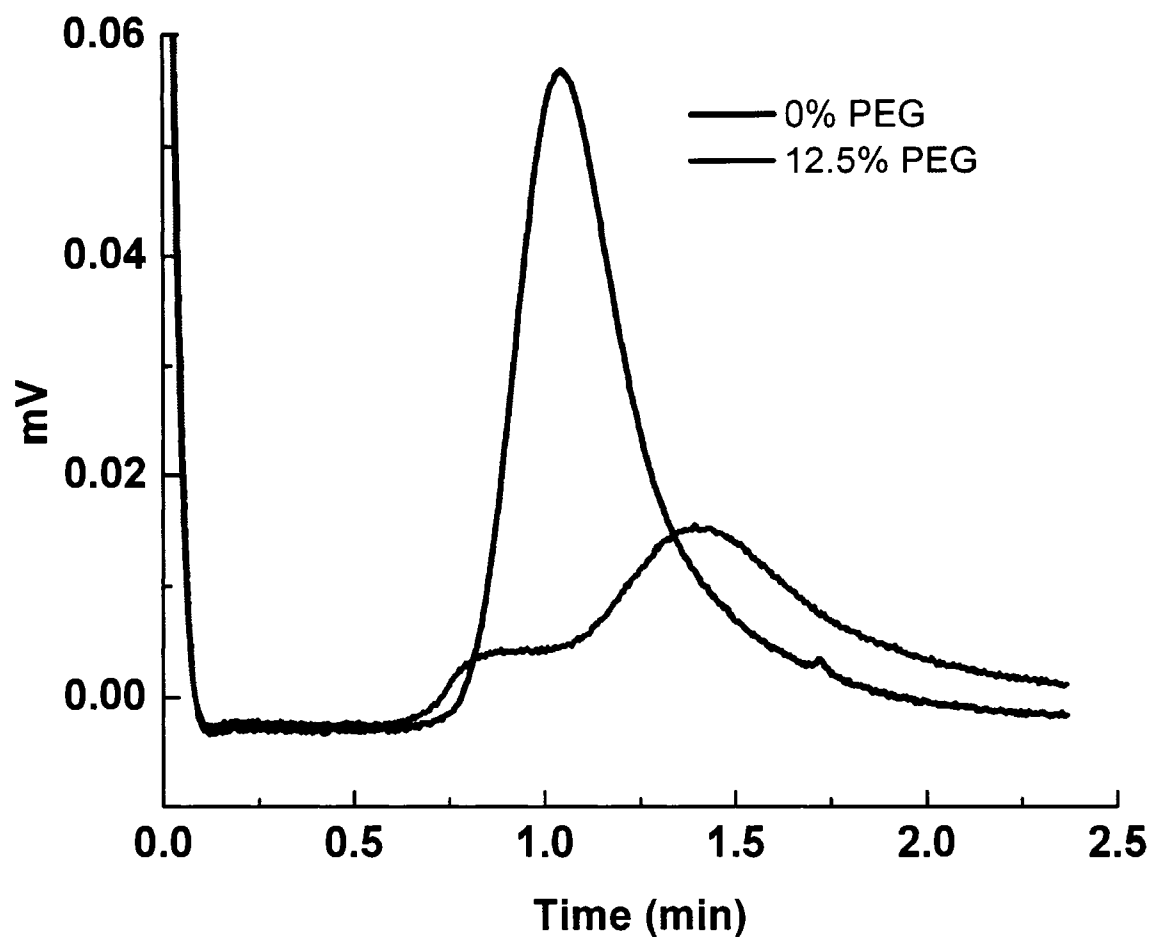


Figure 5.1.5. RHO at different PEG concentrations, 0% (Black) and 12% (Red) measured by small scale by SIC. Instrumental settings: Mobile phase: 10 mM TRIS, flow rate: 60  $\mu$ L/min, injection volume 0.5  $\mu$ L, wavelength 280 nm.

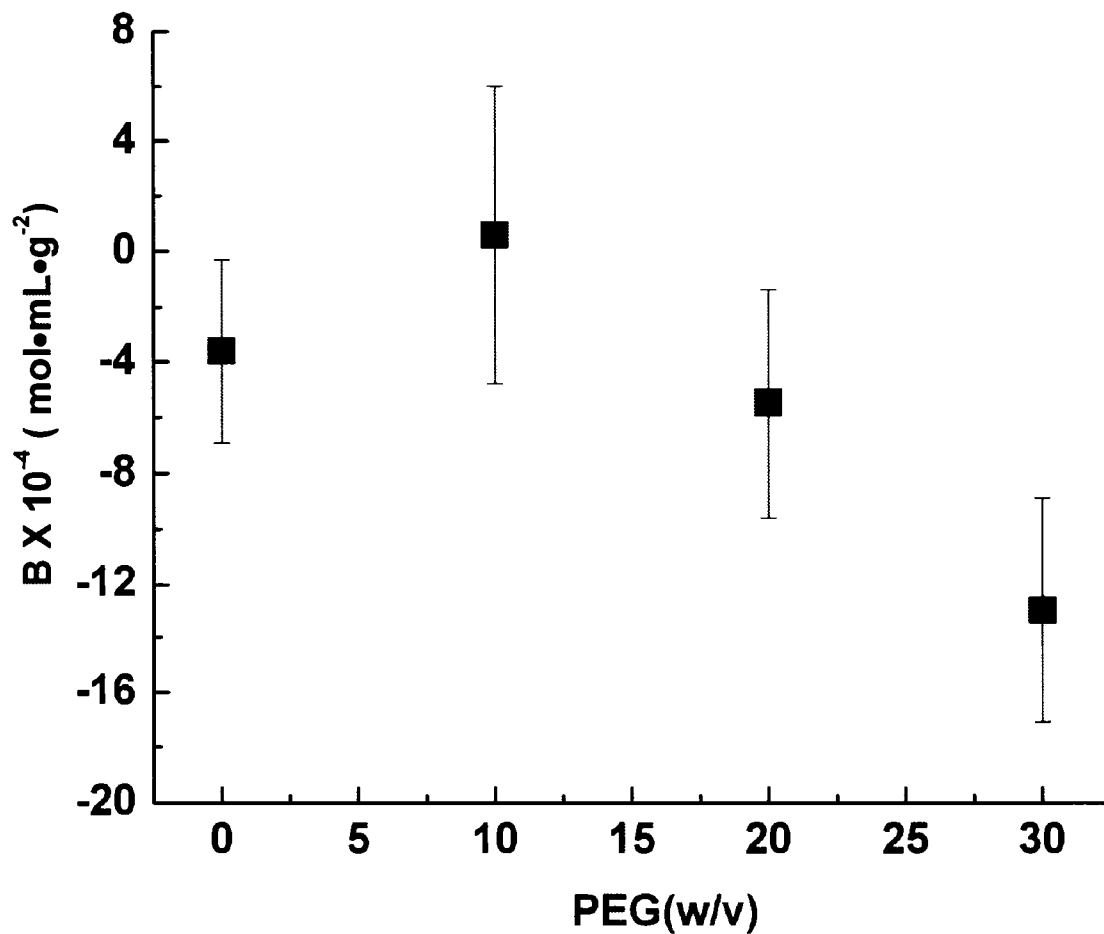


Figure 5.1.6. The effects of different PEG concentrations (0 to 30% w/v) at pH 8.5. 0.5% C<sub>8</sub>E<sub>4</sub>, 20 mM TRIS-HCl, 20mM NaCl. Experimental Condition: Flow rate 25  $\mu$ L/min, injection volume 0.5  $\mu$ L, wavelength 280 nm.

**5.3.4. Effects of Glycerol.** Glycerol is another common additive that is used to increase the solubility of membrane protein.<sup>5, 23, 24</sup> The effects of different glycerol concentrations at 0 to 30% w/v at pH 4.5, 0.1 M sodium acetate, 0.2 mM CaCl<sub>2</sub> are shown in Figure 5.1.7. Sample chromatograms of increasing glycerol concentration in solution are shown in Figure 5.1.7.A. As the percentage of glycerol in solution increases, the elution time of OmpX increases from 3 to 4 minutes. Additionally, the peaks broaden and peak height decreases for OmpX with increasing glycerol. The viscosity of the buffer increased with increasing glycerol causing the peaks to elute off the column longer. The effects of B values for glycerol are shown in Figure 5.1.7.B. As the percentage of glycerol increases protein solvent interactions are favored. At 0% glycerol, B increased by  $10 \times 10^{-4} \text{ mol mL g}^{-2}$  at 30% glycerol. The reason for the apparent disconnect between increasing elution times and trending of B to more positive values is due to the viscosity of glycerol and the use of acetone to adjust for changes in viscosity. Acetone corrects for differences in the viscosity of the buffer caused by the addition of different buffers, in this case glycerol. B values measured for 10 to 20% glycerol are in the range of the crystallization slot. When the concentration of glycerol is 30%, B values are above the crystallization slot, favoring protein-solvent interactions.

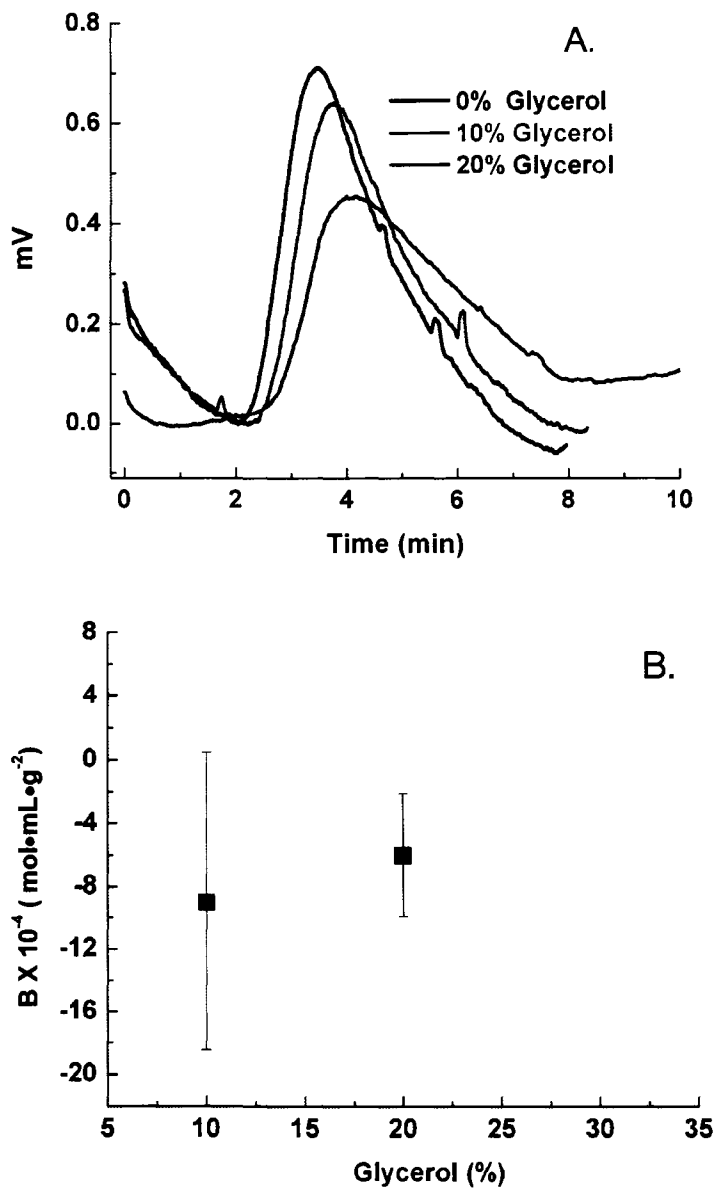


Figure 5.1.7. Effects of different glycerol concentrations on OMPX at 0 to 30% at pH 4.5, 0.1 M sodium acetate, 0.2 mM  $\text{CaCl}_2$ . Figure A shows chromatograms of OmpX vs glycerol 0% (Black), 10% (Red) and 20% (Blue). Experimental Condition: Flow rate 25  $\mu\text{L}/\text{min}$ , injection volume 0.5  $\mu\text{L}$ , wavelength 280 nm.

**5.3.5. Effects of Crystallization Co-solvent.** OmpX has been crystallized with 2-propanol, CaCl<sub>2</sub>, sodium acetate and co-solvents as shown in., Figure 5.1.7.<sup>9-</sup>

<sup>25</sup> Small scale SIC was used to measure the change in B for each cosolvent added to the buffer, for the purpose of stabilizing OmpX and to promote the weak two body interactions needed for crystallization. CaCl<sub>2</sub> was held constant at 0.2M for all screening experiments. Additionally, glycerol was also present in all screening experiments at 20% (v/v). Sodium acetate is a common biological buffer suitable for pH 4.6. Additionally, sodium acetate at concentrations greater than 0.1 M will decrease B resulting in salting out of the protein. As the concentration of sodium acetate increases from 0 to 0.3M in the presence of 0.2 M CaCl<sub>2</sub>, pH 4.5, B decreases from  $-13 \times 10^{-4}$  to  $-16 \times 10^{-4}$  mol mL g<sup>-2</sup>. When the concentration of the 2-propanol was increased from 0 to 30% (v/v) from  $-10 \times 10^{-4}$  to  $-20 \times 10^{-4}$  mol mL g<sup>-2</sup>, resulting in a decrease in B. The B values for 2-propanol and sodium acetate in the presence of glycerol and CaCl<sub>2</sub> are below the crystallization slot, explained in chapter 1.

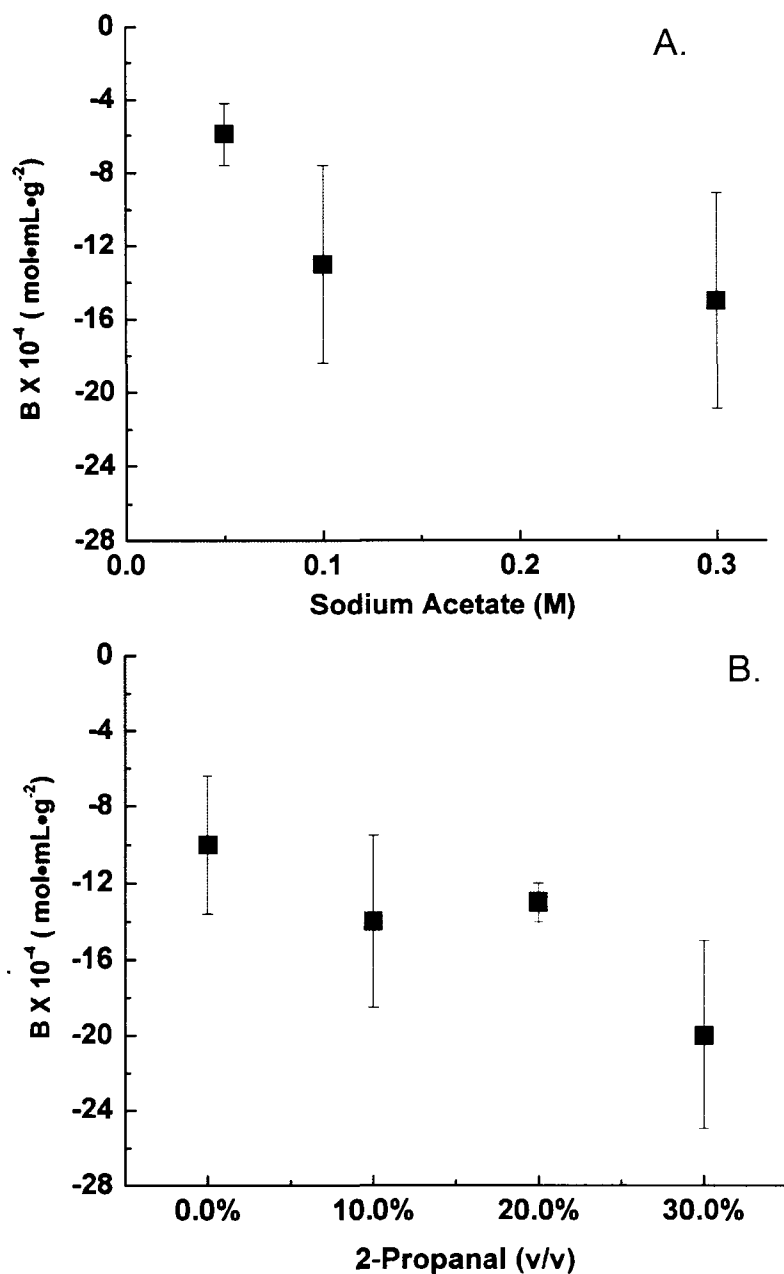


Figure 5.1.7. The effects of different 2-propanol (B) (0 to 30%) and sodium acetate (A) (0.05 to 0.3 M) at pH 4.6, 20% Glycerol, 200 mM CaCl<sub>2</sub>, 100 mM sodium acetate. Experimental Condition: Flow rate 25  $\mu$ L/min, injection volume 0.5  $\mu$ L, wavelength 280 nm.

**5.3.6. Effects of Glycerol and E<sub>8</sub>C<sub>4</sub>.** The effects of mixing different glycerol concentrations at 0 to 30% and E<sub>8</sub>C<sub>4</sub> 0.25 to 0.76 M at pH 4.5, 0.1 M sodium acetate, 0.2 mM CaCl<sub>2</sub> are shown in the bar graph in Figure 5.1.8. As concentration of glycerol increased from 0 to 20 %, at 0.25 M at E<sub>8</sub>C<sub>4</sub>, B decreased from  $-3.2 \times 10^{-4}$  to  $-7 \times 10^{-4}$  mol mL g<sup>-2</sup>. The same trend in B was observed when the concentration of glycerol increased from 0 to 20% at 0.50 M E<sub>8</sub>C<sub>4</sub>. When the concentration of E<sub>8</sub>C<sub>4</sub> increased above the CMC (0.5 M) at 0.75 M, B values for 0 and 10% glycerol were between  $-1.9 \times 10^{-4}$  to  $-1.8 \times 10^{-4}$  mol mL g<sup>-2</sup>. When glycerol was increased to 20% in presence of 0.75% E<sub>8</sub>C<sub>4</sub>, B decreased to  $-3.5 \times 10^{-4}$  mL mol g<sup>-2</sup>).

The effects of glycerol on the colloidal stability of OmpX are dependent on the addition of different co-solvent. The addition of E<sub>8</sub>C<sub>4</sub> to the buffer is causing glycerol to decrease B compared to its effect in Figure 5.1.8. When the concentration of E<sub>8</sub>C<sub>4</sub> is below the CMC the protein-protein and protein-solvent interactions are dominated by glycerol. When the concentration of E<sub>8</sub>C<sub>4</sub> exceeds the CMC, glycerol has a minimal effect on B. This observation agrees with past experiments with proteorhodopsin (Chapter 3). E<sub>8</sub>C<sub>4</sub> is a nonionic detergent, was used because of its ability to maintain the structural stability of OMPX. Membrane proteins are soluble then the concentration of the detergent was above the critical micelle concentration (CMC), for E<sub>8</sub>C<sub>4</sub> is 0.5 M. The data highlights once more the importance of the detergent for stabilizing membrane proteins.

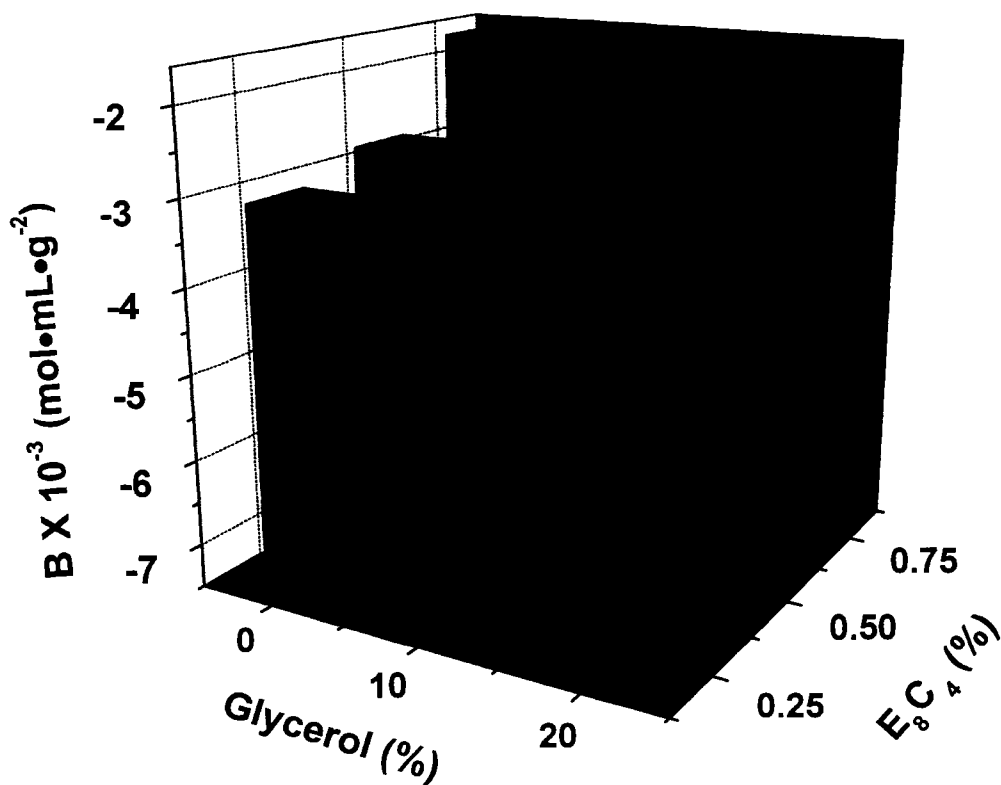


Figure 5.1.8. The effects of different concentration glycerol and E<sub>8</sub>C<sub>4</sub> at pH 4.6, 20% Glycerol, 200 mM CaCl<sub>2</sub>, 100mM sodium acetate. Experimental conditions: flow rate 25 μL/min, injection volume 0.5 μL, wavelength 280 nm.

**5.4. Conclusion.** Miniaturizing SIC has advanced in stages, each improving until the project reaches the ultimate goal of microchip SIC. Trending B for RHO using a conventional HPLC was not possible because of the limited amount of material. Use the small scale SIC allowed for the measurement of B for RHO as a function of PEG concentration. As the percentage of PEG increased, the physical stability of RHO decreased. PEG is an important co-solvent used to induce membrane protein crystallization and increasing concentrations of PEG have been shown to cause a decreased in B.<sup>6, 7, 26, 27</sup> Trending the change in B for RHO and OmpX demonstrates small scale SIC is able to measure the change and magnitude of two-body interactions, using less than 1 mg of material.

#### **5.5. Reference.**

1. Loll, P. J., Membrane protein structural biology: the high throughput challenge. *Journal of Structural Biology* **2003**, 142, (1), 144-153.
2. Degrip, W. J., Thermal-Stability of Rhodopsin and Opsin in Some Novel Detergents. *Methods in Enzymology* **1982**, 81, 256-265.
3. Stowell, M. H. B.; Rees, D. C., Structure and Stability of Membrane-Proteins. *Advances in Protein Chemistry, Vol 46* **1995**, 46, 279-311.
4. Ramon, E.; Marron, J.; del Valle, L.; Bosch, L.; Andres, A.; Manyosa, J.; Garriga, P., Effect of dodecyl maltoside detergent on rhodopsin stability and function. *Vision Research* **2003**, 43, (28), 3055-3061.
5. Camara-Artigas, A.; Brune, D.; Allen, J. P., Interactions between lipids and bacterial reaction centers determined by protein crystallography.

*Proceedings of the National Academy of Sciences of the United States of America* **2002**, 99, (17), 11055-11060.

6. Loll, P. J.; Hitscherich, C.; Aseyev, V.; Allaman, M.; Wiencek, J.,  
Assessing micellar interaction and growth in detergent solutions used to  
crystallize integral membrane proteins. *Crystal Growth & Design* **2002**, 2,  
(6), 533-539.
7. Hitscherich, C.; Aseyev, V.; Wiencek, J.; Loll, P. J., Effects of PEG on  
detergent micelles: implications for the crystallization of integral  
membrane proteins. *Acta Crystallographica Section D-Biological  
Crystallography* **2001**, 57, 1020-1029.
8. Berger, B. W.; Gendron, C. M.; Lenhoff, A. M.; Kaler, E. W., Effects of  
additives on surfactant phase behavior relevant to bacteriorhodopsin  
crystallization. *Protein Science* **2006**, 15, (12), 2682-2696.
9. Pautsch, a.; Vogt, J.; Model, K.; Siebold, C.; Schulz, G. E., Strategy for  
membrane protein crystallization exemplified with OmpA and OmpX.  
*Proteins-Structure Function and Genetics* **1999**, 34, (2), 167-172.
10. Stoorvogel, J.; Vanbussel, M. J. a. W. M.; Tommassen, J.; Vandeklundert,  
J. a. M., Molecular Characterization of an Enterobacter-Cloacae Outer-  
Membrane Protein (OmpX). *Journal of Bacteriology* **1991**, 173, (1), 156-  
160.
11. Fernandez, C.; Hilty, C.; Wider, G.; Guntert, P.; Wuthrich, K., NMR  
structure of the integral membrane protein OmpX. *Journal of Molecular  
Biology* **2004**, 336, (5), 1211-1221.

12. Arnold, T.; Poynor, M.; Nussberger, S.; Lupas, A. N.; Linke, D., Gene duplication of the eight-stranded beta-barrel OmpX produces a functional pore: A scenario for the evolution of transmembrane beta-barrels. *Journal of Molecular Biology* **2007**, 366, (4), 1174-1184.
13. Vogt, J.; Schulz, G. E., The structure of the outer membrane protein OmpX from Escherichia coli reveals possible mechanisms of virulence. *Structure with Folding & Design* **1999**, 7, (10), 1301-1309.
14. Berger, B. W.; Gendron, C. M.; Robinson, C. R.; Kaler, E. W.; Lenhoff, A. M., The role of protein and surfactant interactions in membrane-protein crystallization. *Acta Crystallographica Section D-Biological Crystallography* **2005**, 61, 724-730.
15. Garavito, R. M.; Ferguson-Miller, S., Detergents as tools in membrane biochemistry. *Journal of Biological Chemistry* **2001**, 276, (35), 32403-32406.
16. Gohon, Y.; Popot, J. L., Membrane protein-surfactant complexes. *Current Opinion in Colloid & Interface Science* **2003**, 8, (1), 15-22.
17. Helenius, a.; Simons, K., Solubilization of Membranes by Detergents. *Biochimica Et Biophysica Acta* **1975**, 415, (1), 29-79.
18. Eshaghi, S.; Hedren, M.; Nasser, M. I. A.; Hammarberg, T.; Thornell, A.; Nordlund, P., An efficient strategy for high-throughput expression screening of recombinant integral membrane proteins. *Protein Science* **2005**, 14, (3), 676-683.

19. Odahara, T., Stability and solubility of integral membrane proteins from photosynthetic bacteria solubilized in different detergents. *Biochimica Et Biophysica Acta-Biomembranes* **2004**, 1660, (1-2), 80-92.
20. Smith, P. K.; Krohn, R. I.; Hermanson, G. T.; Mallia, a. K.; Gartner, F. H.; Provenzano, M. D.; Fujimoto, E. K.; Goeke, N. M.; Olson, B. J.; Klenk, D. C., Measurement of Protein Using Bicinchoninic Acid. *Analytical Biochemistry* **1985**, 150, (1), 76-85.
21. Plant, a. L.; Locasciobrown, L.; Haller, W.; Durst, R. a., Immobilization of Binding-Proteins on Nonporous Supports - Comparison of Protein Loading, Activity, and Stability. *Applied Biochemistry and Biotechnology* **1991**, 30, (1), 83-98.
22. Payne, R. W.; Nayar, R.; Tarantino, R.; Del Terzo, S.; Moschera, J.; Di, J.; Heilman, D.; Bray, B.; Manning, M. C.; Henry, C. S., Second virial coefficient determination of a therapeutic peptide by self-interaction chromatography. *Biopolymers* **2006**, 84, (5), 527-533.
23. Berger, B. W.; Garcia, R. Y.; Lenhoff, A. M.; Kaler, E. W.; Robinson, C. R., Relating surfactant properties to activity and solubilization of the human adenosine A(3) receptor. *Biophysical Journal* **2005**, 89, (1), 452-464.
24. Prive, G. G., Detergents for the stabilization and crystallization of membrane proteins. *Methods* **2007**, 41, (4), 388-397.
25. [Anon], Spontaneous formation of detergent micelles around the outer membrane protein OmpX. *European Biophysics Journal with Biophysics Letters* **2005**, 34, (6), 694-694.

26. Loll, P. J.; Allaman, M.; Wiencek, J., Assessing the role of detergent-detergent interactions in membrane protein crystallization. *Journal of Crystal Growth* **2001**, 232, (1-4), 432-438.
27. Tessier, P. M.; Vandrey, S. D.; Berger, B. W.; Pazhianur, R.; Sandler, S. I.; Lenhoff, A. M., Self-interaction chromatography: a novel screening method for rational protein crystallization. *Acta Crystallographica Section D-Biological Crystallography* **2002**, 58, 1531-1535.

## Chapter 6. Developing Microchip SIC

**6.1. Introduction.** This chapter discusses the progress that was made in developing a monolithic column for microchip SIC. For the microchip SIC to be a viable alternative to small scale SIC, a microchip that can withstand high mobile phase velocities is needed. Additionally, the stationary phase should be easily introduced into the microchip channel and allow for on column protein immobilization to reduced column preparation time. If these goals are reached, a device could be produced that would consume protein on the sub-milligram scale. Additionally, the microchip SIC would greatly increase sample throughput, making it possible for large screening studies to be performed over short time periods.

**6.2. Designing the SIC Microchip.** The first design of the SIC microchip was a PDMS-glass chip developed and reported by the Henry group.<sup>1</sup> This first microchip design demonstrated the ability to accurately measure changes in B for a lysozyme versus NaCl screening study.<sup>1</sup> The problem with this early microchip design was the material used to construct the device failed at high mobile phase velocities. For this device, the mobile phase velocities were lowered, resulting in retention times for lysozyme in the 10 to 15 minute range, greatly limiting the throughput of the device.<sup>1</sup> To solve this problem microchip could be constructed with rigid materials that would not fail at high mobile phase velocities. CE has been miniaturized to the microchip scale for a number of years

with chips constructed with a wide range of materials. From this field of research, a number of materials were identified that would be suitable for constructing a SIC microchip that would stand high mobile phase velocities.<sup>2, 3</sup> The one important difference between CE and SIC was adding a stationary phase to the microchip channel. Additionally, early experiments showed it was very difficult to slurry pack the stationary phase into a 350  $\mu\text{m}$  wide x 600  $\mu\text{m}$  high microchip channel, because of the size of the small percentage of particles. For this reason, the data presented in this chapter is focused on developing a monolithic SIC column.

**6.3. Alternate Stationary Phase.** A monolithic column is a single piece of continuous porous material consisting of a network of meso and through pores.<sup>4</sup> The advantages of a monolithic column come from the ability to optimize the separation by controlling the size and distribution of the throughput pores and mesopores.<sup>5-7</sup> Additionally, a monolithic column can be can be polymerized in situ, thus avoiding the problem of slurry packing the microchip channel.<sup>8, 9</sup> Finally, monolithic columns have a much lower pressure drop than traditionally packed columns. For this work the monolithic column needs to withstand a pH range of 3 to 10 and have functional groups for protein immobilization. A number of different stationary phases have been developed, including the methacrylate based stationary phases that was used for these early experiments.<sup>5, 6, 8</sup> A methacrylate column was used here because of its ability to withstand a wide pH range. Additionally, the column chemistry has epoxide groups that can be used to

immobilize proteins by different types of coupling chemistries, including Schiff base, CDI and DSC method.<sup>5, 6, 10</sup> The stationary phase developed in this chapter required the measurement of pore size distribution in a non-destructive manner that could be applied to a microchip column.

**6.4. Measuring Pore Size Distribution.** Pore size distribution in polymer-based monolithic columns has been measured by mercury intrusion, nitrogen adsorption and chromatographic methods.<sup>11</sup> Mercury intrusion measures pore size distribution by measuring the force applied to the mercury to fill pores of different sizes.<sup>11-13</sup> The force needed to fill pores increases as the size of the pore decrease, caused by the high surface tension of mercury.<sup>12</sup> Mercury intrusion was not used because it would have destroyed the stationary phase and the fittings required for attaching it to a microchip could not withstand the high pressures.<sup>12</sup> Nitrogen adsorption measures pore volume by tracking changes in pressure as the nitrogen adsorbs on to the surface. The method would have required the material be grounded up and placed in the instrument and temperature be lowered by liquid nitrogen.<sup>5-7</sup> This method was not used because it would have also destroyed the monolithic column. Inverse size exclusion chromatography (ISEC) is a chromatographic method that measures the pore size distribution of the column by changes in retention time of chemical probes of known molecular sizes.<sup>13</sup> This chromatographic method is nondestructive and can be modified for measuring the pore size distribution of the monolithic column in a microchip format.

## **6.5. Materials and Methods.**

**6.5.1. Chemicals and Reagents.** The following chemicals and materials were used as received for these experiments: hydrochloric acid, sodium hydroxide, potassium phosphate and sodium chloride (Fisher, USA). Ethylene glycol dimethacrylate (EDMA), 2,3-Epoxypropyl methacrylate (GMA), cyclohexanol, dodecanol and acetonitrile were purchased from Sigma. BCA, a colorimetric protein assay kit, was purchased from Pierce. 2,2'-Azobis(isobutyronitrile) (AIBN) was purchased from TCI. 2-(N-Morpholino)ethanesulfonic acid monohydrate (MES) and was purchased from Acros Organics. Lysozyme was used as received from Cal BIO.

**6.5.2. Microchip Fabrication using Thermoset Polyester.** The thermoset polyester microchip was constructed with the help of Brian M. Dressen using previously published methods.<sup>14</sup> The master mold was constructed from a silicon wafer following the methods and procedures published in literature.<sup>3</sup> A brief summary of the procedure is given here. The silica wafer was washed with soap and rinsed with DI water three times and once with acetone. The wafer was allowed to dry in an oven at 40°C for 2 hours. The clean wafer was then coated with SU-8-2100 followed by a ramp to 500 rpm at 100 rpm/second for 10 seconds, followed by a ramp to the final spin speed of 1000 rpm at 300 rpm/second. The coated silicon wafer was then soft baked for 6 min at 65°C, followed by 60 minutes bake at 95°C. The design of the mask was a straight

channel with a tapered end and printed on a transparency using a 2,400 DPI printer. The mask was then placed on top of the coated silicon model and exposed at 100% to 40 seconds. The mask was then removed and the silicon wafer was post baked for 1 minute at 65°C, followed by 15-minute bake at 95°C. The master mold was then washed with developer leaving a raised channel structure for molding.

The patterned master mold was exposed to HMDS by vapor at room temperature over for 12-hour period in a desiccator. After the vapor deposition, the TEP was added to the patterned master and exposed to 50% UV for 110 min for initial cure. The TEP with the imprinted channel was then removed and sealed to another blank TEP by exposing the to 50% UV for 4 times each 15 sec long. The chip was baked at 65°C for 5 min followed by 60 min bake at 95°C. The last step was attaching the micro fittings to the chip by thermoset glue.

**6.5.3. Polymerizing the Monolithic Stationary Phase.** The methacrylate monolithic column was composed of a mixture of functional monomer (GMA), cross-linker (EDMA), porogen (cyclohexanol and dodecanol) and a radical initiator (AIBN).<sup>6,7</sup> The percentages of chemicals used are for the monolithic column 24% GMA, 16% EDMA, 25% cyclohexanol, 0.1% AIBN and 35% of dodecanol.<sup>6,7</sup> The mixture was sonicated for 6 min and nitrogen was bubbled through for 6 min to remove oxygen. The mixture was then filled into a column and both ends were sealed. The monolithic column was formed by filling column

with the polymer mixture and sonicated for 3 min and polymerization at 80°C for 12 hours.<sup>6,7</sup>

**6.5.4. ISEC.** Dextran and polystyrene molecular weight probes were used to characterize the pore size of the monolithic column. The ISEC experiments used an LC instrument equipped with a Waters 501 pump, a Shimadzu SIL-9A autosampler and an HP 1047A RI detector. The RI detector was flushed with solvent at 0.4 ml/min for a hour to allow the instrument to warm up to 34°C. Parameters used for ISEC experiments are as follows, flowrate 0.3mL/min, injection volume 32  $\mu$ L. Data was collected with Labview software and data was analyzed with Origin 7.

**6.5.5. BCA.** BCA is the standard method used in this thesis to measure the amount of protein coupled to the stationary phase. For the monolithic column a length of monolith column was removed from the column and washed three times with coupling buffer. After the third wash, the volume of column and buffer was increased to 100  $\mu$ L and 2 mL of working reagent was added. The other steps in the BCA followed the procedure supplied by Pierce and given early in this thesis.

## **6.6. Data and Discussion.**

**6.6.1. Prototype of the SIC Microchip.** The prototype TEP SIC microchip is shown in Figure. 6.1.1. A failure test to determine the maximum operating pressure was performed on the microchip by blocking one end of the chip and

attaching a nitrogen tank with a pressure regulator on the other end. The chip was submerged underwater to detect leaking gas. The results indicated the chip could withstand pressures up to 700 psi. When the pressure exceeded 700 psi the glue on fittings failed. Problems during the fabrication of the chip were experienced when the TEP was removed from the mold creating ripping at the channel and resulting in irregular channels, Figure 6.1.1. Problems experienced with the first prototype can be overcome by changing the fabrication process and fittings.

To overcome the problems with the first prototype, a number changes would have been made in the chip construction. First, the chip material would have been changed to poly(methyl methacrylate), (PMMA) the channel would have been embossed and solvent sealed.<sup>6,7</sup> Also, the chip would be tapped, so the fitting could be attached without glue. The next problem would be adding the stationary phase into the chip channel in a time effective manner. Early attempts of slurry packing the SIC microchip, failed because of the particle size distribution with a few very large particles blocking the opening of the channel. To overcome the problem with slurry packing the next few section focuses on the effort made toward developing a monolithic stationary phase for SIC.



Figure 6.1.1. A prototype the TEP Microchip SIC, the fittings attached on the chip by glue.

**6.6.2. Methacrylate Based Stationary Phase.** Methacrylate based monolithic stationary phases have been used for number years for affinity chromatography. The functional monomer has an exposed epoxide group, which allows for protein immobilized by a number of different chemistries. Additionally, the material does not have the pH limitations of silica-based monolithic columns. The initial studies focused on the ability to adjust the pore sizes by changing the percentages of cyclohexanol and dodecanol. The polymer samples were first coated with a 5 nm layer of gold to allow SEM images. The SEM images were taken of the gold coated methacrylate polymer using a 15 kV setting for 35 and 40% dodecanol, Figure 6.1.2. The average pore size of the polymer increased as concentration of deodecaol increased. Other groups have documented the increase in pore size with increasing dodecanol. (R) In addition, surface morphology changes with

increasing dedocanol form 40 to 35%. A problem with surface charging occurred even with a 5 nm coating of gold, caused by the porous nature of the material.

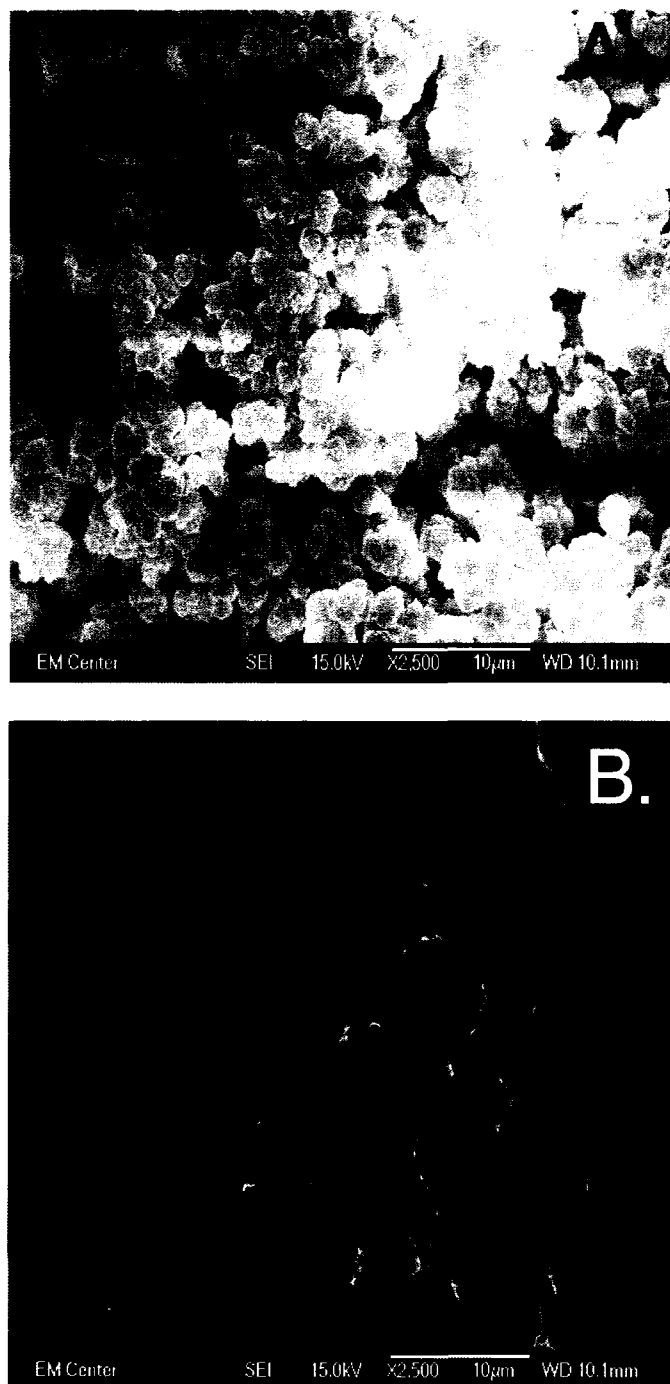


Figure 6.1.2. SEM images take of two monolithic columns with increasing DOOH concentrations, 35% DOOH (A), 40% DOOH (B)

**6.6.3. ISEC of the Methacrylate Polymer.** ISEC was used to measure the pore size distribution of the monolithic column. Initial experiments used polystyrene standards with narrow size distributions with THF as a mobile phase. These standards were used because of their low cost and the ability to detect at 280 nm, Figure 6.1.3. As the molecular weight of the polystyrene increased, the probe was excluded from a larger percentage of the pores, resulting in shorter retention time. In Figure 6.1.3, two different slopes are shown, corresponding to the macropore (excluded pore zone) and mesopore (internal pore zone).<sup>4</sup> The intersection of the two lines is the largest excluded pore diameter mesopore network.<sup>4</sup> Macropores are through pores that have a size range of 1.5 to 2  $\mu\text{m}$  and are a network of flow channels that allow the analyte access to the entire column.<sup>4</sup> The mesopores are side channels off the flow channel network that vary in size between 10 to 20 nm.<sup>4</sup> The porosity of the monolithic column has 75%, and is dependent on the macropores.

The defined intersection of the mesopore and macropore networks indicates the mobile phase and standards used for ISEC are not interacting with stationary phase. The problem with the experiment was the mobile phase used, THF causes the methacrylate polymer to swell. In addition the polystyrene standards are not representative of globular proteins. For the above reason, the standards and the mobile were changed for ISEC to phosphate buffer and dextrane probes.

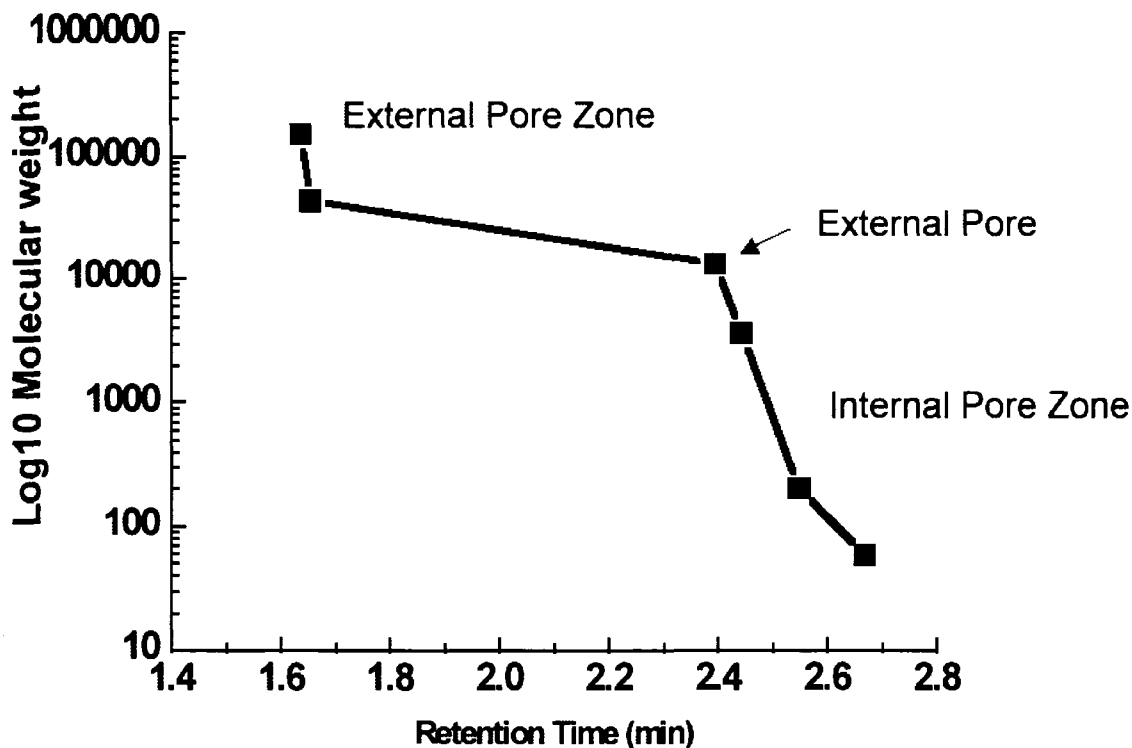


Figure 6.1.3. Trending the change in polystyrene probes of increasing molecular weight. Instrumental settings: Mobile phase THF, 0.1 mL/min, injection volume 5  $\mu$ L, detector set at 280 nm.

**6.6.4. ISEC with Dextran Standards.** Using dextran probes required the RI detector, because dextran lacks a strong UV chromophore. Changing the detector to RI resulted in an increase in noise, not seen with the UV detector. RI detectors are known to be among the least sensitive so this result is not surprising. Figure 6.1.4. shows the chromatograms of increasing molecular weight dextran probes versus the normalized  $K_d$  for two monolithic columns. The steep slope for 40% DOOH from 1 to 0.1 below the 100,000 MW probe size, indicates a large pore size distribution. The pore size distribution for 35% DOOH was smaller than 40% DOOH indicated by the intersection of the slopes at 124,000, kD. Unlike previous

ISEC, there is an increase in noise for the dextrane compared to the polystyrene. The ISEC data and SEM data were used to choose 35% dodecanol for all future experiments. 35% dodecanol was chosen for the smaller pore size distribution and resulting increase in surface area available for protein immobilization. The change in  $k_d$  values of ISEC slope for the two monolithic columns agreed with pore size distribution of the SEM images in section 6.1.3.

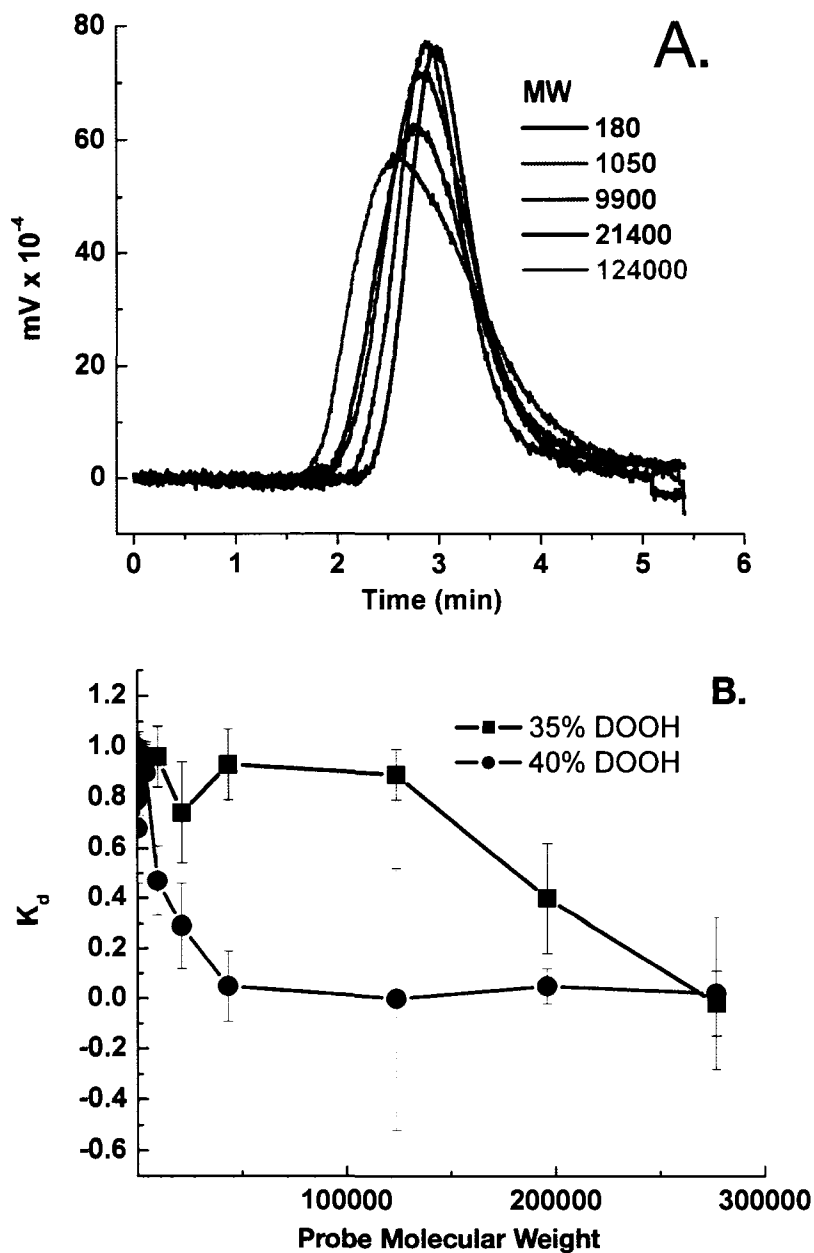


Figure 6.1.4. Trending the change in Dextran probes of increasing molecular weight. Instrumental settings: Mobile phase 120 mM NaCl, 6mM  $\text{Na}_2\text{HPO}_4$ , pH 7 Flowrate: 0.030 mL/min, injection volume 0.5  $\mu\text{L}$ , RI detector.

**6.6.5. Reproducibility of the Polymer.** A common problem with the polymer monolithic columns is reproducing the similar pore size distribution each time a monolithic column is formed. To measure the reproducibility of the monolithic columns SEM and ISEC were used to measure the pore size distribution. SEM images were taken for two monolithic columns formed using the same polymer mixture, Figure 6.1.5. The SEM images show a difference in the pore size distribution when comparing the A with B. The SEM data was not quantitative because of the difficulty of measure the pore sizes and the poor SEM image quality. ISEC was used to quantitatively measure the pore size distribution for two monolithic columns, Figure 6.1.6. ISEC data shows two different size pore size distribution measured for two monolithic columns from the same polymer solution. The SEM and ISEC data agrees with other accounts of the difficulty of reproducing the similar pore size distribution, for polymer monolithic columns. For reproducing similar pore size distribution the polymerization parameters need to be carefully controlled.<sup>15</sup>

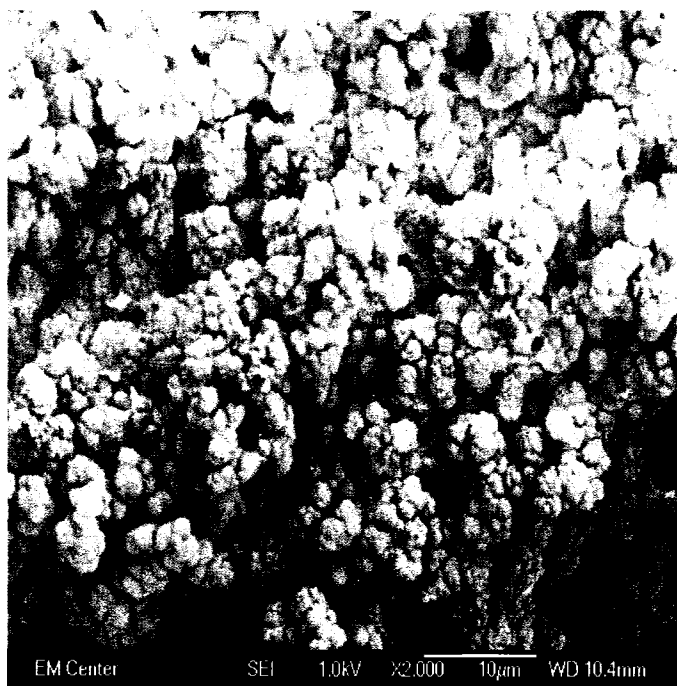
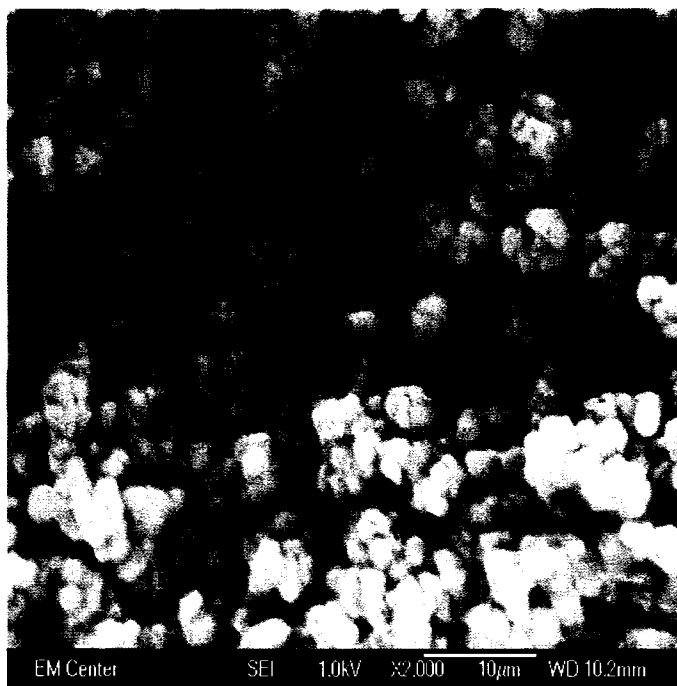


Figure 6.1.5. SEM images of two horizontal samples taken of two monolithic columns of the methacrylate polymer column.

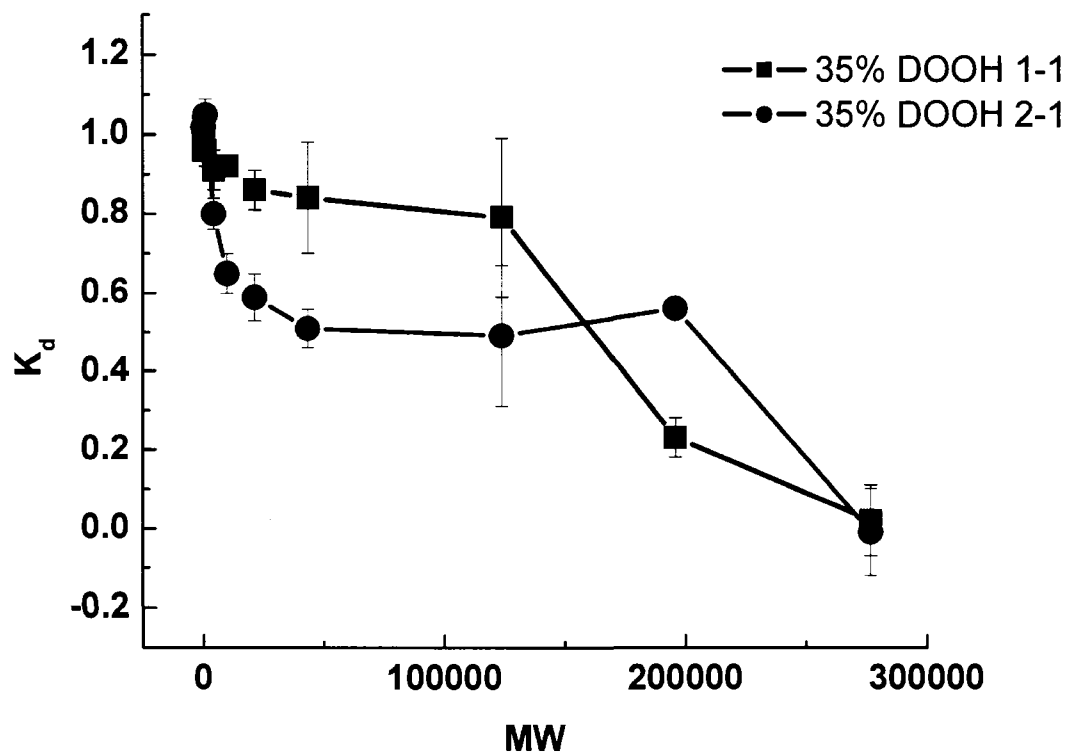


Figure 6.1.6. Measured reproducibility of the monolithic column with the same DOOH concentration by ISEC. Instrumental settings: Mobile phase 120 mM NaCl, 6mM Na<sub>2</sub>HPO<sub>4</sub>, pH 7, flowrate 0.030 mL/min, injection volume 0.5  $\mu$ L, RI detector.

**6.6.6. On Column Immobilization of Lysozyme.** One of the goals for monolithic column was the ability to immobilize the protein on the column in chip, followed by measuring the coupling density without destroying the stationary phase. The experiments were performed with lysozyme. The first set of experiments were to simply determine if lysozyme could be immobilized on column by simply flowing the protein through the stationary for long period of time measured hours. Figure 6.1.7 (A) shows that lysozyme can be immobilized on column by pumping the protein through the stationary phase at very low flow rates for time period exceeding 12 hours.

The next step was determined if the protein coupling density could be determined by indirect methods that would not destroy the stationary phase. The most promising method was a stop flow method in which the protein was pumped into the column and stopped for 2 minutes, then collected and UV absorbance used to determine protein immobilization density. The amount of protein immobilized on the monolithic column would be determined by measuring the difference in absorbance of the protein in solution. The results of the stop flow method are shown in Figure 6.1.7 (B). At time zero, the protein concentration was measured in solution was 1.90 mg/mL, which would indicate that a percentage of protein was immobilized on the column. At 4 minutes, the lysozyme concentration increased to 2.2 mg/mL in solution, close to the starting concentration of lysozyme, in the buffer. The problem is the large amount of noise in the data after time zero, which makes it impossible to determine when the immobilization of

lysozyme ended. The noise in the data could be due to the protein-protein interactions of the immobilized protein and mobile protein.

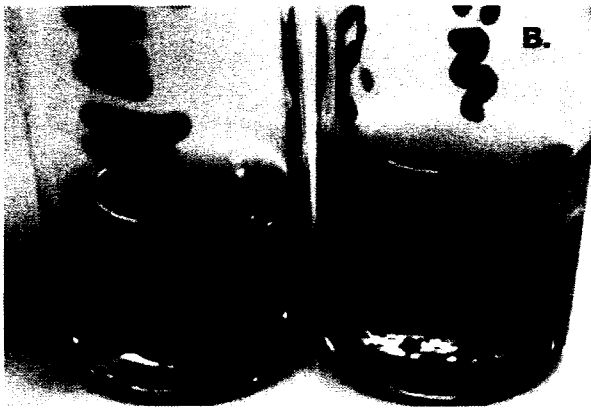
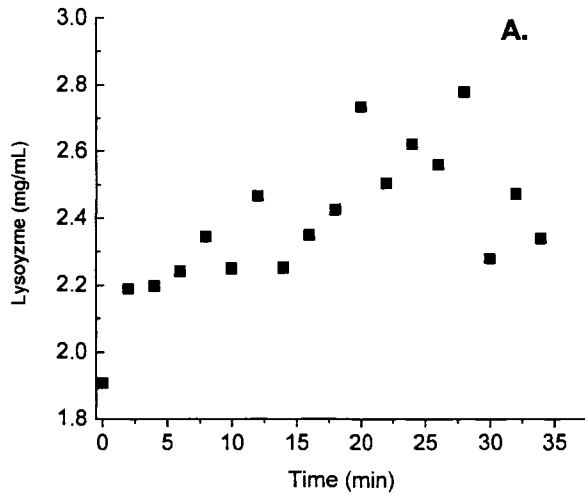


Figure 6.1.7. Trending the change in absorbance of lysozyme in the mobile phase during on column immobilization of a monolithic column. Image A shows a control and live column after protein immobilization. Data showing online coupling of lysozyme (A) and (B)

**6.6.7. Monolithic SIC.** After demonstrating protein immobilization, a series of SIC experiments were performed. This experiment shows the ability of the monolithic SIC to measure the change in B for lysozyme at different concentrations of NaCl. Figure 6.1.8, shows the change in B for lysozyme at 0, 0.2, 0.4 and 0.5 M NaCl. Lysozyme peaks are shifted to the left as the concentration of NaCl was increased, indicating attractive interactions. B decreased to negative values when NaCl concentration increased from 0 to 1 M, starting at  $175 \times 10^{-4} \text{ mol mL g}^{-2}$  and ended at  $-75 \times 10^{-4} \text{ mol mL g}^{-2}$ . The trend in B measured for lysozyme with increasing NaCl is similar to conventional SIC and SLS, but the absolute values are much larger. The difference in magnitude is most likely due to protein interacting with stationary phase, which is reflected by the magnitude and the positive B value for 2% NaCl. It may also be due to our inability to accurately measure surface coverage.

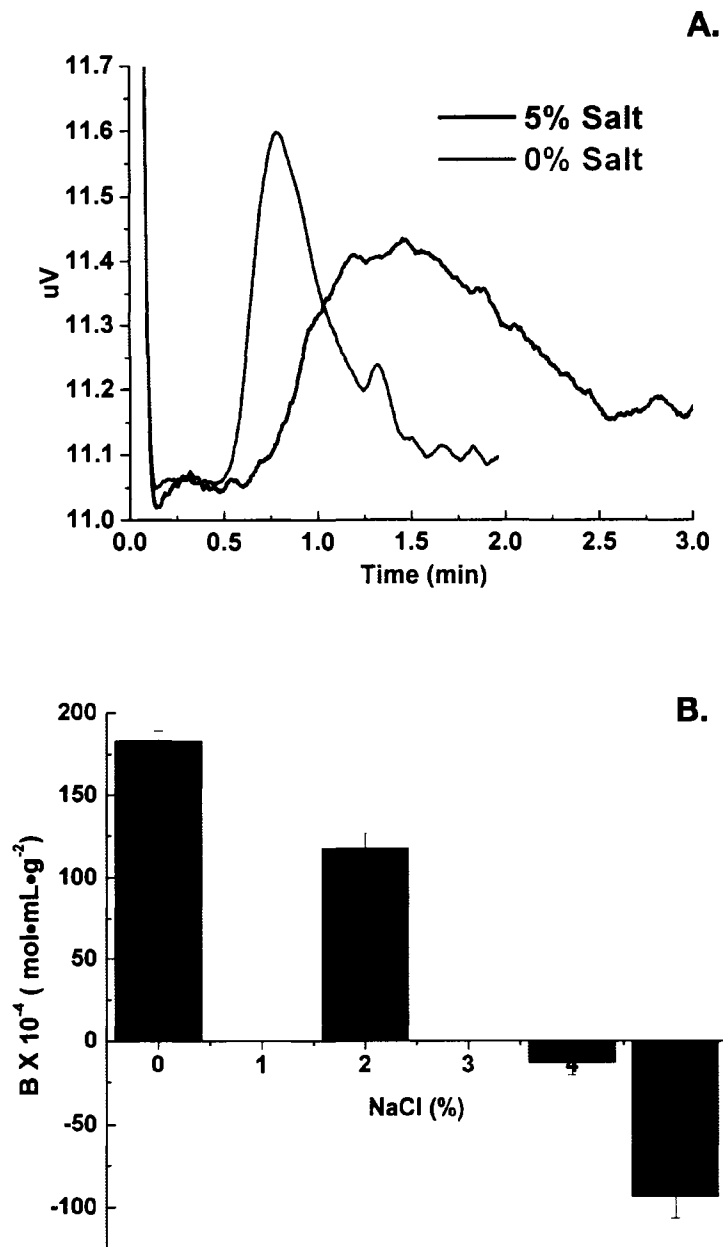


Figure 6.1.8. The effects of increasing NaCl concentration from 0 to 1 M at pH 4.5 of lysozyme, chromatograms (A), B values (B). Instrumental settings: Mobile Phase: 0.1 M Acetic acid, pH 4.5, flowrate =0.01 mL/min, injection volume 0.5  $\mu$ L, wavelength 280 nm

**6.7. Conclusions.** The initial experiments with the monolithic column demonstrated the potential of the micro SIC to measure B. A number of problems need to be addressed before the method could be an effective alternative to the small scale SIC. The construction of the TPE chip as proposed for the microchip SIC needs to be improved to prevent deformed channels in Figure 6.1.1. Later in the development process the epoxide chemistry was found to only work with material. Other types of chemistry require the use of organic solvents that will dissolve and crack the TEP material. Alternative materials can be used to construct the microchip, such as glass or metal. The glass and metal chips would be able to withstand the organic solvents required for formation of the monolithic chemistries. The major limitation would be the expense of making the chips.

The next problem is the lack of reproducibility in pore size distribution of the monolithic columns. If the project was continuing I would propose the use of silica monolithic columns, because its able to reproduce the same pore size distribution and chemistry to immobilize proteins is will documented.<sup>16</sup> Lastly a method needs to be determined to measure the protein coupling density with greater accuracy.

**6.8. Reference:**

1. Garcia, C. D.; Hadley, D. J.; Wilson, W. W.; Henry, C. S., Measuring protein interactions by microchip self-interaction chromatography. *Biotechnology Progress* **2003**, 19, (3), 1006-1010.

2. Henry, C. S., *Microchip capillary electrophoresis: methods and protocols*. Humana: Totowa, NJ, 2006; Vol. 339, p 237.
3. James, P. L., *Capillary and Microchip Electrophoresis and Associated Microtechniques*. 3 ed.; CRC Press, Taylor & Francis Group: Boca Raton, FL, 2008; p 1567.
4. Al-Bokari, M.; Cherrak, D.; Guiochon, G., Determination of the porosities of monolithic columns by inverse size-exclusion chromatography. *Journal of Chromatography A* **2002**, 975, (2), 275-284.
5. Mallik, R.; Hage, D. S., Affinity monolith chromatography. *Journal of Separation Science* **2006**, 29, (12), 1686-1704.
6. Jiang, T.; Mallik, R.; Hage, D. S., Affinity monoliths for ultrafast immunoelectroextraction. *Analytical Chemistry* **2005**, 77, (8), 2362-2372.
7. Hage, D. S.; Austin, J., High-performance affinity chromatography and immobilized serum albumin as probes for drug- and hormone-protein binding. *Journal of Chromatography B-Analytical Technologies in the Biomedical and Life Sciences* **2000**, 739, (1), 39-54.
8. Guiochon, G., Monolithic columns in high-performance liquid chromatography. *Journal of Chromatography A* **2007**, 1168, (1-2), 101-168.
9. Vissers, J. P. C., Recent developments in microcolumn liquid chromatography. *Journal of Chromatography A* **1999**, 856, (1-2), 117-143.
10. Zou, H. F.; Huang, X. D.; Ye, M. L.; Luo, Q. Z., Monolithic stationary phases for liquid chromatography and capillary electrochromatography. *Journal of Chromatography A* **2002**, 954, (1-2), 5-32.

11. Miyabe, K.; Guiochon, G., Characterization of monolithic columns for HPLC. *Journal of Separation Science* **2004**, 27, (10-11), 853-873.
12. Courtois, J.; Szumski, M.; Georgsson, F.; Irgum, K., Assessing the macroporous structure of monolithic columns by transmission electron microscopy. *Analytical Chemistry* **2007**, 79, (1), 335-344.
13. DePhillips, P.; Lenhoff, a. M., Pore size distributions of cation-exchange adsorbents determined by inverse size-exclusion chromatography. *Journal of Chromatography A* **2000**, 883, (1-2), 39-54.
14. Vickers, J. a.; Dressen, B. M.; Weston, M. C.; Boonsong, K.; Chailapakul, O.; Crokek, D. M.; Henry, C. S., Thermoset polyester as an alternative material for microchip electrophoresis/electrochemistry. *Electrophoresis* **2007**, 28, (7), 1123-1129.
15. Eeltink, S.; Rozing, G. P.; Schoenmakers, P. J.; Kok, W. T., Practical aspects of using methacrylate-ester-based monolithic columns in capillary electrochromatography. *Journal of Chromatography A* **2006**, 1109, (1), 74-79.
16. Poole, C. F., *The Essence of Chromatography*. Elsevier Science B.V.: Amsterdam, 2003; p 925.

## 7. Dissertation Summary.

**7.1. Summary.** The work presented in this dissertation has been focused on advancing the ability to measure B by SIC for therapeutic proteins and peptides, using new immobilization chemistries and miniaturizing the method and equipment. By introducing new immobilization chemistries proteins and peptides were immobilized on the stationary phase with coupling densities greater than 2 mg/ mL. The first therapeutic agent was peptide in which a large screening study measured B as a parameter for screening conditions that improved colloidal stability. The work was the first time B was measured for a peptide. When correlating B values with solubility data provided by Lilly, both data sets agreed in pH trend. The second therapeutic agent was a single chain antibody where B was used as a parameter to indicate changes in the colloidal stability. The data generated from the screening study was used to successfully choose solvent/co-solvent system, which improved the solubility of the fragment. The increase in solubility of LB-005 allowed it to advance to the next stage of development, one step closer to a commercial product. Additionally, B was used to compare the differences in the colloidal stability of a mutant of LB-005 that had improved colloidal stability; the B measured for the mutant agreed with the company's data. Studies of comparing LB-005 with the mutant are the first time B has been shown differences in colloidal stability caused by two-point mutations. The last group of proteins examined by SIC was several types of membrane proteins. Membrane proteins are difficult to work with because of their hydrophobic nature that requires using detergent above their CMC to be stable in aqueous solutions. The

presence of the detergent above the CMC does not increase the chemical noise for SIC like it does for SLS. SIC was able to measure B in the presence of micelles. For this reason it was used to measure the changes in colloidal stability of the three membrane proteins, pR, RHO and OMPX in complex buffers. SIC makes it possible to quantitatively trend the colloidal stability of membrane proteins in detergents and co-solvent, which has not been practical using SLS. The data collected for pR is the first step to increasing our understanding of how detergents and co-solvents effect the physical stability of membrane proteins. The amount of analyte available for the screening studies and the cost of the co-solvents for the above work allowed the work to be performed on the HPLC. In many cases the amount of material available was less than 1 mg, which prevents the traditional HPLC from being used.

The next stage of my work was to develop a scaled down SIC method for measuring B for proteins and peptides using less than 1 mg material. To accomplish this goal, SIC parameters were characterized to understand the effects of decrease column volume, flow rates and injection volume on B. Characterization studies indicated the need to decrease the flow rate to less than 0.1 mL/min for column lengths less than 5 cm. For this reason, I developed a instrument that could handle flow rates of less than 0.1 mL/min and a lab view program that could collect the data for analysis. The developed instrument the B values for lysozyme were measured and when compared to SLS and conventional scale the data sets, were the same. The instrument made it

possible to measure B for a protein using less than 1 mg, making it practical to perform limited screening study for low abundant proteins. Additionally, the instrument consumed less than 10 mL of mobile phase per condition and decreasing the cost of the analyses by consuming less than 1 mg of expensive co-solvents. The development of the small scale instrument and software made it possible to measure B for two membrane proteins RHO and OMPX. The B for the two membrane proteins was first to be measured by SIC and demonstrates B values can be made using less than 1 mg for a limited screening study. The stage of my work was to develop microchip SIC for measuring B for rapid screening studies using less than 0.1 mg of material.

The third stage of my work was to development of a microchip SIC that could further decrease sample consumption and run time. The first goal was to develop a microchip that would not fail at high flow rates. The prototype TPE microchip was able to handle 700 psi without failing. The next stage in the work was developing a stationary phase support that could be formed in channel and withstand a wide range of pH conditions, and allow for a number of different immobilization chemistries. A first generation monolithic stationary phase was developed that allowed for protein immobilization and could have been formed in the microchip channel. The rest of the work focused on developing analytical methods to measure the pore size distribution and coupling densities of the protein. Early results demonstrate that the microchip SIC using a polymer monolithic column could work with further development.

**7.2. Future Work.** The future work for the project will focus on three areas, measuring B for more proteins, measuring the effect of novel co-solvent, and developing the microchip SIC. This lab has demonstrated the ability of SIC to measure B values for a limited number of proteins, peptides and membrane proteins. Large group of proteins are important in industry and pharmaceutical field have limited amount of quantitative data about colloidal stability. Early developmental pharmaceutical proteins typically have limited amounts of material due to low yields, caused by small recovery during purification steps and storage. Simple screening experiments using B as an analysis parameter has been used to improve colloidal stability and potentially improving yields.

The next stage is screening for novel co-solvents that would improve the colloidal stability of biopolymers. This would be particularly useful for the industry application since co solvent for therapeutic applications need approval by the FDA, a lengthy and very time-consuming process. New co solvent have been shown effective stabilizers and effective crystallizing agents for a model proteins and membrane proteins. Screening new and old co-solvents against a large number of biopolymers representing different classes of proteins and peptide is needed. B values, along with other physical methods to characterize conformational stability would be of great value to the protein and processing community. Performing large screening studies using small amounts of protein would require a modified SIC method including a SIC instrument with a low dead volume. Scaling down the SIC method to the microchip scale would greatly

improve the use of this method for a broader range of proteins, especially those in early stage development where material available is limited.

## APPENDIX 1: RESEARCH PROPOSAL

### Coupling HPLC to microchip CE for the detection of aminoglycoside antibiotics.

Robert W. Payne, Department of Chemistry, Colorado State University  
Original Research Proposal

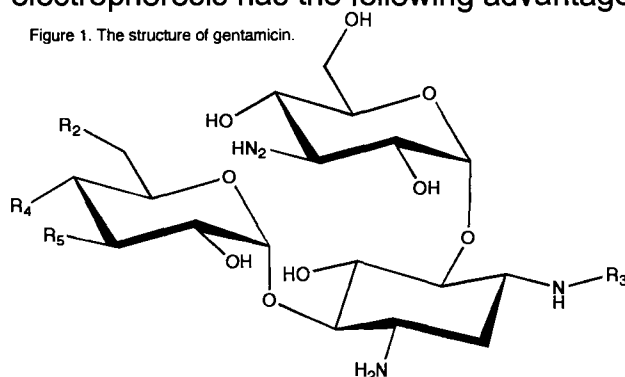
#### A. Specific Aims.

Antimicrobial agents have been successfully used for years in treating infections that were once deadly for humans and animals.<sup>1-3</sup> The use of antimicrobial agents in livestock feed has increased revenues by promoting animal growth by improving an animal's ability to absorb nutrients in feedstock.<sup>2-4</sup> A 1995 report estimated that 8163 megagrams of antibiotics are used in the livestock industry, yearly.<sup>3, 4</sup> Due to the poor absorption properties of antibiotics through the intestinal gut wall, potentially 75 to 90% of the antimicrobial agent is excreted as the parent compound in the urine and manure and then enters the environment.<sup>3, 4</sup> A major concern with the use of antimicrobial agents is the potential for developing antibiotic resistant strains of bacteria, especially in surface water.<sup>5, 6</sup>

Aminoglycosides are among the more commonly used antibiotics in the livestock industry.<sup>3</sup> Compared to other antibiotics, aminoglycosides are difficult to detect because they lack a strong chromophore and are difficult to resolve with common separation methods, Figure 1.<sup>7</sup> The most common method to quantify aminoglycosides in environmental samples is based on derivatization of the sample with a strong chromophore, followed by separation by LC and detection by UV detection.<sup>8, 9</sup> An alternative to UV absorption is mass spectrometry (MS), which gives qualitative information in addition to quantitative data.<sup>1</sup> Electrochemical methods, such as pulsed electrochemical detection (PED), provide an alternative for detecting aminoglycosides that do not require sample derivation or expensive instrumentation.<sup>10</sup>

Separating aminoglycosides using liquid chromatography is difficult because of the similarity of the structures.<sup>7</sup> Additionally, impurities in environmental samples increase the difficulty of separating and quantifying aminoglycosides, requiring increased peak capacity and resolution for separation by LC methods.<sup>11</sup> An alternative method to LC is capillary electrophoresis (CE).<sup>7</sup> Capillary electrophoresis has the following advantages over LC: band broadening is due to

Figure 1. The structure of gentamicin.



diffusion since there is no mass transfer band broadening, reduced consumption of samples and reagents and increased throughput. Microchip CE has the advantages of CE, while allowing for miniaturization and further decrease in sample consumption. Quantifying aminoglycosides in environmental samples requires additional sample

preparation and purification to remove impurities, increasing the required resolution needed for a single stage separation.<sup>11</sup> Ultimately, however, LC and CE individually lack the selectivity for separation of aminoglycosides from environmental samples. In this case, a multidimensional separations technique could provide the peak capacity and resolution needed to detect and quantify low concentration aminoglycosides in environmental samples.<sup>12, 13</sup>

The increased resolution of a multidimensional separation comes from the orthogonality of the separation mechanisms of LC and CE.<sup>14</sup> The goal of this proposal is to develop a novel two-dimensional LC-CE instrument for separation of aminoglycosides in environmental samples. Coupling LC to CE can be accomplished by off-line and on-line methods.<sup>7</sup> Off-line coupling occurs when the effluent from the first stage separation is manually transported to the second stage of the separation, typically by collecting fractions.<sup>15</sup> Off-line coupling of LC to CE is simple and inexpensive, but disadvantages are loss of analyte due to adsorption onto the transfer container and decreased reproducibility due to manual sample handling.<sup>15</sup> In on-line coupling, the LC effluent is injected directly into the CE column. The advantages of on-line coupling of LC to CE is increased reproducibility, automation and decreased operator involvement.<sup>15</sup> The limitations of on-line coupling are increased system complexity, peak broadening caused by dead volume at the interface and the potential for longer analysis times.<sup>14, 15</sup> Furthermore, for on-line coupling of LC to CE the interface needs to account for differences in volumetric flow rates for LC (mL) versus CE ( $\mu$ L-nL).<sup>14</sup> *Here, a simple design for a zero dead volume interface between LC and microchip CE for the multidimensional separation of aminoglycosides is proposed.* To accomplish this goal the following aims are proposed:

1. Develop a zero dead volume interface between the eluent of an HPLC column and a CE microchip.
2. Demonstrate a two-dimensional separation of a mixture of standard aminoglycosides using the integrated system.

3. Analyze simulated environmental samples using the proposed microchip design and validate the data with accepted LC methods.

The zero dead volume interface design will simplify the on-line interface between the LC to microchip CE when compared to current on-line coupling interfaces.<sup>16</sup><sup>17</sup> The design requires no additional hardware or controls such as switching valves, optically gated injections and/or transversal buffer flow.<sup>17, 18</sup> The zero dead volume interface will be integrated onto the microchip CE decreasing cost and overall instrumental complexity. The design will allow for direct on-line coupling from LC to microchip CE with minimal peak broadening and loss of analyte. Additionally, the design of the zero dead volume interface will allow for detection and quantification of aminoglycosides in complex environmental samples. The resulting analyses will be simpler, easier and more cost effective in terms of equipment and analyst time using the proposed LC-Microchip-CE-PAD design.

**B. Background.** Aminoglycosides are commonly added to livestock feed as antimicrobial agents for aerobic gram-negative bacteria.<sup>3, 4</sup> Aminoglycosides are used to kill gram negative bacteria by inhibiting protein synthesis.<sup>19</sup> Development of resistant strains of bacteria is a health concern, since these strains can lead to hospitalization and more expensive and toxic antibiotics for treatment. A concern with the use of aminoglycosides is the development of the resistant strains of bacteria caused by the over use in the livestock industry.<sup>3, 4</sup> In humans, aminoglycosides are used in the treatment of *pseudomonas aeruginosa*, *salmonellae* and *tuberculosis*.<sup>4</sup> The potential for the resistant strains of bacteria to enter the human food chain through meat products and surface water is a major concern, because of the potential for resistant strains of bacteria.<sup>3, 4</sup> Already there are reports of bacteria found in rivers across the United States that are resistant to ampicillin.<sup>4, 6</sup> As a result the extent of aminoglycoside contamination needs to be determined through careful monitoring. This proposal will allow for easier detection and quantification of aminoglycosides, improving the ability to monitor the quality of surface water.<sup>6, 20</sup>

Aminoglycosides are amino-function-containing carbohydrates linked via a glycoside bond, Figure 2.<sup>19</sup> This class of antibiotics is typically characterized by one major component, such as the presence of  $-\text{CH}_3\text{NH}_2$  at R3 and minor components, differences of H and primary alcohol. For example, gentamicin variants have 5 major variable groups, C<sub>1</sub>, C<sub>2</sub>, C<sub>3</sub>, C<sub>1a</sub>, C<sub>1b</sub>, C<sub>2b</sub>, increasing the difficulty in separating each component due to their similar structures. Aminoglycosides as a group lack a strong chromophore, are water-soluble and are usually charged because of the amino groups. The nonvolatile nature of the aminoglycoside requires sample derivatization for gas chromatography (GC) analysis. As a result HPLC and CE are the two main methods for separation of the aminoglycosides in environmental samples. Other antibiotics relevant to livestock industry are seen in levels below  $0.1 \mu\text{g L}^{-1}$  in river samples, while

wastewater taken from a hospital detected concentrations of gentamicin between 0.1 to 7.4  $\mu\text{g} \times \text{L}^{-1}$ .<sup>20, 7, 12, 19</sup>

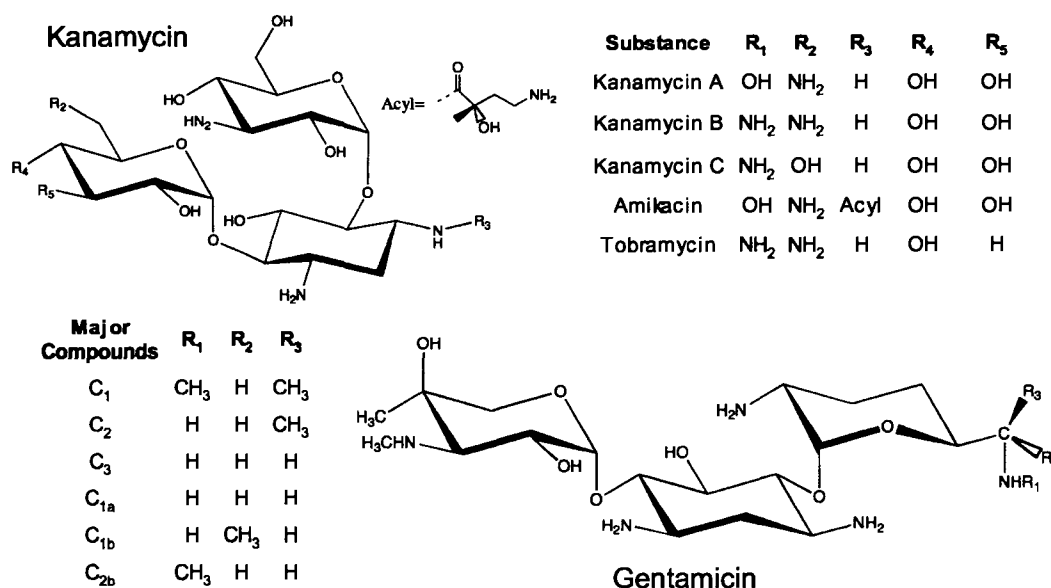


Figure 2. A list of aminoglycosides commonly used in livestock and the major structures of gentamicin.

**Liquid Chromatography.** The LC methods that have been used to separate aminoglycosides includes reverse phase (RP), ion pairing, ion exchange and normal phase.<sup>13</sup> The polar and ionic nature of aminoglycosides increases the difficulty of separating aminoglycosides by reverse phase methods.<sup>13</sup> Normal phase is also difficult without sample derivatization since aminoglycosides are not readily soluble in organic compounds.<sup>13</sup> A common method used to separate aminoglycosides is ion-pair chromatography (IP), where the analyte is paired with pentane and heptane.<sup>13</sup> Ion-exchange is not widely used because run parameters such as buffer pH, ionic strength and temperature must be constant.<sup>13</sup> Furthermore, separating aminoglycosides is complicated due to the need for sample derivatization prior to separation coupled with offline purification and low throughput.

**Capillary Electrophoresis.** Two CE modes are commonly used for separating aminoglycosides, capillary zone electrophoresis (CZE) and micellar electrokinetic chromatography (MEKC).<sup>7, 21, 22</sup> For the CZE separation the analyte is separated by applying a potential along the length of a capillary, causing differences in migration for the analyte according to the charge-to-size ratio.<sup>7</sup> CZE has been used to separate kanamycin, gentamicin and tobramycin with a LOD of 9  $\mu\text{g}/\text{mL}$  using absorbion.<sup>7, 22</sup> For MEKC amikacin, genamicin and netilmicin are separated based on their partitioning with micelles.<sup>7, 21</sup> CE has further been miniaturized to the microchip scale for the analysis of penicillin and ampicillin as a way to decrease sample consumption and analysis time.<sup>16</sup> The main drawback to using CE is the sample treatment needed before sample injection and the lack of sensitivity due to small injection volumes. This is especially true for complex

matrices such as environmental samples. The CE methods described above in general lack selectivity needed to resolve aminoglycosides from closely related compounds in environmental samples.

**Detector Modes.** Despite the fact that aminoglycosides lack a strong chromophore, UV is the most common mode of detecting them in LC and CE separations.<sup>12, 13</sup> UV detection requires derivatizing the sample, most commonly with 1,2-phthalic dicarboxaldehyde (OPA) in either pre- or post-column mode.<sup>8</sup> Another mode of detection that requires derivatizing the sample is fluorescence.<sup>21</sup> Derivatizing the sample increases analysis time and careful control of derivatizing parameters is required for reproducible results and stability of the derivatized sample. Alternatively, aminoglycosides have been detected with UV without derivatizing the sample. Complexing the sample with borate enhances detection at low wavelengths (~206 nm).<sup>23</sup> This mode of detection has only been used with CE and has poor selectivity.<sup>23</sup> Mass spectrometry (MS) and NMR have also been used to detect aminoglycosides and both give structural information, but are expensive.<sup>1, 24</sup>

Electrochemical detection of aminoglycosides requires no sample derivatization and is less expensive than MS or NMR.<sup>1, 24</sup> The electrochemical detection modes used to detect aminoglycosides include the potential gradient detector (PGD), conductivity detection and fast Fourier cyclic voltammetry, all of which have comparable sensitivity to UV.<sup>25, 26</sup> The primary problem with electrochemical detection of aminoglycosides is fouling of the electrode surface. An alternative electrochemical mode of detection is pulsed electrochemical detection (PED), which uses a cleaning step during the run to reduce electrode fouling.<sup>10</sup> PED is an attractive mode for detecting aminoglycosides because it does not require sample derivatization, is less expensive compared to MS/NMR and does not suffer from electrode fouling.<sup>10, 23, 24</sup>

**Summary.** Individually CE and LC lack the selectivity and resolution for the separation of aminoglycosides in complex environmental samples.<sup>12</sup> Additionally, CE methods require off column sample preparation, which increases analysis time and decreases method reproducibility. The development of a high throughput LC-CE two-dimensional separation system should allow effective separation of these analytes from complex media. Developing a zero dead volume interface between HPLC and microchip PED will increase peak capacity and resolution of the aminoglycosides, improving the monitoring of aminoglycosides in environmental samples. The high throughput LC-CE two-dimensional separation system will greatly improve the detection and quantification of aminoglycosides in environmental samples, which will allow for better monitoring of aminoglycosides in the surface water.

**C. Methods and Experimental Design.** The design and development of the zero dead volume interface between LC and microchip CE for the detection of aminoglycosides in surface water samples will occur in three stages. The work

will result in a robust LC-microchip-CE system for the detection of aminoglycosides and other electrochemically active compounds found in environmental complex matrices.

**C.1. Design and Optimizing.** The zero volume interface shown in Figure 3 will be designed to adjust for flow volume differences between the LC and microchip CE systems as well as isolate LC bulk hydrodynamic flow from the electroosmotic flow (EOF) of CE. The goal of this section is to optimize channel dimensions and the flow parameters of HPLC, Waste and Injection channels. Changing the height and width of the three channels will determine backpressure, peak broadening and sample transfer efficiency. These three variables will be monitored during the optimization of the zero volume interface.

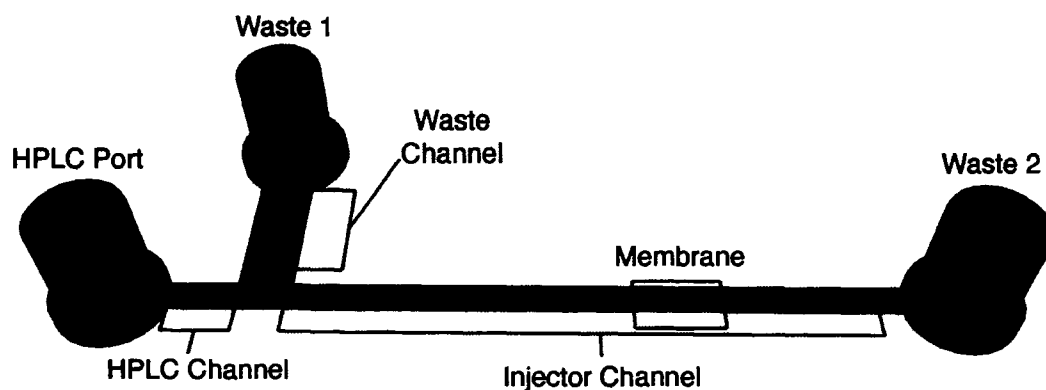


Figure 3. Proposed Design of the Zero Volume Interface integrated onto the microchip-CE

The interface adjusts for differences in LC flow by splitting a large percentage of it to Waste 1 and a small fraction towards Waste 2. The amount of flow split between the channels will be dependent on the channel cross-section and length. Backpressure may be a source of chip failure through leaking at the LC port, structural failure of the material and/or embedded membrane and broadening of the LC peak. The material used to construct the microchip CE with integrated zero volume interface will need to withstand high backpressures. As a result, microchip will be constructed using PMMA, a rigid polymer that can withstand pressures exceeding 1000 psi for solvent bonded chips.<sup>27, 28</sup> Forming channels in PMMA is a common process and will be briefly described here.<sup>29</sup> The channels will be formed in a mold made from the photolithography of SU8 on silicon.<sup>27, 28</sup> The channels will be embossed into PMMA using the SU8 mold under pressure and with temperatures exceeding the  $T_g$  of the material.<sup>27, 28</sup> Wax with a low melting point will flow through the channels and the chip will be solvent sealed with acetone.<sup>27, 28</sup> The rigid nature of PMMA allows for the ports on the interface to be tapped to accommodate finger tight fittings, making the interface with the HPLC simple.<sup>27, 28</sup>

For the optimization process the backpressure will be monitored at each port and at the membrane by pressure transducers attached to microchip as shown in Figure 4. The pressure transducers will be connected to LABVIEW for data collection. Additionally, the chip will be visually inspected for signs of structural failure. Fluorescein isothiocyanate (FITC) will be injected during the optimization process to monitor peak broadening.

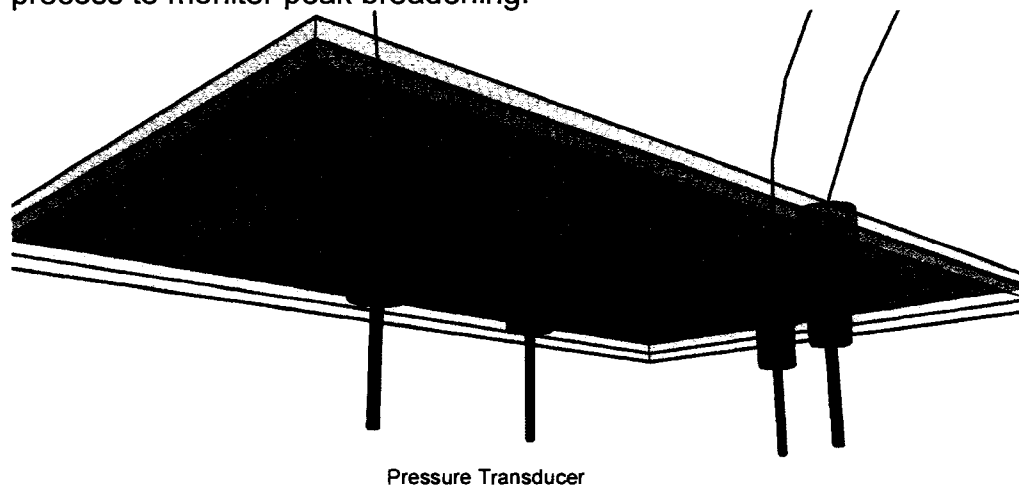


Figure 4. Locations where the pressure transducers imbedded into the PMMA under the waste ports and the membrane.

A membrane will be integrated into the zero volume interface to separate hydrodynamic flow from EOF.<sup>30</sup> The membrane introduces a number of potential problems includes leaking around the edges, membrane failure and the potential for peak broadening.<sup>30</sup> Leaking around the membrane will be detected visually with fluorescent dyes. The flow differences between the LC and microchip CE will be adjusted using the zero dead volume interface, with minimal peak broadening, preserving the peak resolution from the first stage of separation. The design of the zero dead volume interface will allow for a simple and cost effective method for on-line coupling of LC to microchip-CE-PAD, compared to other on-line LC-CE interfaces.

### **C.2. Two-Dimensional Separation of Aminoglycosides.**

The second phase will integrate the zero dead volume interface with microchip CE for the analysis of aminoglycosides with LC-Microchip-CE-PAD, Figure 5. To keep the ionic strength as low as possible, the LC column will be RP-LC using a C18 column with water-acetone gradient.<sup>13</sup> Additionally, the low ionic strength of the LC effluent will allow sample stacking at the membrane.<sup>5</sup> The second phase will be CZE, which has the selectivity needed to separate gentamicin and kanamycin. Gated injection is proposed because the LC eluent will continually diffuse across the membrane into the CE side of the chip.<sup>31</sup> For gated injection the sample is introduced into the CE when C4 and C2 are grounded, C3 is floating and C1 has a positive potential applied. During separation a positive potential is applied at C3, keeping C1, C2 and C3 the same injection potential. If not enough sample is diffusing across the membrane an alterative approach

would be driving the sample across the membrane electrokinetically by applying a potential at A.3.

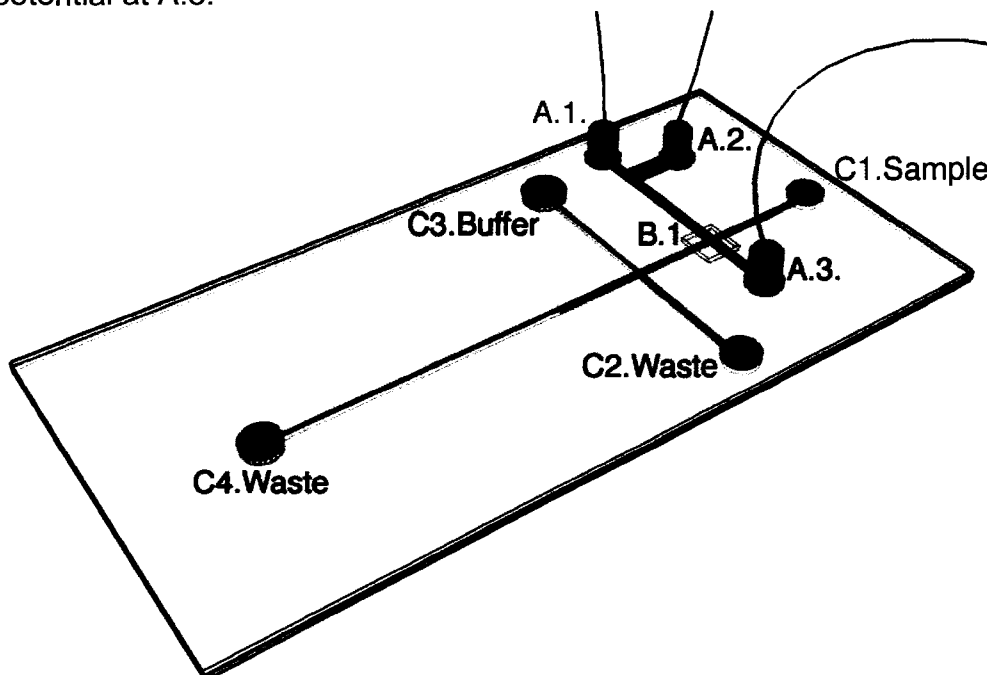


Figure 5. Proposed PMMA microchip design LC-CE-PAD. Zero volume interface integrated on chip (RED), A.1. Flow from LC, A.2. Waste, A.3. Flow out. B.1. Embedded membrane. CE-PAD (Blue)

The detection and separation of the LC-Microchip-CE-PAD will use kanamycin and gentamicin variants. LC flow rates will start at low flow rates, while injecting moderate concentrations of generamcin  $C_1$  and  $C_2$ . For each flowrate the CE voltage and gated injection time will optimize the 2D separation, by monitoring peak height, symmetry and resolution. The optimization process will proceed until peak height, symmetry and resolution is optimized for generamcin  $C_1$  and  $C_2$ .

### C3. Proof of Concept.

Simulated environmental samples will be used to compare the peak height, symmetry and resolution of the 2D LC-microchip-CE-PAD to USP method. Once the 2D LC-microchip-CE-PAD has been validated surface water samples will be analyzed. The channel dimensions for the zero volume interface determined in  $C_1$  will be used, while the separation and detection parameters determined in  $C_2$  will be used.

### D. Summary

The increase in the number of resistant strains of bacteria is a major health issue in every area of the United States, resulting in an increase in hospital stays, cost of treatment and the use of antibiotics with toxic side effects. Because of this, an increase in monitoring the potential source of antimicrobial agents in the environmental is becoming increasingly important. Antimicrobial agents such as aminoglycosides are commonly used but difficult to separate and detect by

common one-dimensional chromatography methods. Here, we propose a simple zero volume interface for on-line coupling of LC to microchip-CE PAD for the detection of aminoglycosides in surface water samples. Additionally, this simple interface can be used with future work for the detection of the aminoglycosides in other complex samples. Finally, the proposed system could be applied in many different applications where single dimension separations do not provide enough peak capacity.

## Reference.

1. Diaz-Cruz, M. S.; Barcelo, D., Determination of antimicrobial residues and metabolites in the aquatic environment by liquid chromatography tandem mass spectrometry. *Analytical and Bioanalytical Chemistry* **2006**, 386, (4), 973-985.
2. Chander, Y.; Gupta, S. C.; Goyal, S. M.; Kumar, K., Perspective - Antibiotics: Has the magic gone? *Journal of the Science of Food and Agriculture* **2007**, 87, (5), 739-742.
3. Kumar, K.; Gupta, S. C.; Chander, Y.; Singh, A. K., Antibiotic use in agriculture and its impact on the terrestrial environment. *Advances in Agronomy, Vol 87* **2005**, 87, 1-54.
4. Campagnolo, E. R.; Johnson, K. R.; Karpati, A.; Rubin, C. S.; Kolpin, D. W.; Meyer, M. T.; Esteban, J. E.; Currier, R. W.; Smith, K.; Thu, K. M.; McGeehin, M., Antimicrobial residues in animal waste and water resources proximal to large-scale swine and poultry feeding operations. *Science of the Total Environment* **2002**, 299, (1-3), 89-95.
5. Dorne, J. L. C. M.; Skinner, L.; Frampton, G. K.; Spurgeon, D. J.; Ragas, A. M. J., Human and environmental risk assessment of pharmaceuticals: differences, similarities, lessons from toxicology. *Analytical and Bioanalytical Chemistry* **2007**, 387, (4), 1259-1268.
6. Ash, R. J.; Mauck, B.; Morgan, M., Antibiotic resistance of gram-negative bacteria in rivers, United States. *Emerging Infectious Diseases* **2002**, 8, (7), 713-716.
7. Garcia-Ruiz, C.; Marina, M. L., Recent advances in the analysis of antibiotics by capillary electrophoresis. *Electrophoresis* **2006**, 27, (1), 266-282.
8. Fabre, H.; Sekkat, M.; Blanchin, M. D.; Mandrou, B., Determination of Aminoglycosides in Pharmaceutical Formulations.2. High-Performance Liquid-Chromatography. *Journal of Pharmaceutical and Biomedical Analysis* **1989**, 7, (12), 1711-1718.
9. Kaale, E.; Van Schepdael, A.; Roets, E.; Hoogmartens, J., Aminoglycoside antibiotics: A decade's overview of capillary electrophoresis analysis. *American Laboratory* **2002**, 34, (21), 22-+.
10. Long, C. Y.; Yang, X. F.; Lee, B.; Ong, C., Optimizing the triple-potential waveform for the pulsed amperometric detection of streptomycin. *Analytical Letters* **2005**, 38, (11), 1759-1767.

11. Giddings, J. C., Concepts and Comparisons in Multidimensional Separation. *Journal of High Resolution Chromatography & Chromatography Communications* **1987**, 10, (5), 319-323.
12. Flurer, C. L., The Analysis of Aminoglycoside Antibiotics by Capillary Electrophoresis. *Journal of Pharmaceutical and Biomedical Analysis* **1995**, 13, (7), 809-816.
13. Isoherranen, N.; Soback, S., Chromatographic methods for analysis of aminoglycoside antibiotics. *Journal of Aoac International* **1999**, 82, (5), 1017-1045.
14. Evans, C. R.; Jorgenson, J. W., Multidimensional LC-LC and LC-CE for high-resolution separations of biological molecules. *Analytical and Bioanalytical Chemistry* **2004**, 378, (8), 1952-1961.
15. Stroink, T.; Ortiz, M. C.; Bult, A.; Lingeman, H.; de Jong, G. J.; Underberg, W. J. M., On-line multidimensional liquid chromatography and capillary electrophoresis systems for peptides and proteins. *Journal of Chromatography B-Analytical Technologies in the Biomedical and Life Sciences* **2005**, 817, (1), 49-66.
16. Garcia, C. D.; Henry, C. S., Direct determination of carbohydrates, amino acids, and antibiotics by microchip electrophoresis with pulsed amperometric detection. *Analytical Chemistry* **2003**, 75, (18), 4778-4783.
17. Bergstrom, S. K.; Dahlin, A. P.; Ramstrom, M.; Andersson, M.; Markides, K. E.; Bergquist, J., A simplified multidimensional approach for analysis of complex biological samples: on-line LC-CE-MS. *Analyst* **2006**, 131, (7), 791-798.
18. Bushey, M. M.; Jorgenson, J. W., Automated Instrumentation for Comprehensive 2-Dimensional High-Performance Liquid-Chromatography Capillary Zone Electrophoresis. *Analytical Chemistry* **1990**, 62, (10), 978-984.
19. Kaale, E.; Govaerts, C.; Hoogmartens, J.; Van Schepdael, A., Mass spectrometric study to characterize thioisindole derivatives of aminoglycoside antibiotics. *Rapid Communications in Mass Spectrometry* **2005**, 19, (20), 2918-2922.
20. Coetsier, C.; Lin, L. M.; Roig, B.; Touraud, E., Integrated approach to the problem of pharmaceutical products in the environment: an overview. *Analytical and Bioanalytical Chemistry* **2007**, 387, (4), 1163-1166.
21. Serrano, J. M.; Silva, M., Trace analysis of aminoglycoside antibiotics in bovine milk by MEKC with LIF detection. *Electrophoresis* **2006**, 27, (23), 4703-4710.
22. Oguri, S., Electromigration methods for amino acids, biogenic amines and aromatic amines. *Journal of Chromatography B-Analytical Technologies in the Biomedical and Life Sciences* **2000**, 747, (1-2), 1-19.
23. Curiel, H.; Vanderaerden, W.; Velez, H.; Hoogmartens, J.; Van Schepdael, A., Analysis of underivatized gentamicin by capillary electrophoresis with UV detection. *Journal of Pharmaceutical and Biomedical Analysis* **2007**, 44, (1), 49-56.
24. McLaughlin, L. G.; Henion, J. D.; Kijak, P. J., Multi-Residue Confirmation of Aminoglycoside Antibiotics and Bovine Kidney by Ion-Spray High-Performance Liquid-Chromatography Tandem Mass-Spectrometry. *Biological Mass Spectrometry* **1994**, 23, (7), 417-429.

25. Ganjali, M. R.; Norouzi, P.; Daneshgar, P.; Sepehri, A., Development a new method for the determination of paromomycin in trace amounts by fast Fourier continuous cyclic voltammetry at an Au microelectrode in a flowing system. *Sensors and Actuators B-Chemical* **2007**, 123, (2), 1125-1132.
26. Baltussen, E.; Guijt, R. M.; van der Steen, G.; Laugere, F.; Baltussen, S.; van Dedem, G. W. K., Considerations on contactless conductivity detection in capillary electrophoresis. *Electrophoresis* **2002**, 23, (17), 2888-2893.
27. Sun, X. H.; Peeni, B. A.; Yang, W.; Becerril, H. A.; Woolley, A. T., Rapid prototyping of poly(methyl methacrylate) microfluidic systems using solvent imprinting and bonding. *Journal of Chromatography A* **2007**, 1162, (2), 162-166.
28. Pan, T.; Kelly, R. T.; Asplund, M. C.; Woolley, A. T., Fabrication of calcium fluoride capillary electrophoresis microdevices for on-chip infrared detection. *Journal of Chromatography A* **2004**, 1027, (1-2), 231-235.
29. Kelly, R. T.; Pan, T.; Woolley, A. T., Phase-changing sacrificial materials for solvent bonding of high-performance polymeric capillary electrophoresis microchips. *Analytical Chemistry* **2005**, 77, (11), 3536-3541.
30. Ismagilov, R. F.; Ng, J. M. K.; Kenis, P. J. A.; Whitesides, G. M., Microfluidic arrays of fluid-fluid diffusional contacts as detection elements and combinatorial tools. *Analytical Chemistry* **2001**, 73, (21), 5207-5213.
31. Jacobson, S. C.; Koutny, L. B.; Hergenroder, R.; Moore, a. W.; Ramsey, J. M., Microchip Capillary Electrophoresis with an Integrated Postcolumn Reactor. *Analytical Chemistry* **1994**, 66, (20), 3472-3476.